RELIABILITY ANALYSIS AND ROBUST DESIGN OF METAL FORMING PROCESS

RELIABILITY ANALYSIS AND ROBUST DESIGN OF METAL FORMING PROCESS

By

BING LI

A Thesis
Submitted to the School of Graduate Studies
in Partial Fulfilment of the Requirement
for the Degree
Doctor of Philosophy

McMaster University

DOCTOR OF PHILOSOPHY (2008)
Mechanical Engineering

McMaster University
Hamilton, Ontario

TITLE: Reliability Analysis and Robust Design of Metal Forming Process

AUTHOR: Bing Li

SUPERVISOR: Dr. Tim J. Nye and Dr. Peidong Wu

NUMBER OF PAGES: xv, 192

Abstract

Metal forming processes have been widely applied in many industries. With the severe competition in the market, a reliable and robust metal forming process becomes crucial for the manufacturer to reduce product development time and cost. For the purpose of supplying engineers with an effective tool for a reliable and robust design of metal forming process, this research investigates the application of traditional reliability theory and robust design methods in metal forming processes for the ultimate goal of increasing quality and reducing cost in manufacturing.

A method to assess the probability of failure of the process based on traditional reliability theory and the forming limit diagram (FLD) is presented. The forming limit of a material is chosen as the failure criteria for analysis of reliability.

A study of prediction of forming limit diagrams using finite element simulation without pre-defined geometrical imperfection or material imperfection is presented. A 3D model of the dome test is used to predict the FLD for AA 5182-O. The FE predicted forming limit diagram is in good agreement with the experimental one. The uncertainty sources for the scatter of forming limits are categorized and investigated to see their effects on the shape of FLD.

A novel method of improving the reliability of a forming process using the Taguchi method at the design stage is presented. The thickness-thinning ratio is chosen as the failure criteria for the reliability analysis of the process. A Taguchi orthogonal array is constructed to evaluate the effects of design parameters on the thinning ratio. A series of finite element simulations is conducted according to the established orthogonal array. Based on the simulation results, Taguchi S/N analysis and ANOVA analysis are applied to identify the optimal combination of design parameters for minimum thinning ratio, minimum variance of thinning ratio, and maximum expected process reliability.

A multi-objective optimization approach is presented, which simultaneously maximizes the bulge ratio and minimizes the thinning ratio for a tube hydroforming process. Taguchi method and finite element simulations are used to eliminate the parameters insignificant to the process quality performance. The significant parameters are then optimized to achieve the multiple optimization objectives. The optimization problem is solved by using a goal attainment method. An illustrative case study shows the practicability of this approach and ease of use by product designers and process engineers.

Acknowledgments

I would like to express my sincere gratitude to my co-supervisors, Dr. Tim Nye & Dr. Peidong Wu and former supervisor, Dr. Don Metzger for their invaluable support and guidance during my Ph.D. study. Their advice, patience and encouragement have been extremely helpful for the successful completion of this work. During the past years, I have learned a lot from them, not only in their areas of technical expertise, but also many aspects of the life. My gratitude to them is boundless.

I would also like to express my gratitude to my supervisory committee members, Dr. Mukesh Jain and Dr. Mateusz Sklad. Their valuable discussions and insightful comments profoundly helped me improve the quality of this thesis work.

My thanks also go to Dr. Nye's and Dr. Metzger's group members, Yuqing Ding, Xinjian Duan and Li Pan. I gratefully appreciate their constructive discussions and constant friendship during the course of my Ph.D. study.

Finally, I would like to thank my family, especially my wife Yu Sun, for their support, understanding and countless sacrifices during my Ph.D. period.

Contents

Abstract ..... **iii**

Acknowledgments ..... **v**

List of Tables ..... **ix**

List of Figures ..... **xi**

Chapter 1 Introduction **1**

1.1 Background and Motivation 1

1.2 Research Objectives 4

1.3 Thesis Outline 5

Chapter 2 Literature Review **6**

2.1 Reliability Theory 7

2.2 Forming Limit Diagram 10

2.2.1 Strain Path Effects on FLD 11

2.2.2 Prediction of FLD 12

2.2.3 Uncertainty of Forming Limit 13

2.3 Reliability Analysis of Metal Forming Process 17

2.4 Hydroforming 20

2.4.1 Tube Hydroforming Process 21

2.4.2 Influence of forming parameters on hydroformability 22

2.5 Taguchi Method 23

2.5.1 Historical Background 24

2.5.2 Principle of Taguchi Method 24

2.5.3 Application in Manufacturing 26
2.6 Discussion 28
Chapter 3 Reliability Based on Forming Limit Diagram 29
3.1 Notional Strain and Notional Limit Strain 30
3.2 Reliability Analysis Based on FLD 31
3.2.1 Distribution of Notional Limit Strain 32
3.2.2 Distribution of Notional Strain 33
3.3 Application 34
3.3.1 FEM Simulation 34
3.3.2 Effects of Different Parameters on Hydroformability 37
3.3.3 Reliability of Tube Hydroforming Process 44
3.4 Discussion 49
Chapter 4 Prediction of FLD using FEM 51
4.1 Criteria for Localized Necking 53
4.2 Finite Element Analysis 54
4.2.1 Element Type 57
4.2.2 Mesh Size 57
4.2.3 Material Model 59
4.2.4 Contact Definition 60
4.2.5 Tool Motion 61
4.3 Results and Discussion 64
4.3.1 Forming Limits at Biaxial State 64
4.3.2 Forming Limits from the Uniaxial State 73
4.3.3 Forming Limit at Plane Strain State 80
4.3.4 FE Predicted FLD 88
4.3.5 Uncertainty of Forming Limits 89
4.3.6 FLD Considering Objective and Subjective Uncertainties 104
Chapter 5 Improving Reliability by the Taguchi Method 111
5.1 Reliability Analysis Based on Thinning Ratio 112
5.2 Finite Element Simulation 115
5.3 Taguchi Method 117
5.3.1 Choice of Quality Characteristic 118

5.3.2 Construction of Orthogonal Arrays 118
5.4 Results and Discussion 121
5.4.1 Mean Value Analyses 121
5.4.2 Variance Analysis 124
5.4.3 S/N Analyses 125
5.4.4 ANOVA Analyses 127
5.4.5 Improvement of Reliability 128
Chapter 6 Multi-objective Optimization Based on Taguchi Method 130
6.1 Methodology 132
6.2 Free Bulging Tube Hydroforming Process 133
6.2.1 FEM Simulation 133
6.2.2 Decision of Quality Characteristics and Objective Function 135
6.2.3 Selection of Parameters and Construction of Orthogonal Array 136
6.3 Results and Discussion 138
6.3.1 Effects of Forming Parameters on Hydroformability 138
6.3.2 Multi-objective Optimization of Tube Hydroforming Process 145
6.3.3 Confirmation Experiments 151
6.3.4 Pareto Set 152
Chapter 7 Conclusions 154
7.1 Summary of Conclusions 155
7.2 Contributions 157
7.3 Recommendations for Future Work 158
References 160
Appendix A 176

List of Tables

Table 2.1: Historical background of FLD 11
Table 2.2: The Methods for predicting the FLD 13
Table 2.3: Uncertainty analysis of forming limit 14
Table 2.4: Application of Taguchi method in Manufacturing 27
Table 3.1: Mechanical properties used in the simulation 35
Table 3.2: Maximum effective plastic strain with different mesh sizes 37
Table 3.3: The forming conditions used in the simulation 39
Table 3.4: Layout of simulation and the resulting critical notional strain 40
Table 3.5: Partial derivative of notional strain with respect to each forming parameter.. 47
Table 4.1: Material properties of AA 5182-O (Numisheet 2005) 54
Table 4.2: Effect of mesh size on the thinning rate 58
Table 4.3: Punch displacement for various friction conditions 66
Table 4.4: Layout of simulation with three levels of each parameter 93
Table 5.1: Level of design parameters 119
Table 5.2: Level of noise factors 119
Table 5.5: Design parameters' effects on standard deviation 124
Table 5.6: Design parameters' effects on S/N ratio 126
Table 5.7: Analysis of variance for thinning ratio 127
Table 6.1: Parameters used in the FEM simulation 134
Table 6.2: Level of forming parameters 136

Table 6.3: Taguchi's L_{18} orthogonal array 137
Table 6.4: Bulge ratio values and its S/N ratio 139
Table 6.5: Average S/N ratio of the bulge ratio for each parameter 140
Table 6.6: Thinning ratio values and its S/N ratio 141
Table 6.7: Average S/N ratio of the thinning ratio for each parameter 142
Table 6.8: Analysis of variance for bulge ratio 144
Table 6.9: Analysis of variance for thinning ratio 144
Table 6.10: A full factorial array for three parameters with three levels 146
Table 6.11: Bulge ratio and its S/N ratio 147
Table 6.12: Thinning ratio and its S/N ratio 148
Table 6.13: Optimal combination of parameters and estimated S/N ratio 150
Table 6.14: Comparison between the optimal case and nominal case 151
Table A.1: The critical stress and its relative parameters 188
Table A.2: The regression coefficients of the fuzzy stress 190

List of Figures

Figure 2.1: Schematic view of stress-strength interference model 8
Figure 2.2: Example of forming limit diagram 10
Figure 2.3: Forming limit band in FLD 15
Figure 2.4: Definition of limit state function (Kleiber et al., 2002) 18
Figure 2.5: FLD with marginal zone (Kleiber et al., 2002) 19
Figure 2.6 Forming limit diagram for rimming steel diaphragms bulged in different dies (Van Minh et al., 1974) 19
Figure 2.7: Schematic view of tube hydroforming process (Asnafi et al., 2000) 22
Figure 3.1: Concept of notional strain and notional limit strain 31
Figure 3.2: Notional strain – notional limit strain interference model 32
Figure 3.3: Schematic view of free bulging hydroforming 35
Figure 3.4: Loading path used in the simulation 36
Figure 3.7: Effect of the different parameters on the bulge ratio 43
Figure 3.9: Relationship between notional strain and the forming parameters 48
Figure 4.1: Classification scheme for grids in the neck region (Jain & Allin, 1994) 54
Figure 4.2: Simulation model of dome test 56
Figure 4.3: Geometry of samples used in the simulation 56
Figure 4.4 Different mesh sizes for the blank for plane strain stretching 58
Figure 4.5: Effective stress versus effective plastic strain for AA 5182-O 60
Figure 4.6: Clamp die velocity curve (solid) and corresponding displacement (dashed). 63

Figure 4.7: Punch velocity curve (solid) and displacement curve (dashed) 63
Figure 4.8: Simulation model for biaxial stretching test... 64
Figure 4.9: Deformed mesh of sheet with the punch displacement of 40 mm 65
Figure 4.10: Location of the measuring elements in the biaxial state with $f_c = 0.01$ 68
Figure 4.11: Minor & major strains (a) and thickness strain (b) of measuring elements in the biaxial state with $f_c = 0.01$ 69
Figure 4.12: Location of the measuring elements in the biaxial state with $f_c = 0.05$ 70
Figure 4.13: Minor and major strains of measuring elements in the biaxial state with $f_c = 0.05$ 71
Figure 4.14: Location of the measuring elements in the biaxial state with $f_c = 0.15$ 72
Figure 4.15: Minor and major strains of measuring elements in the biaxial state with $f_c = 0.15$ 72
Figure 4.16: Simulation model for uniaxial tension test... 73
Figure 4.17: Deformation of the sheet with the punch displacement of 40 mm.............. 74
Figure 4.18: Location of the measuring elements in the uniaxial state with $f_c = 0.01$ 75
Figure 4.19: Minor and major strains of measuring elements in the uniaxial state with $f_c = 0.01$ 76
Figure 4.20: Location of the measuring elements in the uniaxial state with $f_c = 0.05$ 77
Figure 4.21: Minor and major strains of measuring elements in the uniaxial state with $f_c = 0.05$ 78
Figure 4.22: Location of the measuring elements in the uniaxial state with $f_c = 0.15$ 79
Figure 4.23: Minor and major strains of measuring elements in the uniaxial state with $f_c = 0.15$ 80
Figure 4.24: Simulation model for plane strain stretching test....................................... 81
Figure 4.25: Deformation of the sheet with the punch displacement of 40 mm.............. 82
Figure 4.26: Location of the measuring elements in the plane strain state with $f_c = 0.01$ 83

Figure 4.27: Minor and major strains of measuring elements in the plane strain state with $f_c = 0.01$ 84
Figure 4.28: Location of the measuring elements in the plane strain state with $f_c = 0.05$ 85
Figure 4.29: Minor and major strains of measuring elements in the plane strain state with $f_c = 0.05$ 86
Figure 4.30: Location of the measuring elements in the plane strain state with $f_c = 0.15$ 87
Figure 4.31: Minor and major strains of measuring elements in the plane strain state with $f_c = 0.15$ 88
Figure 4.32: Comparison between FEA predicted FLD with the experimental one for AA5182-O 89
Figure 4.33: Reference limit strain points for FLD of AA5182-O 94
Figure 4.34: FLDs showing the effect of material yield stress 94
Figure 4.35: FLDs showing the effect of hardening exponent 95
Figure 4.36: FLDs showing the effect of R_{45} 95
Figure 4.37: FLDs showing the effect of R_0 96
Figure 4.38: FLDs showing the effect of R_{90} 96
Figure 4.39: FLDs showing the effect of thickness 97
Figure 4.40: FLDs showing the effect of friction coefficient 97
Figure 4.41: FLDs showing the strain paths obtained with different friction conditions. 98
Figure 4.42: FLDs for different set of measuring element samples 99
Figure 4.43: FLDs for different combinations of strain paths 101
Figure 4.44: FLDs for different number of samples used in each strain path 102
Figure 4.45: FLDs produced by different methods 103
Figure 4.46: 99.9% confidence region of forming limits for element 350 under biaxial stretching state with $f_c = 0.01$ 105

Figure 4.47: 99.9% confidence region of forming limits for element 374 under biaxial stretching state with $f_c = 0.01$ 105
Figure 4.48: 99.9% confidence region of forming limits for element 398 under biaxial stretching state with $f_c = 0.01$ 106
Figure 4.49: 99.9% confidence region of forming limits at biaxial stretching state with $f_c = 0.01$ 106
Figure 4.50: 99.9% confidence region of forming limits at biaxial stretching state with $f_c = 0.05$ 107
Figure 4.51: 99.9% confidence region of forming limits at biaxial stretching state with $f_c = 0.15$ 107
Figure 4.52: 99.9% confidence region of forming limits at plane strain stretching state with $f_c = 0.05$ 108
Figure 4.53: 99.9% confidence region of forming limits at uniaxial tension state with $f_c = 0.05$ 108
Figure 4.54: 99.9% confidence region of forming limit strains for AA 5182-O 109
Figure 4.55: Comparison of FLDs of AA 5182-O 110
Figure 5.1: Resulting thinning ratio-Limit thinning ratio interference model 114
Figure 5.2: Schematic view of the tube hydroforming process 116
Figure 5.3: Finite element mesh and effective strain contour 116
Figure 5.4: Mean values of thinning ratio for each design parameter 122
Figure 5.5: Standard deviation of thinning ratio for each design parameter 125
Figure 5.6: S/N ratio graph for the thinning ratio 126
Figure 5.7: Interaction analysis of parameters A and B 128
Figure 5.8: Reliability of the process with the initial and optimal forming parameters . 129
Figure 6.1: Multi-objective optimization using Taguchi Method 133
Figure 6.2: Average effect diagram of forming parameter on the bulge ratio 140
Figure 6.3: Average effect diagram of forming parameter on the thinning ratio 142
Figure 6.4: Pareto optimal combinations of thinning ratio and bulge ratio 153

Figure A.1: Triangular Fuzzy Number 179
Figure A.2: Fuzzy stress-random strength interference model 184

Chapter 1

Introduction

1.1 Background and Motivation

Metal forming processes such as drawing, extrusion, rolling, forging, sheet metal forming and hydroforming have been widely applied in diverse industries. In metal forming, as much as half of the design time is often consumed by prototype testing and subsequent modifications of the dies, especially when new materials and/or forming processes are used (Cao et al., 2003). With the increasing demand of high-quality products at a minimum cost, reliable and robust design of metal forming processes has become crucial to reduce design cycle times and time to market.

Currently the most widely used method for the failure analysis of sheet metal forming is the well-known forming limit diagram (FLD). The forming limit diagram is a convenient tool for the evaluation of formability and for the determination of the process limitations in sheet metal forming. However, the FLD can only qualitatively show how close a strain state is to failure. In order to quantify the failure probability of the metal forming process, the methodology developed for reliability analysis of structures can be used (Kleiber, 2002). The structure reliability analysis is a probabilistic engineering approach to estimate the probability of failure of a structure from the probability distributions of the contributing factors and modes of failure (Bullough et al., 1999). In metal forming, the forming limit can be applied as the failure criteria for the reliability analysis of the process.

Presently there are a lot of theoretical, numerical and experimental methods to predict the forming limit diagram. All the methods always lead to a forming limit curve (FLC) which separates the safe zone and the necking or fracture zone. Actually what is really determined in the experiments are some discrete points corresponding to the different strain paths (Janssens et al., 2001), so it is more suitable to estimate the results by using the forming limit band than the forming limit curve. On the other hand, the accuracy of the experimental determination of a FLC is also a complex matter as it depends largely on the experimental procedure. Variation of material properties, friction conditions, process parameters and differences in strain path could substantially increase or decrease the level of the FLC. All the above information indicates that the forming limit curve should be treated as a forming limit band with some uncertainties (Kleiber, 2002). Meanwhile the metal forming process has a number of parameters that may affect the quality of the process, such as material constants, geometric dimensions, process control parameters, friction coefficients, etc. Real values of these parameters are known to have a certain scatter around their nominal values, so that the response or performance characteristics, resulting from the process, depend on these uncertain parameters.

Historically, probability theory has been the primary tool for representing uncertainty in mathematical models. Because of this, all uncertainty was assumed to follow characteristics of random uncertainty. However, not all uncertainties are random or objective. Some uncertainties, especially those based on incomplete information are due to subjective sources (Sawyer and Rao, 1999). For instance, in predicting the forming limit diagram of a material, engineering experience and subjective decisions are involved in selecting the experimental method, tooling and specimen geometry, friction condition, method for interpretation of the experimental results. The forming limit strain in the FLD should thus be regarded somewhat as a subjective variable.

The main goal of reliability analysis is to predict and minimize failures while the goal of robust design is to build quality into products and processes. Robust design methods, including the Taguchi method, pioneered by Taguchi (1976, 1977), are an optimization approach that uses a series of experiments (computer-based or physical) to find parameter settings for a design that yield predicted performance to be on target and to be as insensitive to variation in parameter levels as possible. The variation can come from the material properties, dimensional parameters and system or environmental parameters. Usually in metal forming, the forming parameters are determined by theoretical analysis or experience, requiring that a large number of experiments have to be performed to adjust the parameters for optimal or near-optimal forming performance, resulting in a time-consuming and costly procedure. The Taguchi method uses a set of orthogonal arrays to determine parameters configuration and analyze the results. These kinds of arrays allow a smaller number of experiment runs but obtain maximum information and have high reproducibility and reliability (Yang, 1998). Taguchi parameter design can estimate the contribution of each parameter to the forming response and can optimize the forming process through setting of design parameters while reducing the sensitivity of the forming response to sources of variation.

This research is expected to provide engineers with an effective tool for designing a reliable and robust metal forming process, which will be extremely beneficial in the reduction of development time and cost.

1.2 Research Objectives

The objective of this research is to investigate how to apply reliability theory and robust design methods in metal forming processes for the ultimate goal of increasing quality and reducing cost in manufacturing. There are a number of research topics for this objective. In this Ph.D. study, the focus will be on the following tasks:

- Investigate how to combine reliability theory with the traditional failure criteria for evaluating the metal forming process;
- Investigate how to predict the forming limit diagram using finite element simulation by considering both objective and subjective uncertainties;
- Investigate how to evaluate the influence of the forming parameters on the metal forming process and optimize the process for robustness.

1.3 Thesis Outline

The results of this research are reported in six chapters. Chapter 2 presents a review of the literatures relative to this research. A reliability analysis method for the metal forming process based on the forming limit diagram is introduced in Chapter 3. The results of this study have been published (Li et al., 2006). The study of prediction of forming limit diagram using finite element simulation is presented in Chapter 4. The part of the results of this study has been presented at an international conference (Li et al., 2006). The uncertainty analysis of forming limit is also reported in this chapter. In Chapter 5, a method of improving the reliability of metal forming process by using the Taguchi method is reported. The paper based on this study has been published (Li et al., 2007). A study of optimization of the forming parameters, in the metal forming process with the conflicting objectives, is reported in Chapter 6, the Taguchi method is employed to find the most significant parameters for the process. The goal attainment method is used for solving this multi-objective problem. A paper based on this study has been published (Li et al., 2006). Overall results of this research are discussed and summarized in Chapter 7, some conclusions are drawn and recommendations for future studies are made. In appendix, a study of evaluating the reliability of metal forming process by fuzzy sets theory, which has been presented at an international conference (Li et al., 2004), is reported. This part of research is an accomplishment of the author during the course of Ph.D. study even it is not directly contributing to the objectives of this thesis.

Chapter 2

Literature Review

Five areas of previous research bear the most direct relationship to this research. The literature on reliability theory describes the development of the reliability theory to evaluate the reliability of components and systems. The literature on reliability analysis of metal forming process summarizes some previous research works and discusses the new research opportunities in this area. The literature on forming limit diagram mainly focus on the conventional strain-based forming limit diagram. The prediction of FLD using experimental method and numerical method are reviewed. The literature on hydroforming using the experimental method and numerical method is reviewed. The literature on the Taguchi method introduces the brief history of this method and its applications in the manufacturing area.

Each of these five areas will be discussed in depth in subsequent subsections. There is no attempt to discuss all the research in these disciplines, only that which is most directly connected to the main direction of this proposed research is mentioned.

2.1 Reliability Theory

Failure and faults are unavoidable phenomenon in all products or systems and they can show up in multiple forms and in assorted circumstances. The theory of reliability can be considered as the study of failure occurrence in technical equipment. Reliability had a very important impulse after World War II by military researchers due to the significance it has in naval and aeronautical equipment, and in the structure and control of missiles (Collins, 1988). In the seventies, motivated by the special security conditions demanded at nuclear stations, increasing investigations of reliability have been made due to the technological advances and to the complexity of the system (Aven, 1985). Now reliability has become a main aspect in many products and systems, and has been widely studied in many areas.

One of the many definitions of the term 'reliability' throughout the literature is given by Pagès & Gondran (1980). They consider that reliability is the "Capacity of a device to perform a function required within some conditions and during a given duration". Kaufman and his collaborators (1975) gave another definition of reliability, in more mathematical terms. They define reliability as "the probability of the fact that a system accomplishes with some given services, with the fixed utilization conditions and during a given time".

The common reliability analysis methods include (Dupow & Blount, 1997):

- FMEA (failure modes and effects analysis)

- FTA (fault tree analysis)
- Computer simulation programs (i.e. Monte Carlo, SIMULINK)
- SCA (sneak circuit analysis)
- ESS (environmental stress screening)
- RDGT (reliability development/growth testing)
- Experimental test methods
- State-Space Analysis (Markov analysis)
- Stress-Strength Interference Analysis.

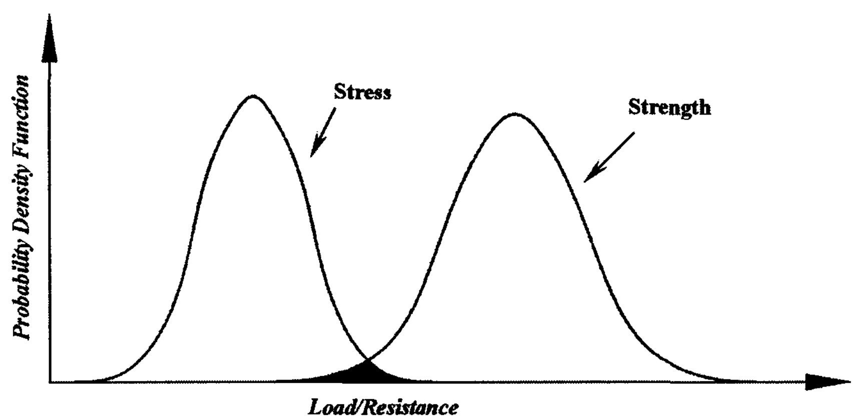

Figure 2.1: Schematic view of stress-strength interference model

For a mechanical or structural component, it is considered to be safe and reliable when the strength or resistance of the component exceeds the value of the stress acting on it. Figure 2.1 schematically shows the stress-strength interference model. Mathematically, the reliability of a component is given by

$$R = P(L - S > 0) = \iint f_{L,S}(l,s)\,dl\,ds \tag{2.1}$$

where L is strength, the resistance effect variable, S is stress, the load effect variable, $f_{L,S}(l,s)$ is the joint density function of L and S.

There are three levels of formal reliability analysis of a structure (Bullough et al., 1999). In the Level 1 formal reliability analysis method, the reliability is not calculated explicitly; instead a set of partial safety factors is applied to each basic variable. Typical examples of Level 2 formal reliability analysis methods are the First Order Reliability Method (FORM) and the Second Order Reliability Method (SORM); these methods in most cases provide only an approximation to the exact value of the reliability. In the Level 3 formal reliability analysis method, the reliability is calculated exactly. The calculation can either be carried out using multiple numerical integration or by Monte Carlo sampling techniques, but there are practical limitations to the number of basic random variables with multiple numerical integration and the Monte Carlo sample techniques only have high statistical accuracy if a large number of cases are simulated.

2.2 Forming Limit Diagram

The forming limit diagram (FLD) has proven to be a useful tool in the formability analysis for sheet metal forming (Graf & Hosford, 1990). The limits of formability in sheet metal operations are described in terms of the principal strains by the forming limit diagram (FLD). The forming limit in a FLD is conventionally described as a curve in a plot of major strain vs. minor strain. If the maximum principal strain is above the forming limit curve, it indicates that necking or fracture failure will happen; otherwise failure will not occur and the process is safe (Stoughton, 2000). As shown in Figure 2.2, for two postulated forming processes for the same material, the maximum strain obtained in process one crosses the forming limit curve, where necking failure will happen, while the maximum strain obtained in process two is below the forming limit cure. Thus, process two is assumed to be safe.

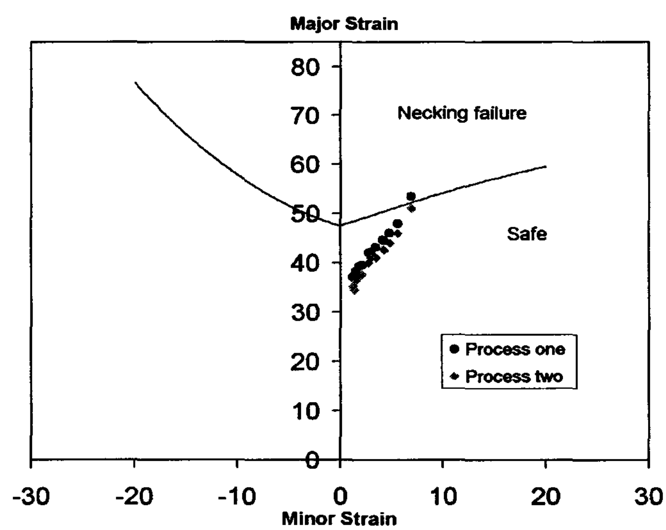

Figure 2.2: Example of forming limit diagram

The historical background of the development of the FLD is shown in Table 2.1.

Table 2.1: Historical background of FLD

Year	Researchers	Main Contributions
1964	Keeler & Backofen	Firstly conducted the study of FLD with the tests of the stretching of circular blanks by a hemispherical punch.
1965	Keeler	Proposed the use of electrochemically-etched grids to measure strain histories and strain distributions as a tool for determining forming limits.
1967	Marciniak & Kuczynski	Proposed the analytical model for limit-strain prediction based on the initial inhomogeneity of a material, now commonly referred to as the M–K theory.
1968	Keeler	Analyzed the strain distributions in the region of biaxial tension in actual stampings to improve part quality and optimize die design using FLD.
1968	Goodwin	Obtained a failure band in both the negative and positive quadrants of minor strain, creating the general form of the forming-limit diagram.
1975	Hecker	Introduced an approach involving the stretching of sheets of various widths over a hemispherical punch to obtain strain ranging from uniaxial tension to balanced biaxial tension.

2.2.1 Strain Path Effects on FLD

Early work in the development of the forming-limit diagram assumed linear strain paths. With the full use of grid-strain analysis and, later, computer simulation, the strain histories in various deep-drawing operations have become more readily identifiable. Shortly after the Keeler–Goodwin FLD had been developed, researchers began to find that, for some materials, such forming limits changed significantly with differences in the strain paths used to collect data points. An early experimental study, performed by Matsuoka and Sudo (1969), investigated the forming limits of aluminum-killed steel sheets that had been subjected to various types of second-stage strains, following first-stage deformation through balanced biaxial tension, uniaxial tension, or a modified drawing operation. More recently, interest in strain-path-dependent forming-limit diagrams for aluminum alloys has been driven by their potential application in the automotive industry. Graf and Hosford (1993) performed experiments using aluminum alloy 2008-T4, prestrained at various levels of uniaxial tension, biaxial tension, and plane strain. They determined that biaxial prestrains generally lower the FLD, whereas plane-strain and uniaxial-tension prestrains generally raise the forming-limit curves.

2.2.2 Prediction of FLD

Three approaches have been proposed and utilized to predict the FLD, namely bifurcation analysis, damage model analysis and Marciniak & Kuczynski analysis as shown in Table 2.2.

Table 2.2: The Methods for predicting the FLD

Method	Main Characteristics	References
Bifurcation analysis	Treat the onset of failure as the condition that leads to plastic instability	Hill (1952) Stören & Rice (1975) Hutchinson and Neale (1978) Xinhai Zhu et al. (2001)
Damage model analysis	Assume micro-defects in the material and forming limit is predicted when the evolution of these micro-defects reaches a limit	Tjotta (1992) Chow et al. (2001)
M-K method	Assume thickness imperfections normal to the principal stress and strain as a groove simulating the preexisting defects in the materials	Marciniak & Kuczynski (1967) Rasmussen (1981) Barata da Rocha & Jalinier (1984) Cao et al. (2000) Yao & Cao (2002) Wu et al. (2003)

2.2.3 Uncertainty of Forming Limit

In spite of the considerable amount of time researchers have spent on the subject of FLD, the concern regarding the accuracy and precision with which a forming limit can be determined has not been sufficiently analyzed. Previous research works regarding this subject are listed in Table 2.3.

Table 2.3: Uncertainty analysis of forming limit

Year	Researchers	Main contributions
1968	Goodwin	Presented the concept of forming limit band
1974	Van Minh et al.	Investigated the probabilistic nature of the forming limits, showed that the scatter in the forming limits must be some manifestation of an intrinsic material property rather than the errors inherent in the experimental method
1992	Narasimhan et al.	Predicted a scatter band in limit strains by repeating the FLD predictions for several differential initial random thickness distribution using Monte-Carlo and finite element methods
2001	Janssens et al.	Statistically evaluated the uncertainty of experimentally characterized forming limits of sheet steel, confirmed that the scatter of the forming limits is due to the material behavior and not to the experimental procedure.

The forming limit curve of a material is usually determined by experimental measurement. Generally errors exist due to the uncertainty in experimental measurements, the material properties, the process conditions and so on, so the forming limit curve is more appropriately described as a forming limit band (Janssens & Lambert, 2001). With the forming limit band (e.g., as shown in Figure 2.3), if a strain point is located under the lower forming limit band boundary, the forming process is safe. If the strain point is located above the upper forming limit boundary, then necking failure is predicted to occur. If the strain point is located between the upper and the lower boundaries, then the forming process is marginal and there is a probability that failure will happen. In the following chapter, the reliability theory will be used to calculate the necking failure probability of the process when the maximum strain obtained is located among the forming limit band. In the particular example shown in Figure 2.2 and Figure 2.3, while the conventional FLD predicts the process is safe, use of the forming limit band allows a probability of failure to be calculated.

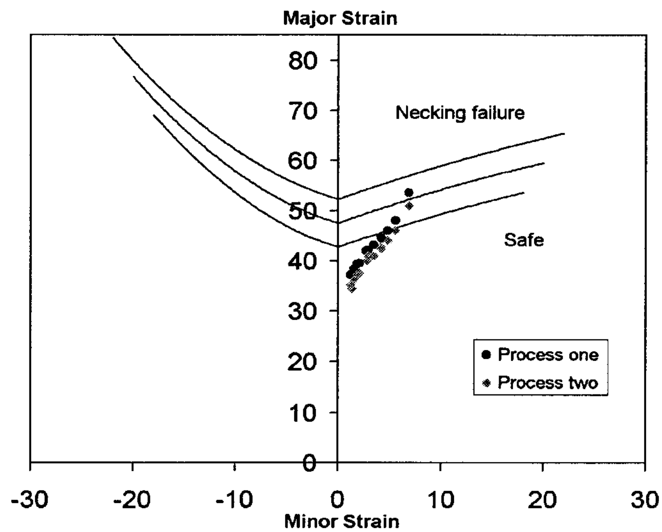

Figure 2.3: Forming limit band in FLD

Uncertainty of forming limit is not just found in the experimentally determined FLDs. Numerically predicted FLDs also see the uncertainty of forming limit due to the assumptions in the models. Horstemeyer (2000) investigated the following parameters which caused the variation of forming limits using FE simulation: finite element code, sheet thickness, type of instability, element type, mesh size and two-stage, non-proportional loading. The influence of sheet orientation, *n*-values, *r*-values, prestrain and sheet thickness on the predicated FLDs has been investigated in Rees's (2001) research on predicting the FLD of automotive sheet metal. Ozturk and Lee (2004) used a dome test for FE simulation to predict the forming limit using ductile fracture criteria, the limit strains were determined by monitoring the thickness strain throughout the simulations. A pre-determined strain value was checked and compared with the thickness strain of each element at each increment, when the condition is satisfied, the major and minor strains were recorded. In this method, the pre-determined strain value is a kind of subjective value which brings the subjective uncertainty of forming limit into the predicted FLD. Wu et al. (2004) presented a mesoscopic approach for constructing the forming limit diagram. It has shown that the following parameters have the effects on the predicted FLDs: strain-rate sensitivity, hardening parameter n, latent hardening parameter q, crystal elastic modulus, texture evolution and the spatial orientation distribution of texture. By directly incorporating the measured grain orientations and their spatial distributions into the finite element model, Wu et al. (2007) numerically simulated the localized necking in AA6111-T4 under stretching. They assumed that localized necking is associated with surface instability, the onset of unstable growth in surface roughening. They found that localized necking depends strongly on both the initial texture and its spatial orientation distribution.

By recognizing that the uncertainty of forming limit exists in both experimentally determined FLD and numerically predicted FLD, in the following chapters, all the potential sources for the uncertainty of FLD observed in the experimental procedure will be classified into two categories: objective uncertainty sources and subjective uncertainty sources. The influence of these uncertainty sources will be investigated through the FE simulations.

2.3 Reliability Analysis of Metal Forming Process

Although reliability theory is now widely applied in various areas, it has not become a main subject of studies in the metal forming field. There are very few reports on reliability analysis of metal forming process in the literature.

Hopperstad et al. (1999) presented the reliability analyses of a plastic forming process. They combined the finite element method and reliability method to obtain the valuable information regarding the influence of various parameters governing the response of the aluminium extrusion during the forming process. Material parameters were modeled as random variables defined in terms of given statistical properties. The probability for the response parameters to stay within specified limits was calculated by means of response surface methods and First Order Reliability Method (FORM)/Second Order Reliability Method (SORM).

The first research report of reliability analysis of sheet metal forming based on the FLD was presented by Arwashan (1999). In this research, the forming limit was defined by FLD_0, which is expressed by a function of sheet thickness and the work hardening exponent. The probability of failure in forming was calculated as the probability of the plane strain to be higher than FLD_0. The author did not take the shape of the FLD into account and assumed the variability in the forming limit is the result of variability in FLD_0.

Kleiber et al. (2002) applied the methodology developed for structural reliability analysis to assess the reliability of a sheet metal forming operation. Forming limit diagrams (FLD) were used as a criterion of material breakage for the process in their research. They indicated that the FLC can be regarded as bounding the safe zone with some probability due to the uncertainties on the evaluation of the FLD caused by the different uncertainties in the process and material parameters.

The FLC was used to construct the limit curve for the reliability analysis in their study. If all the strain points are below the FLC, the limit state function is equal to the distance of the point closest to the FLC (See Figure 2.4). On the other hand, if some of the points are above the FLC the value of the limit state function equals the maximal distance of the point from those above the curve, taken with the minus sign.

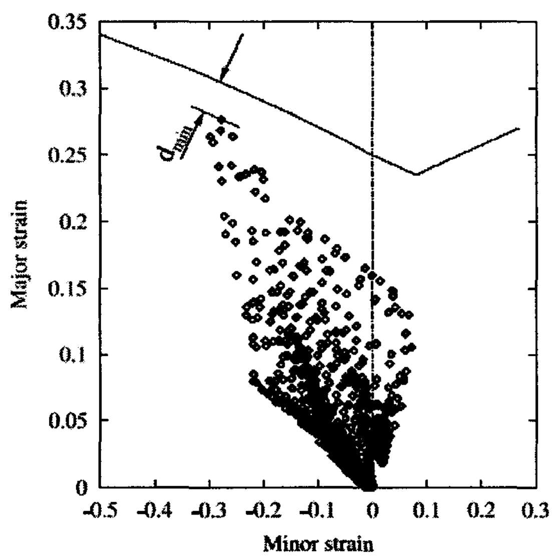

Figure 2.4: Definition of limit state function (Kleiber et al., 2002)

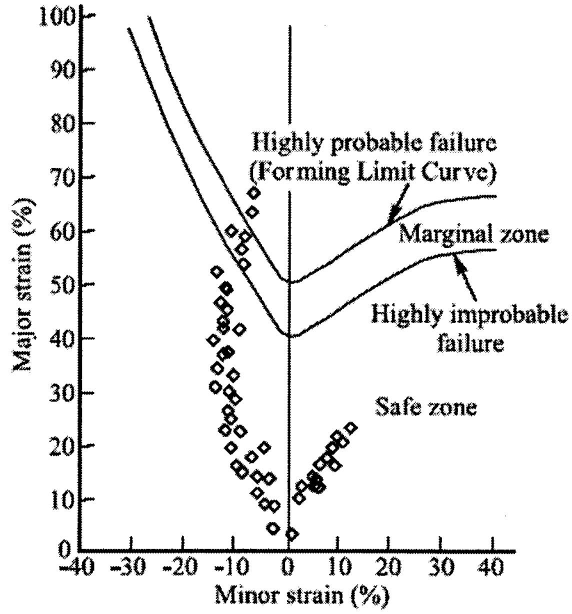

Figure 2.5: FLD with marginal zone (Kleiber et al., 2002)

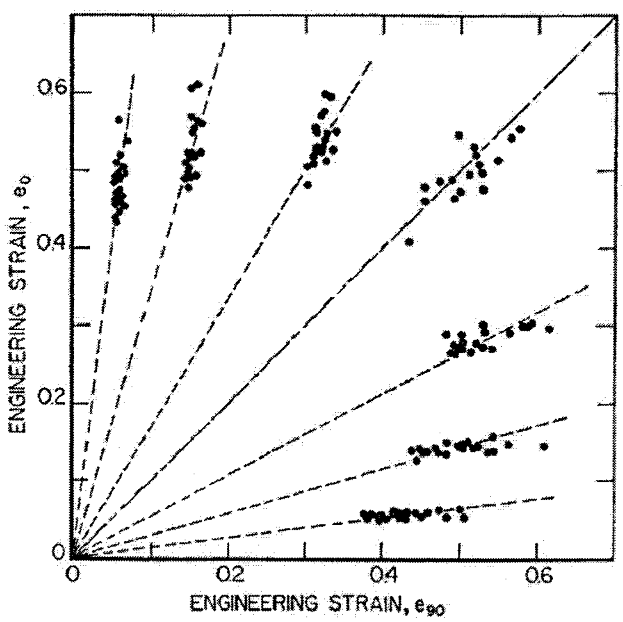

Figure 2.6 Forming limit diagram for rimming steel diaphragms bulged in different dies (Van Minh et al., 1974)

To account for the uncertainties regarding FLC's shape and position, Kleiber et al. introduced the marginal zone below the FLC (see Figure 2.5). The points on the diagram can now be classified depending on their position with respect to the marginal zone as leading to necking type failure with high or low probability.

This paper is a pioneering research report of reliability analysis of metal forming process using the FLD. However, there are some obvious shortcomings in this paper since the authors are experts in reliability research but not the metal forming areas. First, the statistical experimental results of predicting the FLC showed that the strain points tend to spread more along the particular strain path than perpendicular to the estimated curve (see Figure 2.6, Van Minh et al., 1974), so it is not proper to use the distance of the strain point perpendicularly closest the FLC as the value of the limit state function. Second, all the FLCs constructed from the experimental results approximately represent the average limit of a material (Narasimhan et al., 1992; Janssens et al., 2001), so it is inappropriate to set a marginal zone below the FLC rather than offsetting from the FLC based on reliability analysis of forming process point of view.

This research will try to overcome the shortcomings mentioned above and present a reliability analysis model based on the FLD in a different manner.

2.4 Hydroforming

Hydroforming was developed during the late 1940's and early 1950's in response to the need for a lower cost method of producing relatively small quantities of deep drawn parts (Davis, 1945). Since the 1990's it has been attracting increasing attention in many industrial fields, especially in the automotive industry.

2.4.1 Tube Hydroforming Process

Simply stated, hydroforming uses the force of water or hydraulic fluids to shape a single part. There are basically two types of hydroforming: tube and sheet. Tube hydroforming starts from a tube that has been precut into the proper length. The tube may require prebending as a preforming process. The tube is then placed into the die and the die is closed. Hydraulic liquid fills the tube and two side cylinders then close onto the ends of the tube. Simultaneously, the liquid is pressurized and the cylinders are pushed in from the side. The materials of the tube yields and flows into die cavity and the part is formed. A typical tube hydroforming process is shown in Figure 2.7.

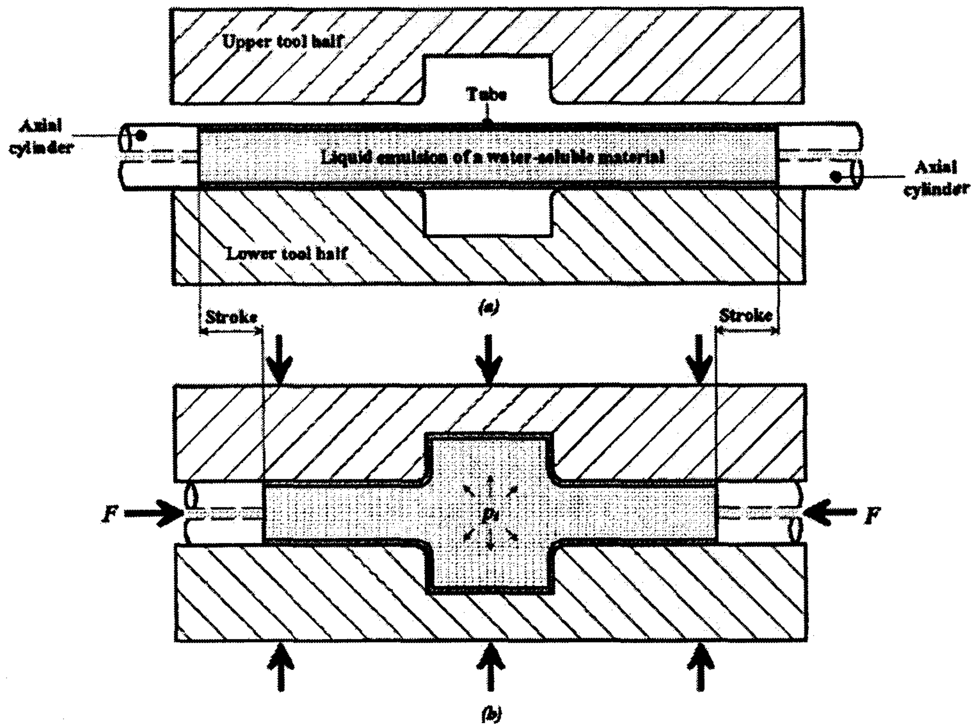

Figure 2.7: Schematic view of tube hydroforming process (Asnafi et al., 2000)

2.4.2 Influence of forming parameters on hydroformability

The influence of material properties and process parameters on the tube hydroforming process has been studied by means of experiments, analytical models and finite element simulations. Carleer et al. (2000) found that the anisotropy parameter and hardening exponent have a large impact on the shape of free expanded tubes, and the anisotropy parameter and friction coefficient have the biggest effect on strain distribution. Manabe and Amino (2002) investigated the parameters influencing tube hydroforming by means of FE simulations and experiments. They suggest that tubular material with a high hardening exponent and high anisotropy parameter should be selected, and good lubrication should be maintained to obtain the uniform wall thickness distribution. Boudeau et al. (2002) used the finite element method to study the influence of material and process parameters on the necking and bursting. Koç and Altan (2002) investigated the effects of the geometry parameters and process parameters in tube hydroforming by a series of 2D FEM simulations. They found the internal pressure and the length of the tube have the greatest effect on the bulge of an axi-symmetric part. Yang et al. (2001) developed a numerical approach that can provide the sensitivity information of internal pressure and axial load on the tube hydroforming process.

2.5 Taguchi Method

Over the second half of the 20th century, optimization found widespread applications in the study of production planning and scheduling systems, resource allocation in financial systems, and in engineering design. All optimization problems are expressed as a mathematical model which presents the optimization objective as a formula. In our research, it will not be appropriate to use traditional optimization methods to find the optimal combination of the forming parameters for a metal forming process in which the performance characteristics can not be expressed as a mathematical formula. The robust design method, also known as the Taguchi method is a proper tool for such kind of optimization problems.

2.5.1 Historical Background

The Taguchi method is named after Dr. Genichi Taguchi, a Japanese electrical engineer. Taguchi (1976, 1977) published his main ideas in two volumes written in Japanese, and popularized his method in the United States and Europe in the late 1980's. Taguchi methods were first introduced to the American automotive industry in March 1982 (Sullivan, 1987). Since 1982, the Taguchi method has been applied in a wide range of areas, from electronics and information technology to process industries and plastics technologies. Users of the Taguchi method have claimed substantial improvements in quality and robustness while simultaneously reducing costs. (Park et al., 1995; Yang et al., 1998; Ko et al., 1999; Huh et al., 2003)

2.5.2 Principle of Taguchi Method

Experimental design methods were developed originally by Fisher (1925). However, classical experimental design methods are complex and not easy to use. Taguchi (1990) proposed to use a special design of orthogonal arrays to study the entire parameter space with a small number of experiments. The experimental results are then transformed into a signal-to-noise (S/N) ratio. Taguchi recommends the use of the S/N ratio to measure the quality characteristics deviating from the desired values. The S/N ratio is defined by

$$S/N = -10\log(MSD) \tag{2.2}$$

where *MSD* is the mean square deviation for the quality characteristic.

Usually, there are three categories of quality characteristic in the analysis of the S/N ratio, i.e. the-lower-the-better, the-higher-the-better, and the-closer-to-nominal-the-better. The mean square deviation for the-lower-the-better quality characteristic is given by

$$MSD = \frac{1}{n}\sum_{i=1}^{n} y_i^2 \tag{2.3}$$

where y_i is the value of the-lower-the-better quality characteristic, n is the number of the tests for a trial condition. The mean square deviation for the-higher-the-better quality characteristic is given by

$$MSD = \frac{1}{n}\sum_{i=1}^{n} \frac{1}{y_i^2} \tag{2.4}$$

where y_i is the value of the-higher-the-better quality characteristic. In the event the-closer-to-nominal-the-better quality characteristic was desired, the mean square deviation would be

$$MSD = \frac{1}{n}\sum_{i=1}^{n} (y_i - S)^2 \tag{2.5}$$

where y_i is the value of the-closer-to-nominal-the-better quality characteristic, and S is the target value.

Regardless of the category of the quality characteristic, a greater S/N ratio corresponds to better quality characteristic. Furthermore, a statistical analysis of variance (ANOVA) is performed to see which process parameters are statistically significant. It uses the sum of squares to partition the overall variation from the average S/N ratio into the contribution by each of the parameters and the error.

The overall average S/N ratio is expressed as

$$\overline{S/N} = \frac{1}{k}\sum_{i=1}^{k}(S/N)_i \tag{2.6}$$

where k is the number of tests in the orthogonal array, $(S/N)_i$ is the S/N ratio of the i^{th} test. The sum of the squares due to the variation from the overall average S/N ratio is

$$SS = \sum_{i=1}^{k}((S/N)_i - \overline{S/N})^2 \tag{2.7}$$

the sum of the squares due to the variation from the average S/N ratio for the i^{th} factor is

$$SS_i = \sum_{j=1}^{l} T_j \times (\overline{(S/N)}_{ij} - \overline{S/N})^2 \tag{2.8}$$

where l is the number of the factor levels , T_j is the number of the tests of the i^{th} factor at the j^{th} level, $\overline{(S/N)}_{ij}$ is the average S/N ratio of the quality characteristic for the i^{th} factor at the j^{th} level. The percentage contribution of i^{th} factor is given by

$$P_i(\%) = \frac{SS_i}{SS} \times 100 \tag{2.9}$$

With the S/N and ANOVA analyses, the optimal combination of the process parameters can be determined.

2.5.3 Application in Manufacturing

The Taguchi method is now widely used in all areas of manufacturing to improve the quality of products and processes as shown in Table 2.4.

In this research, the Taguchi method will be used to optimize the forming parameters while more than one quality characteristics are simultaneously considered for the same metal forming process. A new multi-objective optimization approach will be proposed by integrating the classical mathematical optimization method with the Taguchi method.

Table 2.4: Application of Taguchi method in Manufacturing

Year	Researchers	Main contributions
1995	Park et al.	Investigated the effect of material and process variables on the formability using the Taguchi method in metal forming area.
1999	Ko et al.	Implemented the artificial neural network using the Taguchi method in the multi-stage metal forming process considering workability limited by ductile fracture.
2000	Tarng et al.	Used fuzzy logic in the Taguchi method to optimize the submerged arc welding process, transformed the optimization of multiple performance characteristics into optimization of a single performance index through the fuzzy decision-making logic.
2001	Antony	Used the Taguchi's quality loss function to identify the significant factor/interaction effects and determine the optimal condition for the manufacturing process with multiple quality characteristics by assigning different relative weights to the different quality characteristics prior to optimization.
2002	Duan & Sheppard	Studied the influence of rolling parameters on the subgrain size during the hot rolling of aluminium alloys by the combination of finite element methods with the Taguchi method.
2003	Dhavlikar et al.	Presented a successful application of combined Taguchi and dual response methodology to determine robust condition for minimization of out of roundness error of work pieces for centerless grinding operation.

2.6 Discussion

Based on the findings of reviewing the literatures, the reliability analysis of metal forming process can be carried out based on forming limit diagram. The forming limit diagram which is usually determined by experimental tests can also be predicted analytically and/or numerically. The Taguchi method as the experimental design method is a proper tool for optimizing the process by identifying the most significant parameters and the optimal combination of design parameters. It can be applied to improve the reliability of metal forming process and robust design of the process.

The following chapters detail how these methodologies have been implemented in metal forming process and how the research objectives of this study have been achieved.

Chapter 3

Reliability Based on Forming Limit Diagram

The purposes of this study are to (1) establish a reliability analysis model by combining traditional reliability theory with the Forming Limit Diagram (FLD), and (2) predict the failure probability of a given tube hydroforming process at the initial design stage. A simple tube hydroforming process of free bulging will be analyzed to illustrate the method. As for the tube hydroforming limiting strains, due to a shortage of experimental data, the conventional sheet forming limit data is usually applied (Xing et al., 2001; Nefussi et al., 2002).

3.1 Notional Strain and Notional Limit Strain

Before introducing the reliability analysis method based on the FLD, we present two terms, namely notional strain and notional limit strain. We assume there is a forming process and a particular strain point is plotted on the FLD (point "1" in Figure 3.1), and the forming limit band for the material is as shown in Figure 3.1. A proportional strain path is assumed through this strain point. Because of inherent process variability, the strain at a given location of a formed part will vary from part to part during production, thus the notional strain of that point describes the median of this strain distribution.

The proportional strain path (also shown on the right of Figure 3.1) has three intersection points with the forming limit band, i.e., points "2", "3" and "4". We define the distance from the origin in the FLD to the point "1" as the notional strain of the strain point "1". We also define the distance from the origin to any point between the point "3" and "4" in the strain path as the notional limit strain of the material, the distance from origin point to point "2" will be the mean value of the notional limit strain, and the distance from original point to point "3" and point "4" will be the maximum and minimum values of the notional limit strain along the given strain path.

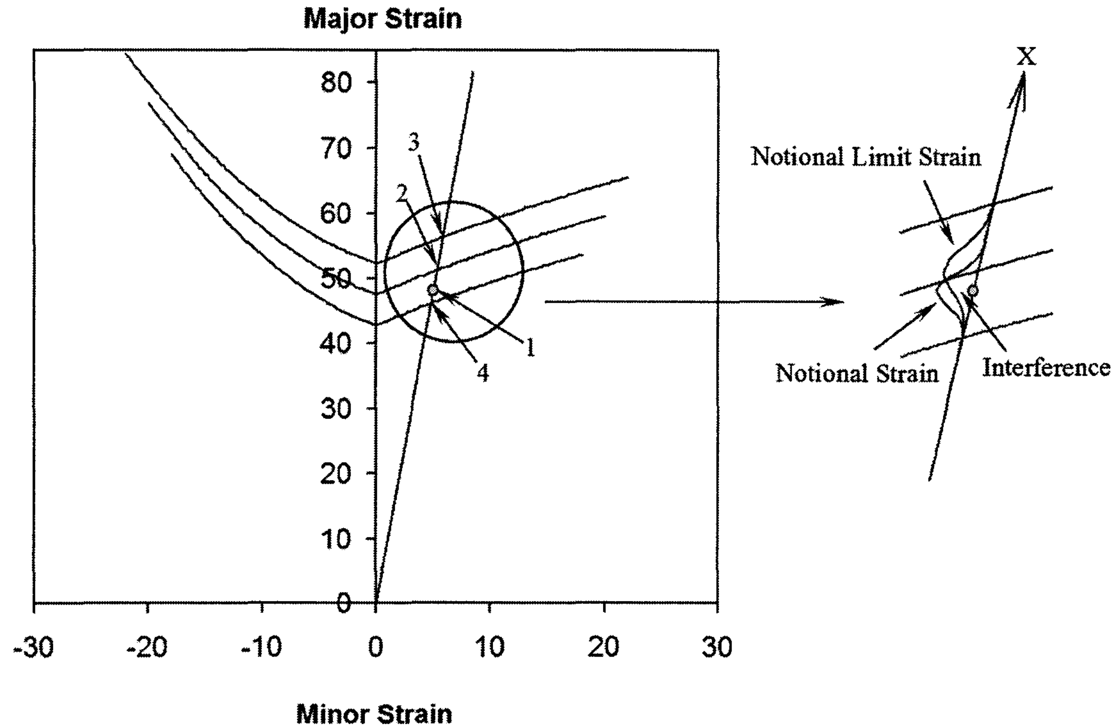

Figure 3.1: Concept of notional strain and notional limit strain

3.2 Reliability Analysis Based on FLD

In our research, we assume that both the notional strain of the tubular blank and the notional limit strain of the material obey the normal distribution. The reliability of the hydroformed tube based on the FLD will then be (Kapur & Lamberson, 1977)

$$R(Z_R) = \frac{1}{\sqrt{2\pi}} \int_{-\infty}^{Z_R} \exp(-\frac{t^2}{2})dt \tag{3.1}$$

where Z_R is the reliability coefficient

$$Z_R = \frac{\mu_{le} - \mu_{ne}}{\sqrt{\sigma_{le}^2 + \sigma_{ne}^2}} \tag{3.2}$$

and μ_{ne} & σ_{ne} and μ_{le} & σ_{le} are the mean values and the standard deviations of notional strain and notional limit strain, respectively.

Traditional reliability theory uses the stress-strength interference model to predict reliability (Rao, 1992). Here we present the notional strain-notional limit strain interference model as shown in Figure 3.2. Notional strain is a function of process variability while notional limit strain represents the distribution of material strength. The overlap area in Figure 3.2 represents the necking failure probability of the forming process. In this case the 'x' axis of the interference model represents the proportional strain path shown in Figure 3.1.

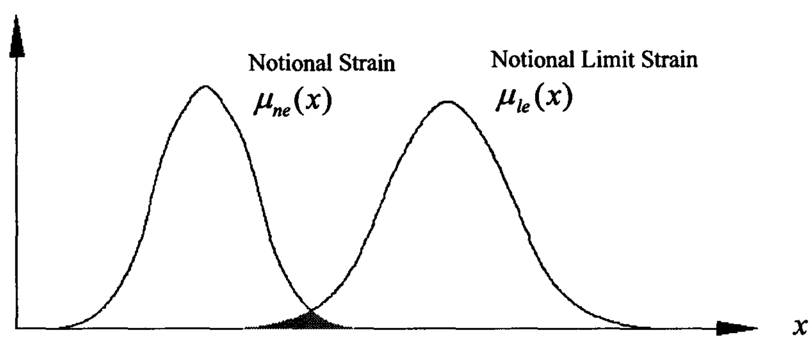

Figure 3.2: Notional strain – notional limit strain interference model

3.2.1 Distribution of Notional Limit Strain

We have assumed the notional limit strain as a random variable following the normal distribution, according to the definition of notional limit strain in Section 3.1. The width of the forming limit band is typically 7% to 10% true strain, depending on the experimental results for a particular material (Janssens et al., 2001). Assuming this band represents plus or minus three standard deviations of the distribution, the standard derivation of the notional limit strain can be obtained approximately as:

$$\sigma_{le} = p\mu_{le} / 3 \tag{3.3}$$

where p is the percent of the true strain of the half width of forming limit band.

3.2.2 Distribution of Notional Strain

The strain distribution of one forming process is dependent on many parameters. We can express the notional strain ε as

$$\varepsilon = f(x_1, x_2, \cdots, x_n) \tag{3.4}$$

where x_i ($i=1, \ldots, n$) are the process parameters that affect the notional strain. Assuming these parameters also obey the normal distribution, then the mean value and the variance of the notional strain can be obtained approximately as (Li et al., 1999)

$$\mu_{ne} = f_{ne}(\mu_{x_1}, \mu_{x_2}, \cdots, \mu_{x_n}) \tag{3.5}$$

$$\sigma_{ne}^2 = \sum_{i=1}^{n} \left[\left. \frac{\partial f_{ne}}{\partial x_i} \right|_{x_i = \bar{x}_i} \right]^2 \sigma_{x_i}^2 \tag{3.6}$$

where $\mu_{x_i}, \sigma_{x_i}^2$ ($i = 1, \cdots, n$) are the mean value and the variance of x_i and $\bar{x}_i$ is the average value of x_i.

3.3 Application

3.3.1 FEM Simulation

Simulations have been performed using the explicit FEM code H3DMAP (Sauvé, 1999). The finite element computer code H3DMAP version 6.2 is a general three-dimensional structural analysis package that has been developed at Ontario Hydro to solve a wide variety of problems encountered by the corporation. The current version of the code has been successfully applied to solve the nonlinear problems including the manufacturing processes involving metal forming. The code has been extensively benchmarked and verified using a number of cases for which either experimental results or classical solutions are available. The salient feature of H3DMAP is the nonlinear explicit transient dynamic/steady state option for the finite deformation of solids. A robust 3-D contact algorithm is included to permit accurate modeling of bodies undergoing sliding at material interfaces. It is based on the master-slave sliding concept and provides significant code capabilities in the area of crashworthiness and manufacturing area.

Figure 3.3 shows the hydroforming process of free bulging of a straight tube with simultaneously applied internal pressure and axial force. Due to the axisymmetry of the deformed tube, by considering that the computer CPU is not an issue for this application, one-eight of the tubular blank and the tooling were modeled. The tooling was modeled as a rigid body. The tube material is assumed to be isotropic elastic-plastic obeying the

Ludwik-Hollomon hardening relationship, $\sigma = k\varepsilon^n$. Table 3.1 shows the material properties of the tubular blank.

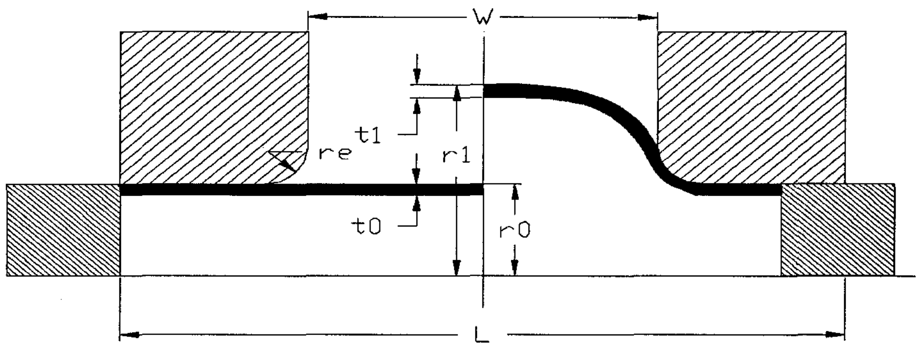

Figure 3.3: Schematic view of free bulging hydroforming

Table 3.1: Mechanical properties used in the simulation

ρ, kg/m3	E, GPa	K, MPa	n	σ_y, MPa	σ_u, MPa	ν
7850	205	537	0.227	240	350	0.3

During simulation of the forming process, the loading path strategy described by Manabe and Amino (2002) was used. In this strategy, the internal pressure and the axial load are applied according to the following equation of nominal stress ratio *m* (Yoshitomi, 1987)

$$m = \frac{\sigma_\phi}{\sigma_\theta} = \frac{(F - P_f A_0)/A}{P_f R_i / t_0} \tag{3.7}$$

where σ_θ is the circumferential stress, σ_ϕ is the axial stress, P_f is the forming internal pressure, F is the axial load, R_i is the inner radius of the tube, A_0 is the inner surface area of the tube, A is the cross-sectional area of the tube, and t_0 is the thickness of the tube.

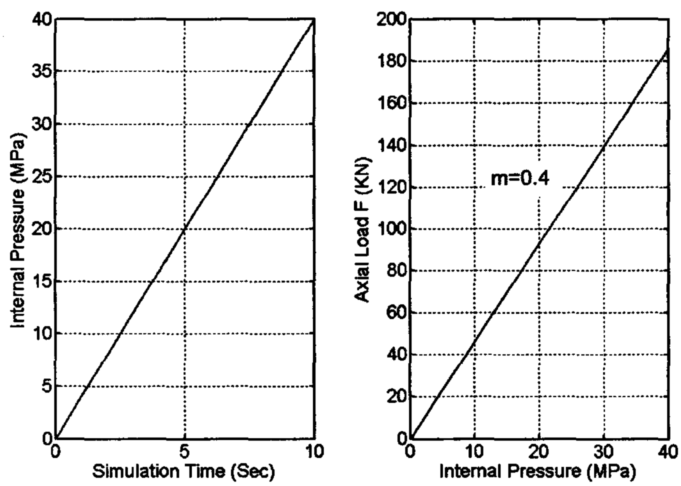

Figure 3.4: Loading path used in the simulation

Figure 3.4 shows the loading path used in the simulation. Internal pressure is applied linearly with the simulation time and axial load is applied in proportion to the internal pressure.

Different mesh sizes for the tubular blank are investigated for its effects on the simulation results. Table 3.2 shows the maximum effective plastic strains of the deformed tube corresponding to the different mesh sizes. In model No.1, 3 layers (3 elements) through the thickness with 1800 elements on each layer are defined. In model No.2, 5 layers (5 elements) through the thickness with 1800 elements on each layer are defined. In model No.3, 5 layers (5 elements) through the thickness with 2400 elements on each layer are defined. It can be seen from Table 3.2 that the variation of the maximum effective strain is quite small, when the mesh size of tube is over 5400 elements. By taking both the mesh quality and computation effectiveness into account, 5 elements through the thickness with the total of 9000 elements are chosen as the mesh size for the tubular blank.

Table 3.2: Maximum effective plastic strain with different mesh sizes

Model	Mesh Size	Maximum effective strain
1	3 elements through the thickness total 5400 elements	0.578
2	5 elements through the thickness total 9000 elements	0.571
3	5 elements through the thickness total 12000 elements	0.568

3.3.2 Effects of Different Parameters on Hydroformability

Generally, there are three groups of parameters that affect the formability of the tube hydroforming process: (a) geometrical parameters: length, radius, thickness, etc.; (b) material parameters: hardening coefficient, strain hardening exponent, etc.; and (c) process parameters: internal pressure, axial load, friction coefficient, etc. (Koç & Altan, 2002).

The parameters of interest in our study are the geometrical parameters including length of the tube (defined by L_0/r_0), thickness (defined by t_0/r_0), die entry radius (defined by r_e/r_0) and bulge width (defined by W/r_0), the material parameter including hardening coefficient (defined by K/σ_y) and hardening exponent (n), and the process parameters including internal pressure (defined by P_f/σ_y), nominal stress ratio (m) and friction coefficient (μ).

In the simulation, each parameter is varied over a range of ±10% from the nominal value, while keeping the rest of the parameters constant, in order to investigate the effect of each parameter on the process. Table 3.3 presents the different parameter values used in the FEM simulation with the outer radius of tube $r_0 = 30$ mm and the yield stress $\sigma_y = 240$ MPa. The nominal values are those in the center column. In total thirty-seven combinations of the forming parameters are evaluated by the finite element simulation (See Table 3.4). The maximum effective strain is found to be in the center of the expansion region (all the elements along the circumferential direction have the same strain value), element 3630 is used as the representative critical element (See Figure 3.5). When the different parameter values in Table 3.3 are used in the simulations, the strain distribution of the critical element 3630 is found (Figure 3.6). The first row in Table 3.4 corresponds to the parameters combination with the nominal values. The resulting notional strains of the critical element (element 3630) are listed in the last column in Table 3.4. Figure 3.7 illustrates the effect of the different parameters on the bulge height. From Figure 3.7, it can be seen that the length of tube, the bulge width, the internal pressure and the hardening coefficient have the greatest effect on the bulge height, with the other parameters having relatively smaller effects.

Table 3.3: The forming conditions used in the simulation

Geometrical parameters					
Length of tube L_0 (mm)	180	190	200	210	220
Thickness of tube t_0 (mm)	1.35	1.425	1.5	1.575	1.65
Die entry radius r_e (mm)	9	9.5	10	10.5	11
Bulge width W (mm)	90	95	100	105	110
Material parameters					
Hardening coefficient K (MPa)	483.3	510.15	537	563.85	590.7
Hardening exponent n	0.2043	0.2157	0.227	0.2384	0.2497
Process parameters					
Internal pressure P_f (MPa)	36	38	40	42	44
Nominal stress ratio m	0.36	0.38	0.4	0.42	0.44
Friction coefficient μ (Coulomb)	0.054	0.057	0.06	0.063	0.066

Table 3.4: Layout of simulation and the resulting critical notional strain

Run No.	L_0/r_0	t_0/r_0	r_e/r_0	W/r_0	n	P_f/σ_y	m	μ	K/σ_y	Notional strain (%)
1	6.667	0.05	0.333	3.333	0.227	0.167	0.4	0.06	2.238	48.2538
2	6.000	0.05	0.333	3.333	0.227	0.167	0.4	0.06	2.238	54.9619
3	6.333	0.05	0.333	3.333	0.227	0.167	0.4	0.06	2.238	52.7630
4	7.000	0.05	0.333	3.333	0.227	0.167	0.4	0.06	2.238	47.4324
5	7.333	0.05	0.333	3.333	0.227	0.167	0.4	0.06	2.238	40.4330
6	6.667	0.045	0.333	3.333	0.227	0.167	0.4	0.06	2.238	47.4798
7	6.667	0.0475	0.333	3.333	0.227	0.167	0.4	0.06	2.238	47.3308
8	6.667	0.0525	0.333	3.333	0.227	0.167	0.4	0.06	2.238	46.6007
9	6.667	0.055	0.333	3.333	0.227	0.167	0.4	0.06	2.238	44.9898
10	6.667	0.05	0.300	3.333	0.227	0.167	0.4	0.06	2.238	44.7365
11	6.667	0.05	0.317	3.333	0.227	0.167	0.4	0.06	2.238	45.4263
12	6.667	0.05	0.350	3.333	0.227	0.167	0.4	0.06	2.238	46.6139
13	6.667	0.05	0.367	3.333	0.227	0.167	0.4	0.06	2.238	47.2692
14	6.667	0.05	0.333	3.000	0.227	0.167	0.4	0.06	2.238	41.1357
15	6.667	0.05	0.333	3.167	0.227	0.167	0.4	0.06	2.238	42.7205
16	6.667	0.05	0.333	3.500	0.227	0.167	0.4	0.06	2.238	50.6125
17	6.667	0.05	0.333	3.667	0.227	0.167	0.4	0.06	2.238	54.8410
18	6.667	0.05	0.333	3.333	0.2043	0.167	0.4	0.06	2.238	45.2590
19	6.667	0.05	0.333	3.333	0.2157	0.167	0.4	0.06	2.238	46.3784
20	6.667	0.05	0.333	3.333	0.2384	0.167	0.4	0.06	2.238	47.7661
21	6.667	0.05	0.333	3.333	0.2497	0.167	0.4	0.06	2.238	48.1477
22	6.667	0.05	0.333	3.333	0.227	0.150	0.4	0.06	2.238	37.5016
23	6.667	0.05	0.333	3.333	0.227	0.158	0.4	0.06	2.238	41.4760
24	6.667	0.05	0.333	3.333	0.227	0.175	0.4	0.06	2.238	49.9498
25	6.667	0.05	0.333	3.333	0.227	0.183	0.4	0.06	2.238	54.7431
26	6.667	0.05	0.333	3.333	0.227	0.167	0.36	0.06	2.238	46.5237
27	6.667	0.05	0.333	3.333	0.227	0.167	0.38	0.06	2.238	46.8054
28	6.667	0.05	0.333	3.333	0.227	0.167	0.42	0.06	2.238	45.7625
29	6.667	0.05	0.333	3.333	0.227	0.167	0.44	0.06	2.238	46.0603
30	6.667	0.05	0.333	3.333	0.227	0.167	0.4	0.054	2.238	47.0816
31	6.667	0.05	0.333	3.333	0.227	0.167	0.4	0.057	2.238	47.3291
32	6.667	0.05	0.333	3.333	0.227	0.167	0.4	0.063	2.238	47.3565
33	6.667	0.05	0.333	3.333	0.227	0.167	0.4	0.066	2.238	47.2305
34	6.667	0.05	0.33	3.33	0.227	0.167	0.4	0.06	2.014	52.6197
35	6.667	0.05	0.33	3.33	0.227	0.167	0.4	0.06	2.126	50.6250
36	6.667	0.05	0.33	3.33	0.227	0.167	0.4	0.06	2.349	45.0626
37	6.667	0.05	0.33	3.33	0.227	0.167	0.4	0.06	2.461	42.2415

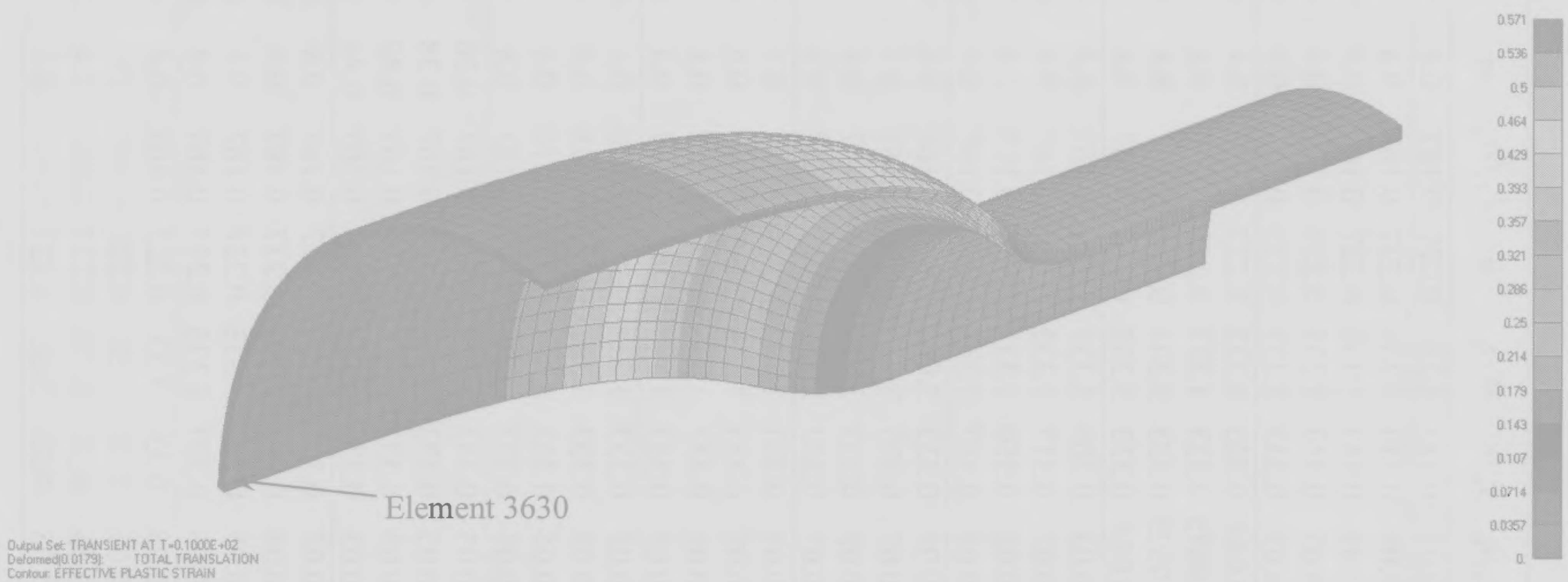

Figure 3.5: Effective strain contour of hydroformed tube

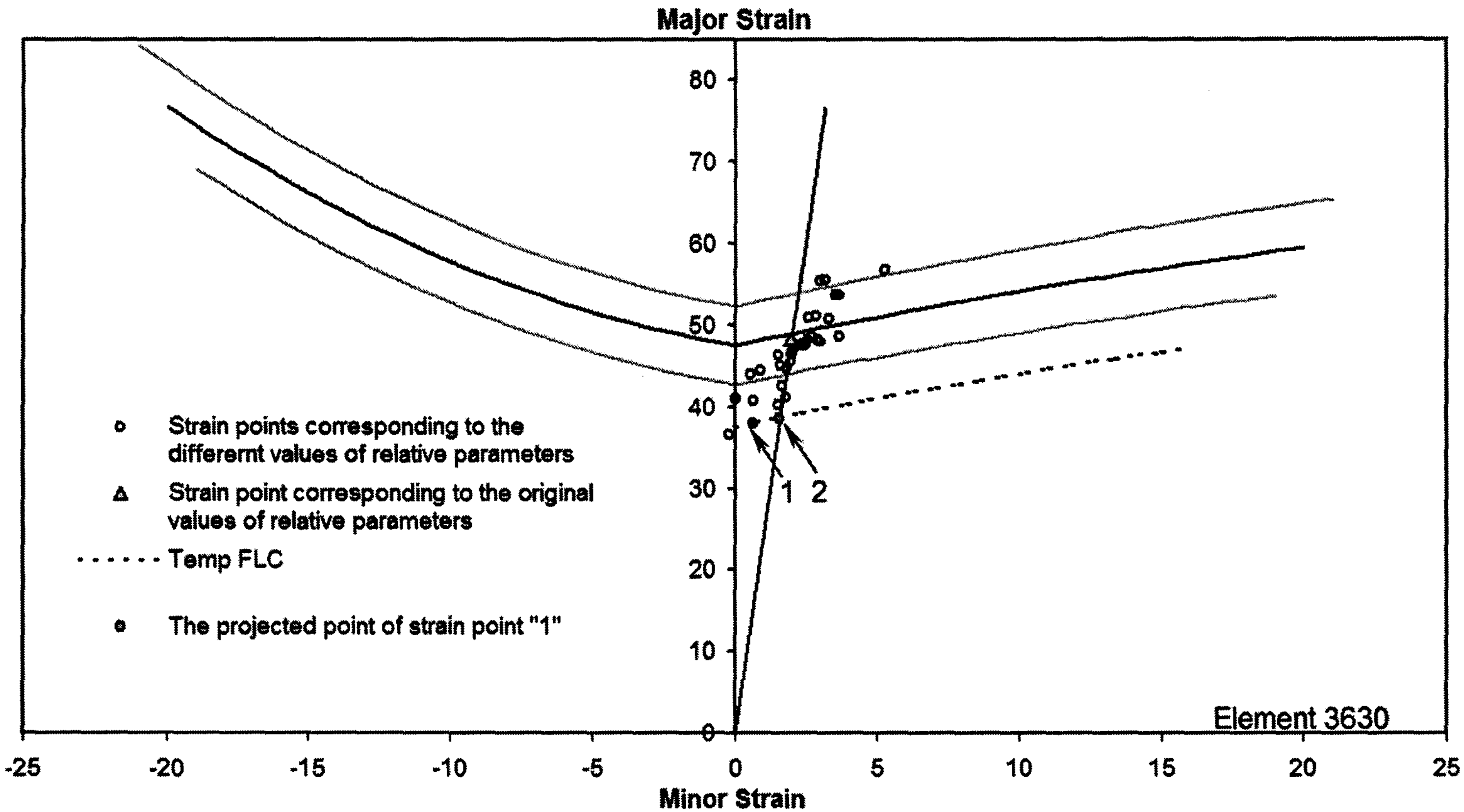

Figure 3.6: Strain distribution of element 3630

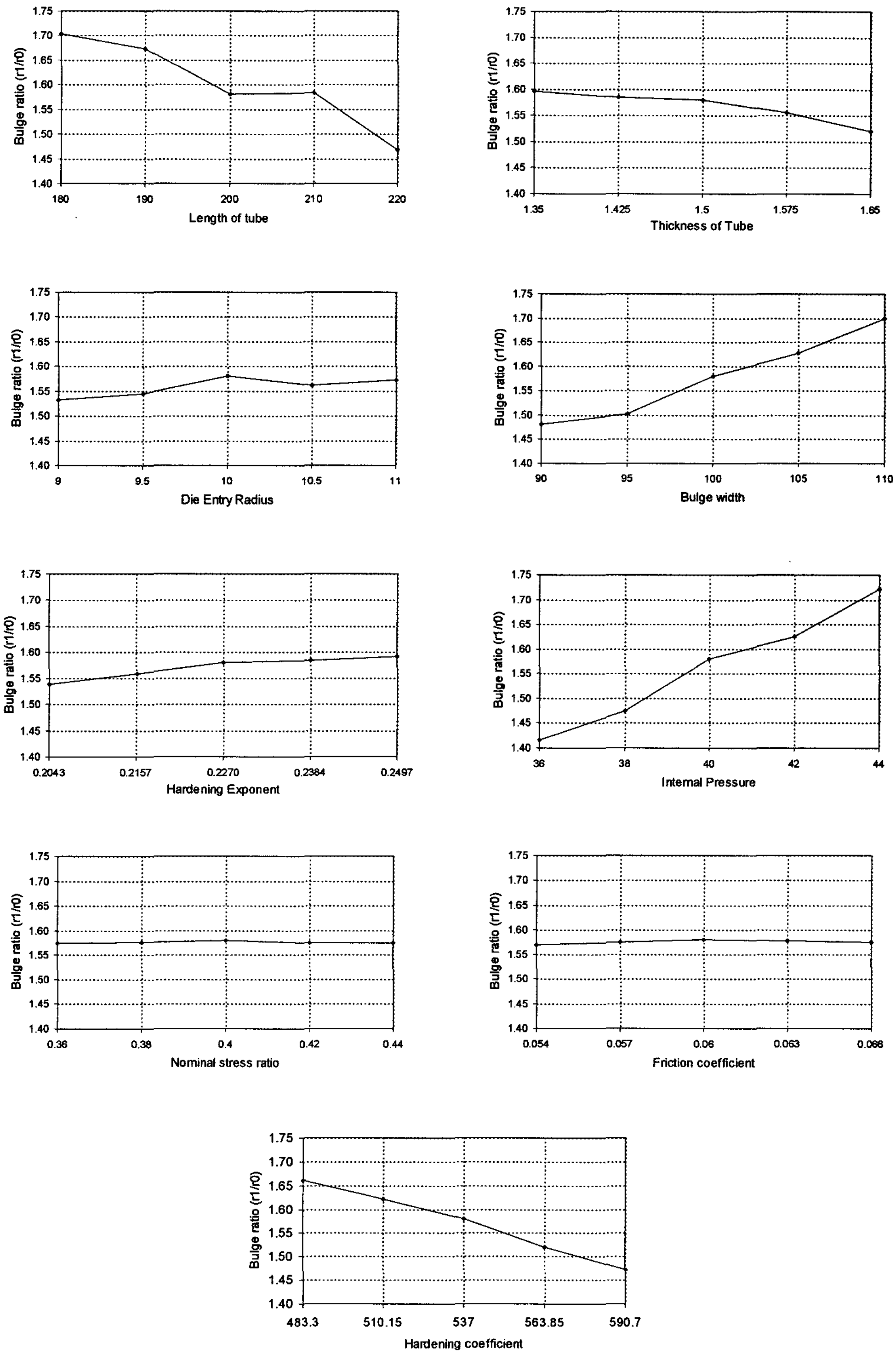

Figure 3.7: Effect of the different parameters on the bulge ratio

3.3.3 Reliability of Tube Hydroforming Process

The principle strains of all the elements of the hydroformed tube from the FEM simulation using the nominal parameter values (Run #1, Table 3.4) are shown in Figure 3.8. Because of rotational symmetry of this process, each strain point in Figure 3.8 actually represents a series of similar strain points of the elements in the same hoop. What appears to be five strain 'paths' in the FLD is the result of using five elements in the thickness direction in our FEM model.

The strain path corresponding to the distribution axis in Figure 3.2 was taken through the strain point of element 3630 for the nominal parameter value case. Using a polynomial representation of the forming limit curve, the mean value of notional limit strain along this strain path is μ_{le} = 49.3337. Assuming the width of the forming limit band as 10% of the mean, then p in Eq. (3.3) is 0.05, so the standard derivation of notional limit strain is σ_{le} = 0.8222.

All the strain points of element 3630 corresponding to the various values of the process parameters are shown in Figure 3.6. (In every simulation case, the critical strain occurred in element 3630.) Taking the strain path through the nominal case strain point as a local coordinate axis, the strain points for all cases were projected to this axis. The projections were made parallel to the FLC, using the offset curve "Temp FLC". Points along this curve have the same probability of necking failure. For instance, the point "2" in Figure 3.6 is the projected point of the strain point "1". Applying this method results in all strain points being projected onto the strain path, and consequently a normal distribution may be fitted to the strain data.

The mean value of notional strain of element 3630 is obtained directly. Equation (3.6) is used to evaluate the standard derivation of notional strain as a function of each parameter. Figure 3.9 shows the relationship of the strain of element 3630 to each forming parameter. This data is used to fit a second-order polynomial, to represent the function f_{ne} in Eq. (3.6). Table 3.5 shows the mean value and standard deviation of each forming parameter and the partial derivative of notional strain with respect to each parameter. After calculating, we get the mean value of notional strain of element 3630 μ_{ne} = 48.2538 and the standard deviation σ_{ne} = 4.7562.

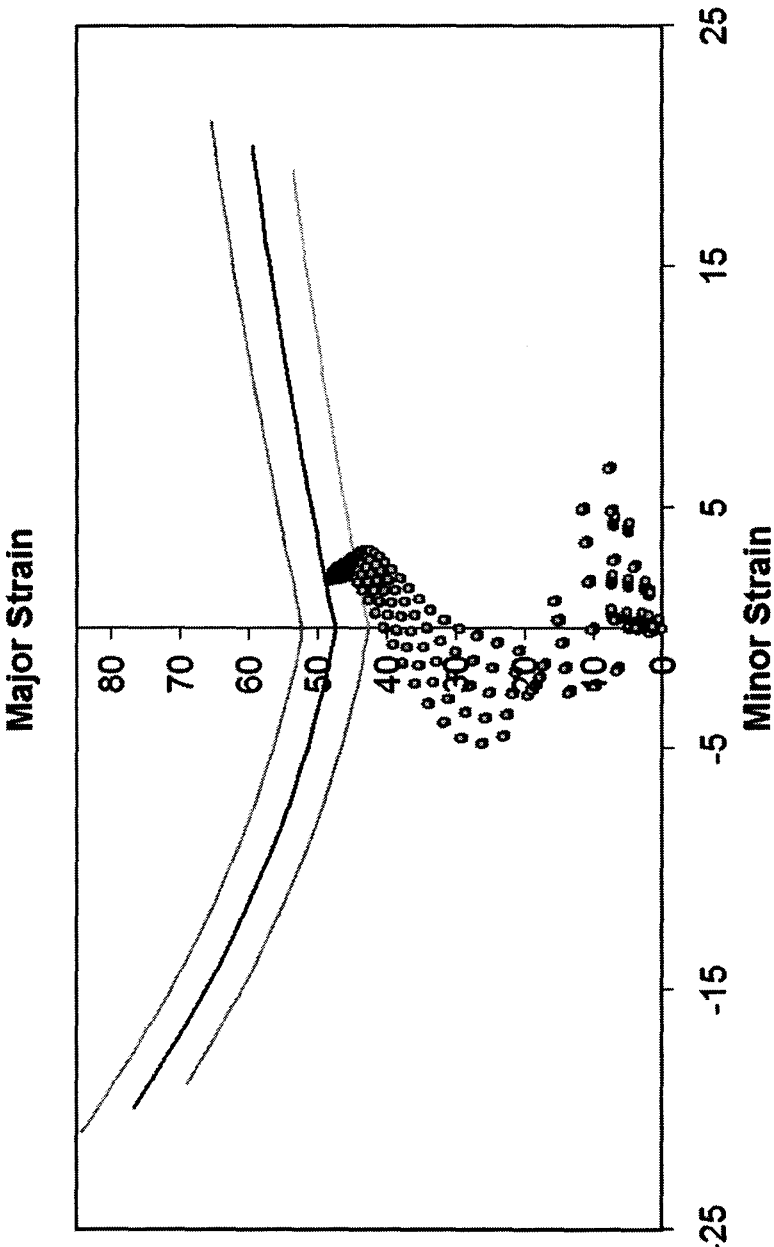

Figure 3.8: Strain distribution of hydroformed tube

Table 3.5: Partial derivative of notional strain with respect to each forming parameter

X_i	L_0	t_0	r_e	W	n	P_f	m	μ	K
Mean Value	200	1.5	10	100	0.227	40	0.4	0.06	537
Standard derivation	6.6667	0.05	0.3333	3.3333	0.0076	1.3333	0.0133	0.0020	17.9
$\frac{\partial f_{ne}}{\partial x_i}$	-0.3439	-7.6135	1.2506	0.7061	63.1286	2.1478	0.1114	10.8400	-0.0980

From Eq. (3.1), we can obtain the reliability of the element 3630 R=58.85%. Since the strain of element 3630 is the critical strain of the hydroformed tube, then the reliability of this hydroforming process is 58.85%, i.e., the necking failure probability of the process is 41.15%.

If a specific reliability is required for this process, the designer can alter the process and product design at the initial design stage and use this approach to predict the resulting reliability. Indeed, data generated during the analysis can be plotted as in Figure 3.9 to present sensitivity information that would aid in selecting the parameters to change, and the directions of change.

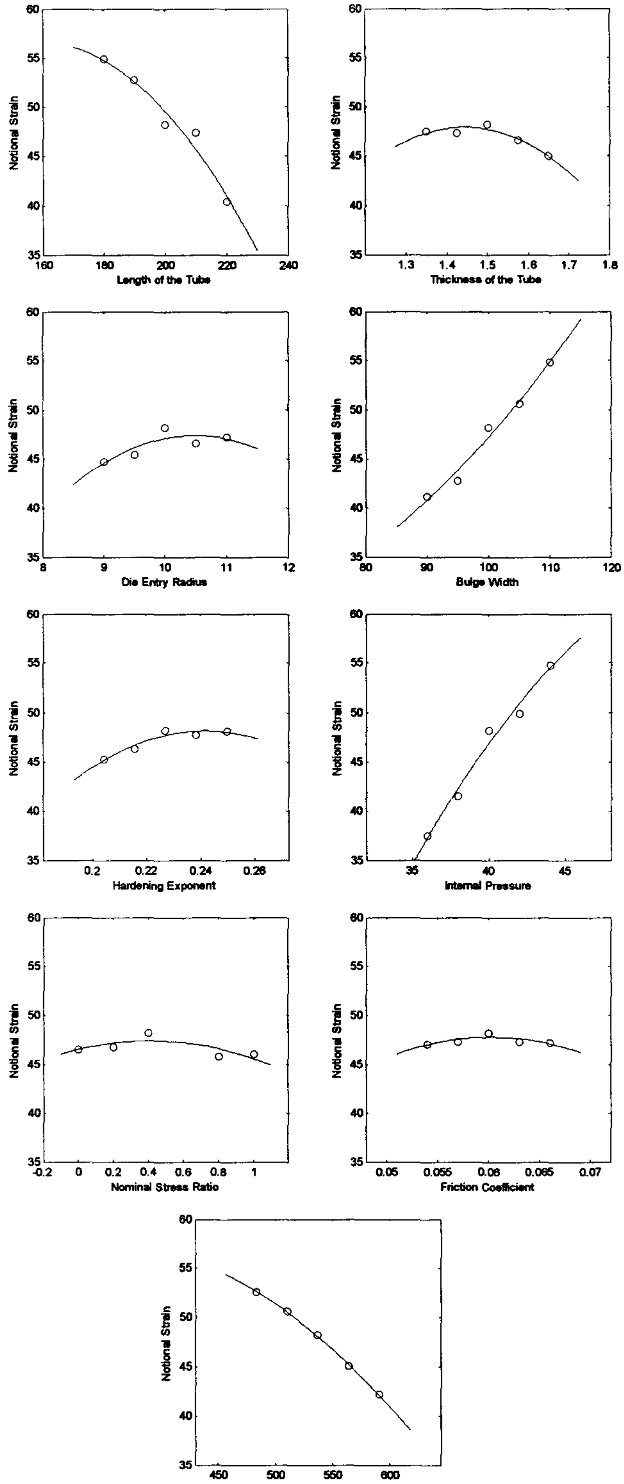

Figure 3.9: Relationship between notional strain and the forming parameters

3.4 Discussion

It is a relative new area in the metal forming field by using forming limit diagram to predict the reliability of a metal forming process. As mentioned in literature review, Kleiber et al. (2002) applied the structural reliability analysis method to evaluate the reliability of a sheet metal forming operation using the forming limit diagram as the criteria of material failure. Two methodology issues of this paper have been summarized in Section 2.3, one is regarding the orientation of the scatters of strain points, and another is regarding the marginal zone of forming limit. In our study, improvements have been made in both aspects. First, the notional strain and notional limit strain are defined as the distance from the origin to certain strain point along a particular strain path. Such kind of definition is conformable with the statistical experimental observation, in which the strain points tend to spread more along the particular strain path than perpendicular to the estimated curve (Figure 2.6, Van Minh et al., 1974). Second, the forming limit band offsetting the forming limit curve, with the same upper and lower percentage is used to present the uncertainty of the strain limits. Such kind of presentation reflects the actual practice better than the marginal zone below the FLC, because the FLC constructed from the experimental results usually represents the average strain limit of a material (Janssens et al., 2001).

The methodology presented in this study will be still applicable if a stress space FLD is chosen as the failure criteria for metal forming process. The notional strain and notional limit strain are assumed to follow the normal distribution in this study since it is simple and easy to use. However, other formats of probability distributions such as triangle, lognormal and weibull can also be chosen to describe the strains if the experimental statistical data are available, but the methodology will be identical.

The approach described here is meant to be applied at the initial product design stage. As such, it allows process validation to be performed before any time or cost has been spent building tooling. In addition to predicting process reliability, this approach also provides sensitivity information that can be used to modify process designs to improve the reliability.

Chapter 4

Prediction of FLD using FEM

As introduced in Chapter 2 and 3, the Forming Limit Diagram (FLD) of a material is generally determined by experimental measurements. However, the experimental determination of a FLD is a time-consuming procedure and a large scatter of forming limit is usually obtained in the experimental measurements (Wu et al., 2003). As a result, various numerical methods have been used to determine the forming limit diagram. Most numerical methods for FLD studies have been based on the so-called M-K approach developed by Marciniak and Kuczynski (1967). By using the M-K approach, a basic assumption has to be made that an initial imperfection exists in the form of a groove. Many researchers have shown that the initial thickness inhomogeneity in the M-K approach has a significant influence on the predicted results (Graf and Hosford, 1993, 1994; Tang and Tai, 2000). A great of number of efforts have been made to predict the FLD by introducing different types of initial inhomogeneities in the numerical simulation such as assigning texture components randomly to the sheet (Wu et al., 2004) and postulating a heterogeneous distribution of mechanical properties through the starting material (Duan et al., 2005). On the other hand, the studies using FEM without implementing a pre-defined imperfection have increased. Takuda et al. (2000) predicted the forming limit strains of sheet metals by combining the finite element simulation with ductile fracture criteria. The in-plane biaxial stretching test was simulated and the limit strains were determined by substituting the values of stress and strain obtained from the finite element simulation into a ductile fracture criteria. Ozturk and Lee (2004) did similar research to analyze forming limits by the combination of finite element simulation with the ductile fracture criteria, but they used the out-of-plane formability test for the simulation.

The purpose of this study is to develop a practical approach to predict the forming limit diagram of sheet metals by finite element simulation. The basic idea is to simulate the real experimental test for determination of FLD. There are several types of tests used to determine the FLD such as uniaxial tensile test, hydraulic bulge test, punch stretching test, Keeler test, Hecker test, Nakazima test, Marciniak test and Hasek test (D. Banabic, 2000). The Nakazima test (also called the dome test) is chosen for simulation in this study to predict the FLD. Nakazima test is carried out with a hemispherical punch and a circular die. By varying the width of the specimen and the lubricant, both side of the FLD curve can be predicted. The assumption behind using the dome test is that the compressive stresses normal to the sheet, frictional shear stresses and sheet curvature existing in the test can be regarded as kind of "imperfection". So neither pre-defined geometrical imperfections nor material imperfections will be applied in the simulation model. The forming limit strains will be obtained based on the proposed localized necking criteria.

4.1 Criteria for Localized Necking

Jain and Allin (1994) experimentally analyzed the variability of FLDs by conducting hemispherical punch stretching tests and Marciniak punch stretching tests. They classified the grids measured in the vicinity of the neck into four categories (see Figure 4.1): (a) necked: grids which contained the entire neck width; (b) partially necked: grids which partially contained the neck width; (c) unnecked: grids just lying outside the neck and (d) safe: grids at least one grid length away from the neck. The major and minor strains of the unnecked grids were used to determine the FLD. Takuda et al. (2000) measured the strains at the nearest lattice close to the fracture site as the limit strains of necking in their experimental work. They found the plastic deformation almost ceases outside of the necking after the localized necking happens, while the deformation at the necking region progresses under plane-strain condition to fracture.

In this study, hemispherical punch stretching tests conducted by Jain and Allin (1994) are used as the referred experimental method for the simulation. The following criterion is proposed to evaluate the forming limit strains for localized necking:

The element just outside the necking area, where both its major principal strain (ε_1) and minor principal strain (ε_2) have no change after localized necking happens, will be chosen as the reference element for measurement of limit strains.

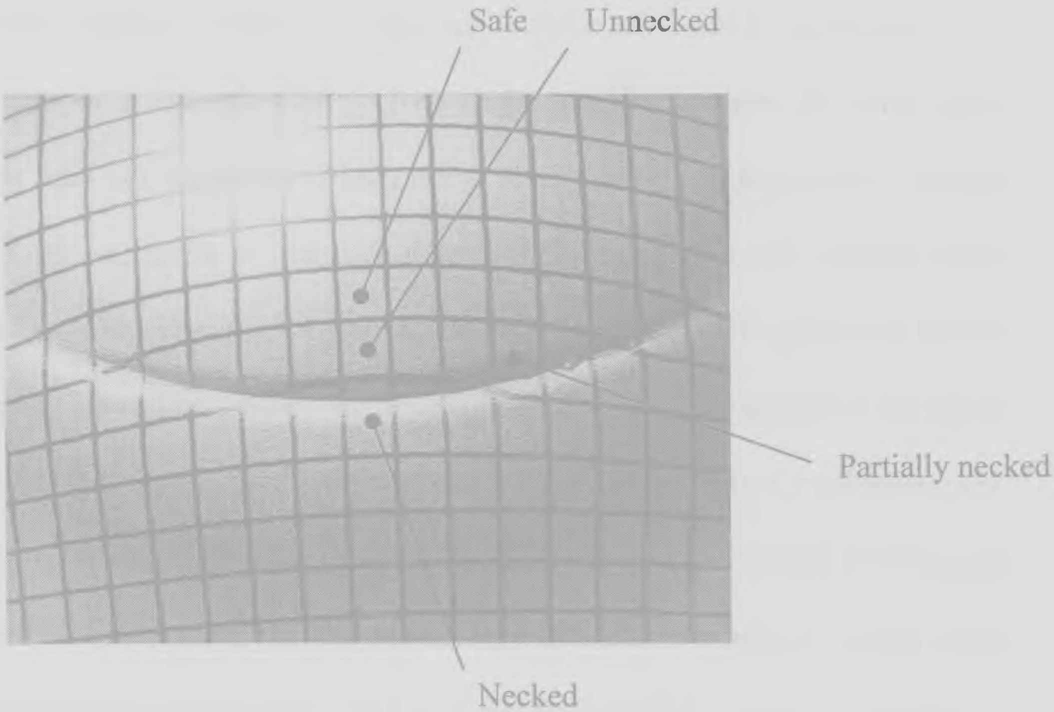

Figure 4.1: Classification scheme for grids in the neck region (Jain & Allin, 1994)

4.2 Finite Element Analysis

Figure 4.2 shows the model for dome test. It is made up of a sheet blank, punch, clamp die and lower die. The clamp die first moves down to clamp the sheet and then the punch moves upward to deform the sheet until failure. Material used in this study is an aluminium alloy AA5182-O with a thickness of 1.0 mm. Table 4.1 shows the material properties of AA 5182-O.

Table 4.1: Material properties of AA 5182-O (Numisheet 2005)

ρ (Kg/mm3)	E (GPa)	ν	σ_y (MPa)	n	K (MPa)	R_0	R_{45}	R_{90}
2700	70.6	0.341	127.7	0.257	459.1	0.957	0.934	1.058

In the simulation, the width of the sample is varied to achieve different forming states. The left sample in Figure 4.3 is used to determine the limit strain for uniaxial tension. The central sample in Figure 4.3 is used to determine the limit strain for plane strain tension. The right sample in Figure 4.3 is used to determine the limit strain for biaxial stretching. Three friction conditions between the punch and the sheet are used to study the effects of friction on the strain path. No lubricant between the punch and the sheet meaning a high friction condition is represented by the friction coefficient of 0.15 at punch sheet interface. A Teflon lubricant between the punch and the sheet meaning an intermediate friction condition is represented by the friction coefficient of 0.05. A polyurethane lubricant between the punch and the sheet meaning a low friction condition is represented by the friction coefficient of 0.01. Due to the geometrical symmetry of three types of sheet blanks (see Figure 4.3), one quarter of the sheet and tooling are modeled in order to improve the computational efficiency. The finite element simulations were performed by the commercial FE software LS-DYNA (LSTC, 2007). LSDYNA is an explicit dynamic FE solver which is very robust for solving dynamic, non-linear, large deformation events and processes including sheet metal forming problems. The significant features of LS-DYNA include fully automatic definition of contact areas, large library of constitutive models, large library of element types, special implementation for the automotive industry (seatbelt, airbag, dummy), and special features for metal forming applications (adaptive mesh). The main application areas of LS-DYNA are crashworthiness, metal forming, and drop testing. Other applications could be limit-load analysis or safety of buildings after an earthquake or after an impact.

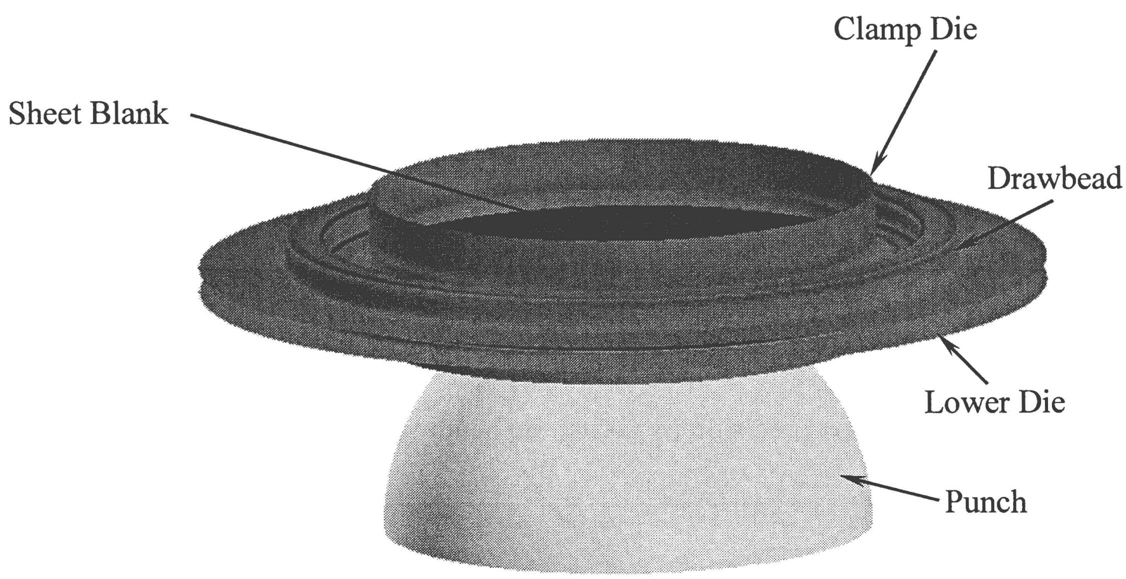

Figure 4.2: Simulation model of dome test

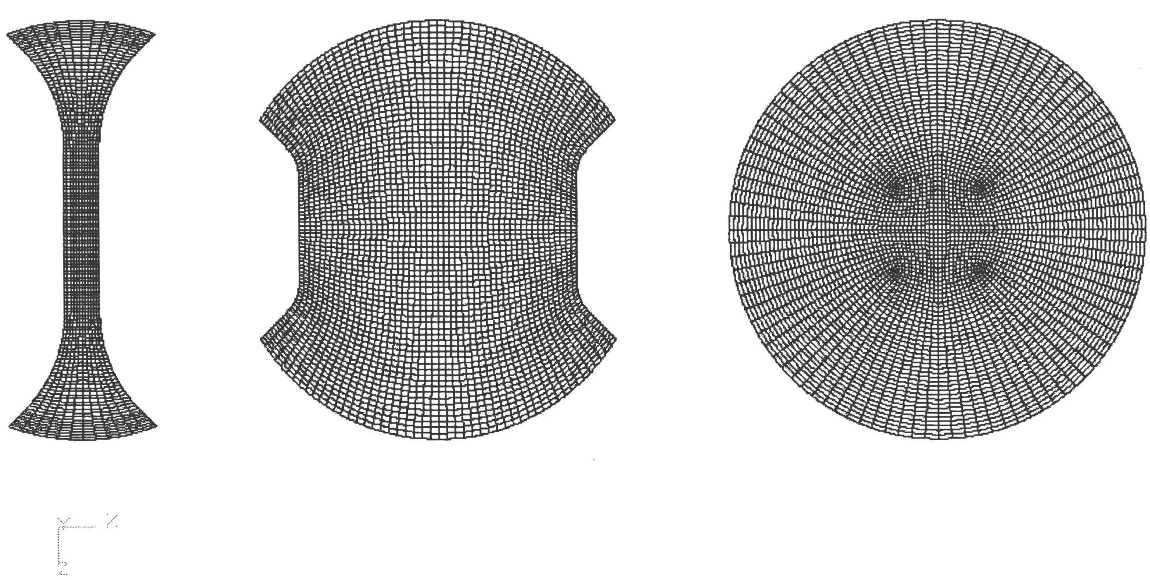

Figure 4.3: Geometry of samples used in the simulation

4.2.1 Element Type

Both the tooling and sheet blank are meshed using shell elements. The tooling including the punch, the clamp die and the lower die are defined as rigid bodies. The Belytschko-Tsay shell element is used for the sheet blank as recommended by Maker and Zhu (2000). The shell element thickness is specified through the thicknesses of its associated nodes. Seven integration points through the thickness were used to ensure enough calculation precision by taking the bending effect into account.

4.2.2 Mesh Size

The choice of mesh size is important to capture the strain distribution of the model accurately. The smaller mesh size can provide more accurate deformation solution but take longer computation time. In order to get a balance between solution accuracy and computational efficiency, the sensitivity analysis of mesh size is performed to define the appropriate mesh size. Four different mesh sizes for the sheet blank are examined to see the effect of mesh size on the results for the plane strain stretching test (see Figure 4.4). Table 4.2 shows the resultant maximum thickness reduction percentages correspond to the different mesh sizes. It can be seen that the maximum thickness reduction percentage changes very slightly when the element size is smaller than 1.65 mm. Although not shown here, similar mesh sensitivity analysis studies have been performed for the uniaxial tension and biaxial tensions tests. It seems that the mesh with an average element size of approximately 1.65 mm should be fine enough for the present study.

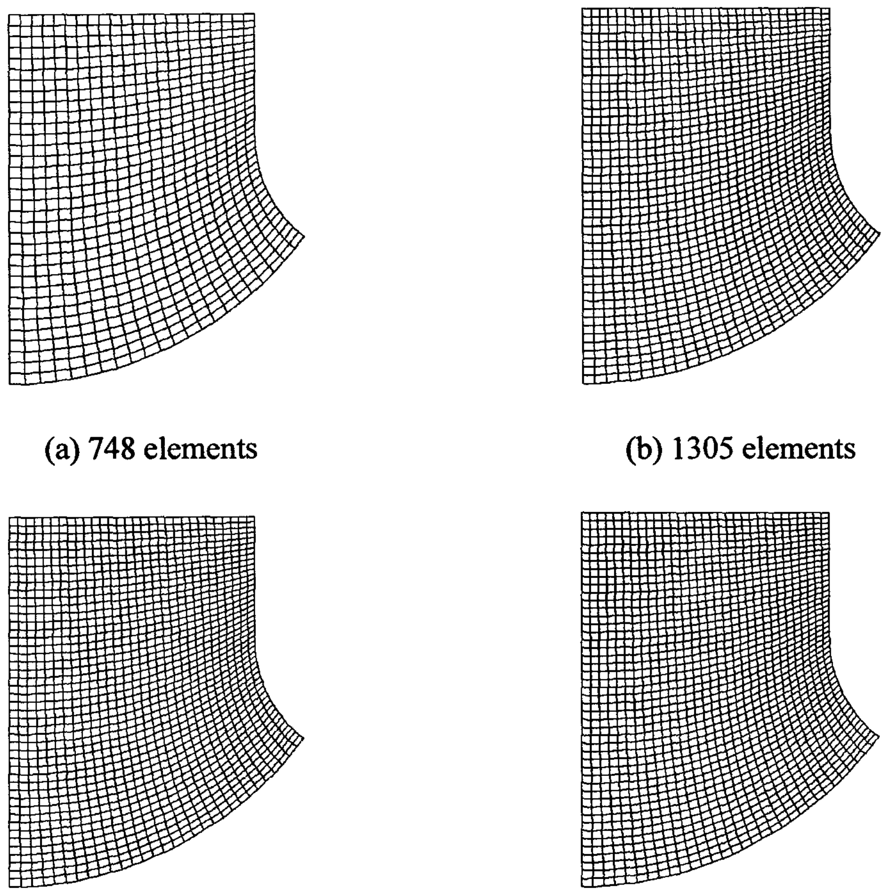

(a) 748 elements (b) 1305 elements

(c) 1380 elements (d) 1457 elements

Figure 4.4 Different mesh sizes for the blank for plane strain stretching

Table 4.2: Effect of mesh size on the thinning rate

Total elements	Element size (mm) (Approximately)	Maximum thickness reduction percentage (%)
748	2.20	39.82
1305	1.70	44.46
1380	1.65	49.37
1457	1.60	49.49

4.2.3 Material Model

There are several material models available in LS-DYNA for sheet metal forming simulation such as types 18, 24, 36 and 37. Material type 18 is the *MAT_POWER_LAW_PLASITICITY. This is an isotropic plasticity model with rate sensitivity which uses a power law-hardening rule. Material type 24 is the *MAT_PIECEWISE_LINEAR_PLASITICITY. This is an isotropic elastic-plastic model in which an arbitrary stress versus strain curve and arbitrary strain rate dependency can be defined in this model. Material type 36 is the *MAT_3-PARAMETER_BARLAT. This model was developed by Barlat and Lian (1989) for modeling sheets with anisotropy under plane stress conditions. Material type 37 is the *MAT_TRANSVERSELY_ANISOTROPIC_ELASTIC_PLASTIC. This model is for simulating transverse anisotropic materials based on Hill's (1948) yield function.

AA 5182-O is an anisotropic material, material type 36 is thus used in this study. The anisotropic constants in Barlat's Yld89 model are obtained through the Lankford parameters R_0, R_{45} and R_{90}. The effective stress-effective plastic strain curve for AA5182-O used in the simulations, which is based on the values of σ_y, K and n in Table 4.1, is shown in Figure 4.5.

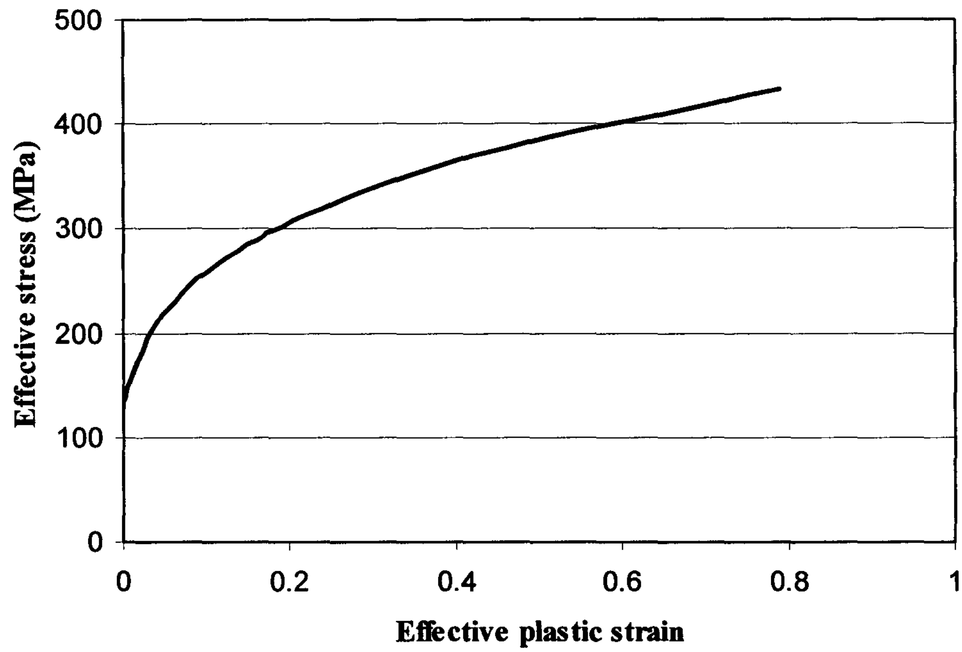

Figure 4.5: Effective stress versus effective plastic strain for AA 5182-O

4.2.4 Contact Definition

There are three contact interfaces defined in the dome test simulations, i.e., the contact interface between sheet blank and punch, sheet bank and clamp die and sheet blank and lower die. LS-DYNA decomposes contact interface into two parts: a slave surface and a master surface. It assumes that slave nodes must not penetrate master segments.

LS-DYNA offers three different contact methods. For most metal forming simulations, the penalty method is recommended (Maker & Zhu, 2000). The penalty method places a normal interface spring between all penetrating nodes and the contact surface. When penetration is detected, fictitious springs between the contacting entities move a penetrating node back to the contact surface. These artificial springs are applied as long as penetration is detected and are removed as soon as penetration ceases (LSTC, 2003).

In this study, the sheet blank is always treated as the slave surface and each rigid tooling component is designated as a master surface. There are many special contact types available in LS-DYNA formulated for sheet metal forming simulations. The contact algorithm used for the dome test simulations in this study is the *CONTACT_FORMING_ONE_WAY_SURFACE_TO_SURFACE as recommended by Maker and Zhu (2000).

4.2.5 Tool Motion

The overall hydraulic press motion in the dome test is simulated numerically through the application of appropriate velocity and displacement boundary conditions. The punch and clamp die are constrained allowing only movement in the Y-direction, which corresponds to the direction of the punch axis. The lower die is fully constrained.

The clamp die motion is specified using a trapezoidal velocity profile as shown in Figure 4.6. The maximum clamp die velocity is 2 mm/ms and the total displacement is 5 mm, which is the height of the drawbead. After the drawbead is fully closed, the velocity constraint is removed and the proper clamping load is applied to the clamp die.

The punch motion is also specified using a trapezoidal velocity profile as shown in Figure 4.7. The punch velocity is held at zero during engagement of the drawbead after which the punch stroke initiates at 3 ms. A maximum punch velocity of 2 mm/ms with a total punch displacement of 40 mm is sufficient to ensure the localized necking happened during the deformation process of the sheet blank.

The overall process motion sequence is as follows:

(1) The punch and clamp die are held in position close to the specimen.

(2) A velocity curve is specified to move the clamp die and engage the drawbead.

(3) After the drawbead is closed, a constant clamping load is applied.

(4) The punch moves via a trapezoidal velocity curve to complete the deformation of the blank.

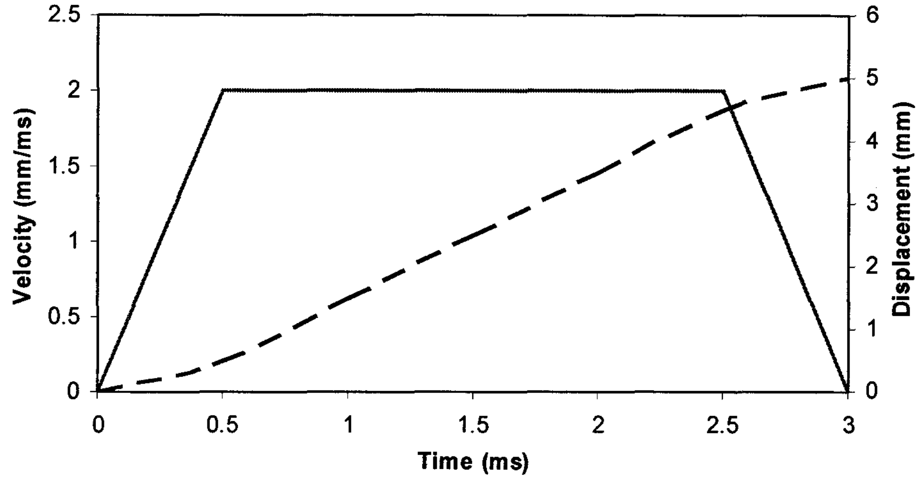

Figure 4.6: Clamp die velocity curve (solid) and corresponding displacement (dashed)

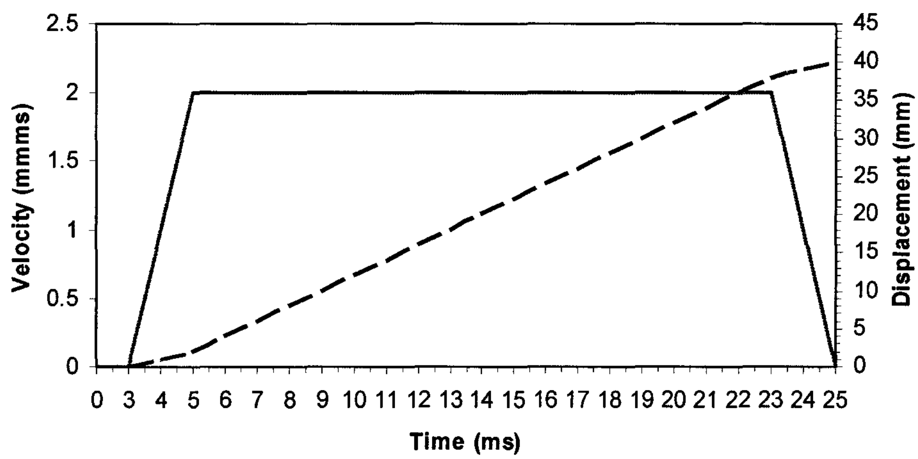

Figure 4.7: Punch velocity curve (solid) and displacement curve (dashed)

4.3 Results and Discussion

As discussed in the foregoing section, different geometries of samples and different friction conditions at the punch sheet interface are used to obtain the forming limits for the different strain paths. The following results are obtained from finite element simulation.

4.3.1 Forming Limits at Biaxial State

Figure 4.8 shows the profile of the simulation model for biaxial stretching test.

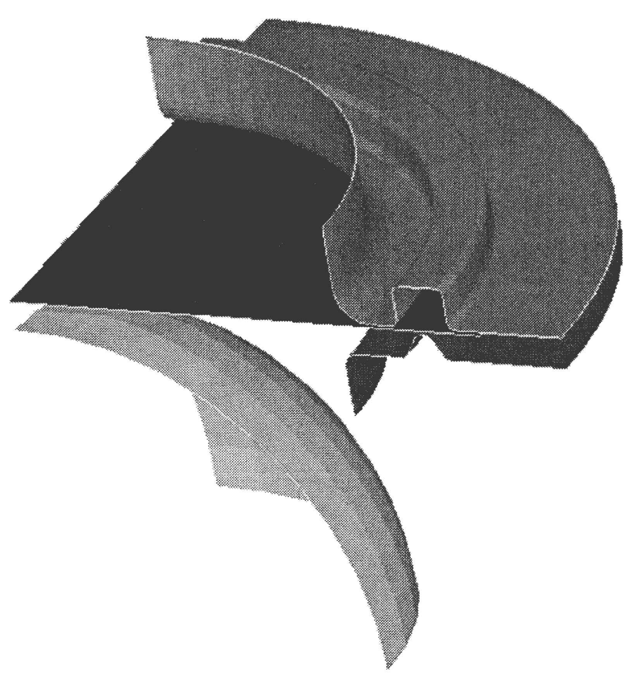

Figure 4.8: Simulation model for biaxial stretching test

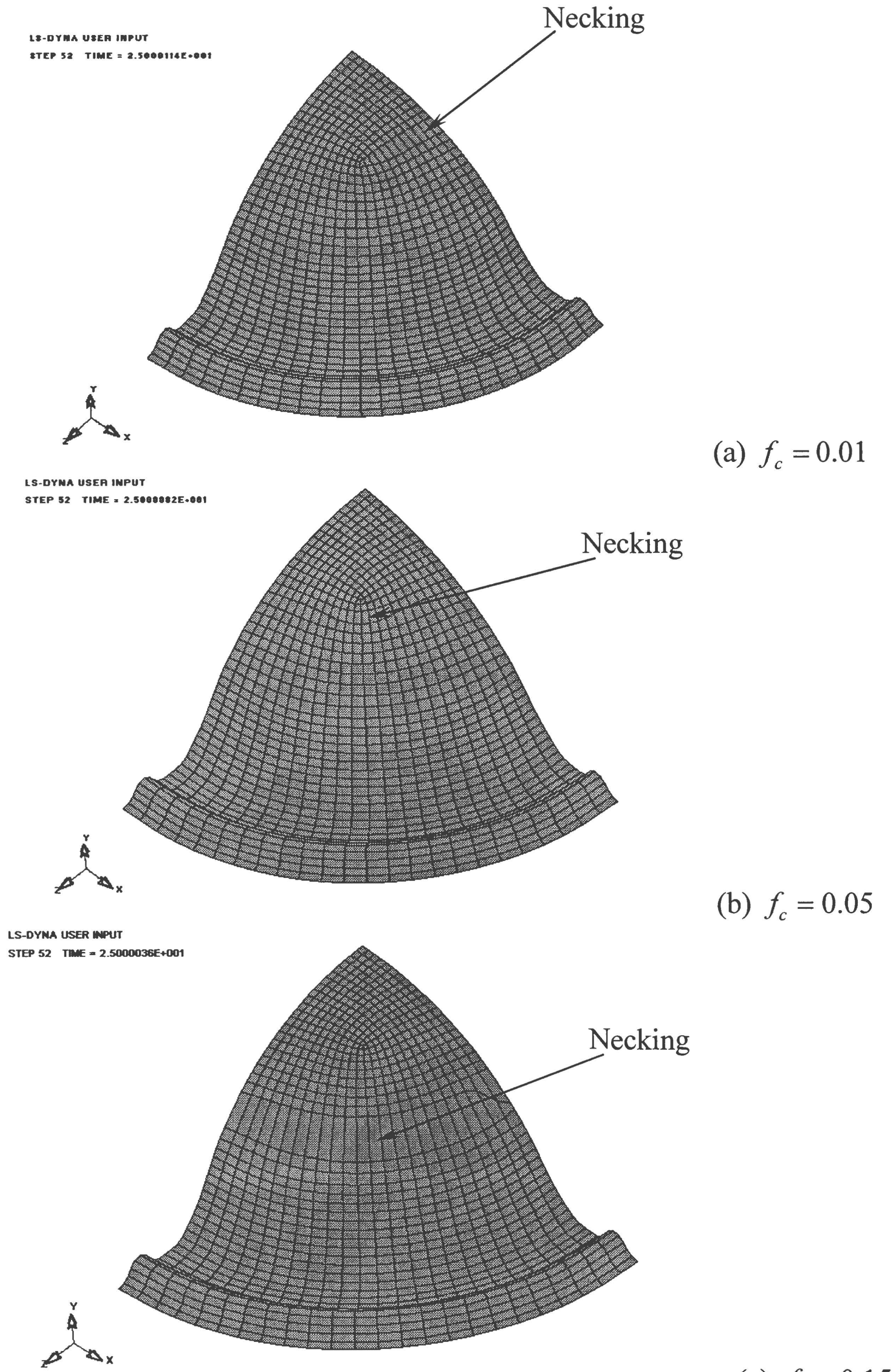

Figure 4.9: Deformed mesh of sheet with the punch displacement of 40 mm

In the experimental method for determining the FLD, it is not easy to stop the test after the localized necking happens, especially for the right hand side of FLD. Sometimes the fractured specimen is used to measure the forming limit strains. The numerical simulation, however, has the advantage of being able to stop the deformation of the blank after the onset of necking and before fracture is reached. Figure 4.9 shows the necking area of blank at the different friction conditions. The lower the friction coefficient, the closer the necking area to the pole. This result is in good qualitatively agreement with experimental results (Hayashi, 1998). When necking happens, the corresponding punch displacement at the different friction conditions is shown in Table 4.3. The friction coefficients in Table 4.3 are estimated and utilized based on the lubrication conditions specified by Jain et al., 2005. The results of the punch displacement at necking are in good agreement with experimental results (Jain et al., 2005)

Table 4.3: Punch displacement for various friction conditions

Lubrication condition estimated	Adopted friction coefficient	Punch displacement at necking (mm)
Dry	0.15	31
Teflon	0.05	38
Polyurethane	0.01	38.875

As discussed earlier, the unnecked elements closest to the necking area are chosen as the measuring elements for determining the limit strains. The criteria for choosing these elements are to see if the ε_1 and ε_2 of the candidate elements have no simultaneous increase after necking happens. With different friction coefficients, the different forming limit strains were obtained.

4.3.1.1 Friction condition with $f_c = 0.01$

In the biaxial stretching test with friction coefficient $f_c = 0.01$, the necking area is shown in Figure 4.10. Three elements, namely, No. 350, No. 374 and No. 398, are chosen as the measuring elements. The minor and major strains of these elements are shown in Figure 4.11 (a). It can be found that the minor and major principal strains of all these three elements have no further increase after simulation time of 23.5 ms, which corresponds to the punch displacement of 38.875 mm. Localized necking is therefore initiated at 23.5 ms. However, the simulation kept running until 25 ms, so a large group of necked elements can been seen in Figure 4.9. The values of ε_1 and ε_2 of the element No. 350, 374 and 398 at 23.5 ms were recorded and were used as the reference points in the biaxial side of the FLD. It is noted that after initiation of necking at t=23.5 ms, these elements have no further thinning (See Figure 4.11 (b)).

All the elements directly adjacent to the necking area are potentially qualified to be the measuring elements. However, some elements' major strains keep increasing while the minor strains have no change or the minor strains keep increasing while the major strains have no change after the onset of necking, it means the thickness strain of these elements are still changing, these elements can not satisfy the criteria, so they can not be chosen. Several elements around the necking area including elements 350, 374 and 398 meet the criteria, the practice of choosing elements 350, 374 and 398 arbitrarily as the measuring elements is to illustrate kind of subjective decisions involved in determining the FLD, i.e., how many elements and which specific ones should be chosen for measurement. For those elements chosen as the measuring elements such as 350, 374 and 398, their minor and major strains at the necking can be found slight difference between each other. It shows the uncertainty of the limit strain due to the decision of how to choose the measuring elements. This issue will be discussed further in the later section.

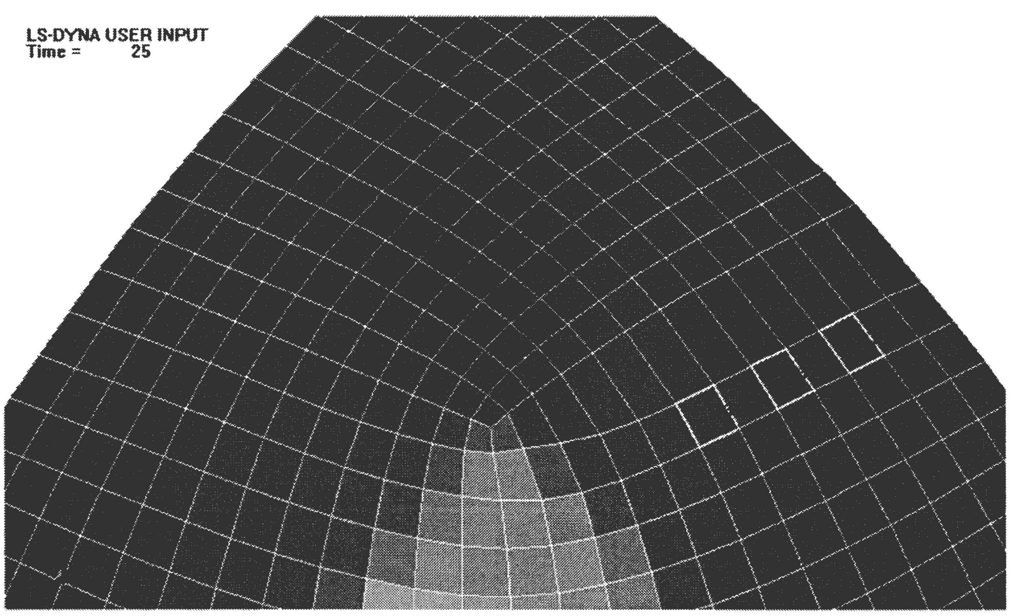

Figure 4.10: Location of the measuring elements in the biaxial state with $f_c = 0.01$

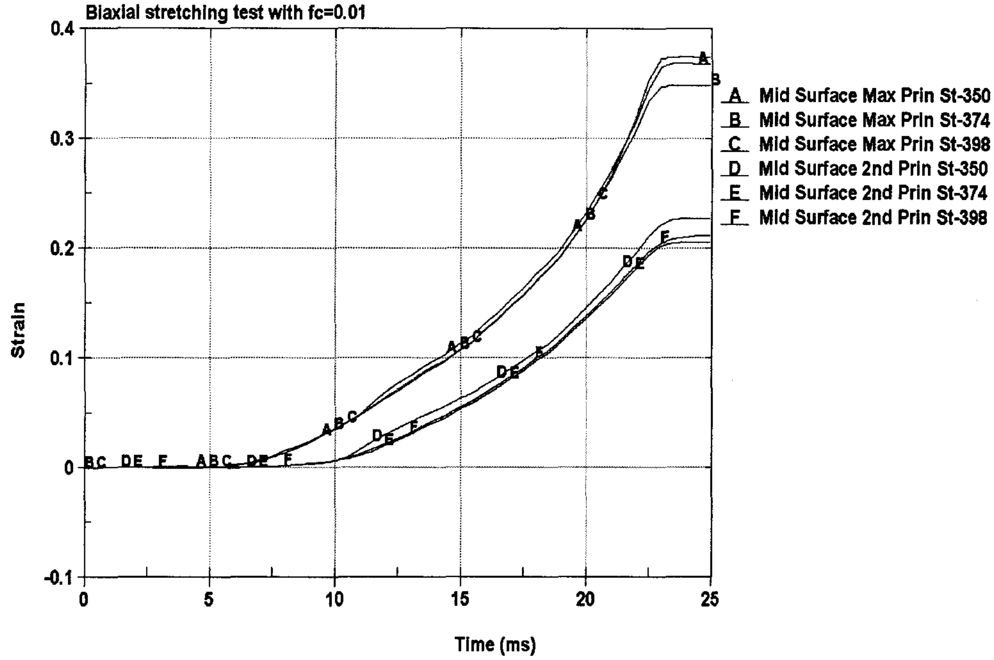

(a)

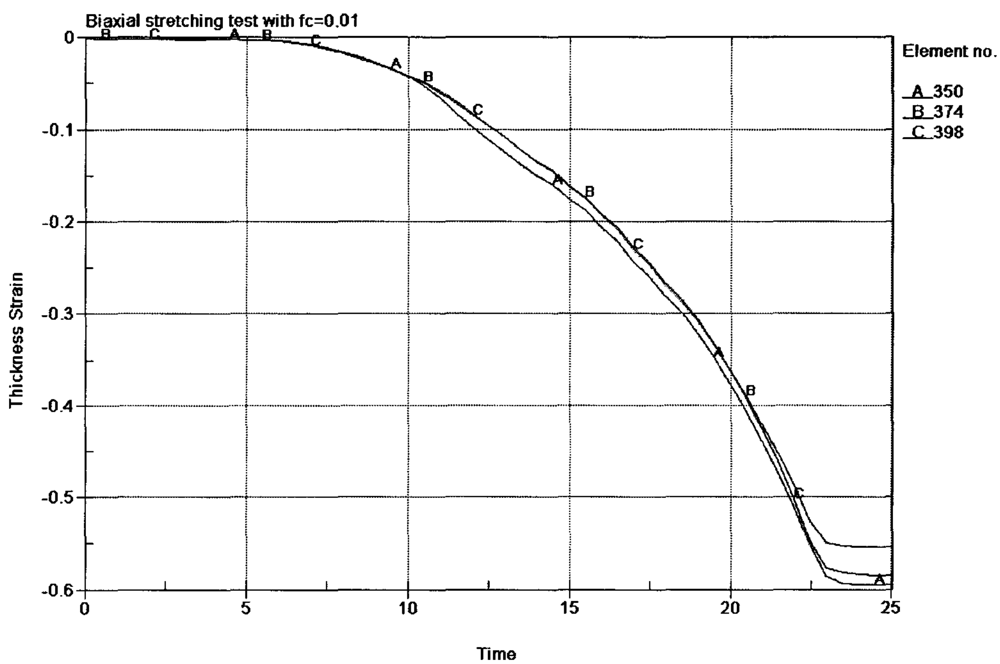

(b)

Figure 4.11: Minor & major strains (a) and thickness strain (b) of measuring elements in the biaxial state with $f_c = 0.01$

4.3.1.2 Friction condition with $f_c = 0.05$

In the biaxial stretching test with f_c = 0.05, the necking area is shown in Figure 4.12. Three elements, namely, No. 194, 278 and 386, are chosen as the measuring elements. The minor and major strains of these elements are shown in Figure 4.13. It can be found that the minor principal strain and major principle strain of all these three elements have no further increase after simulation time of 23 ms, which corresponds to the punch displacement of 38 mm. The values of ε_1 and ε_2 of the elements 194, 278 and 386 at 23 ms were recorded and were used as the reference points in the biaxial side of FLD.

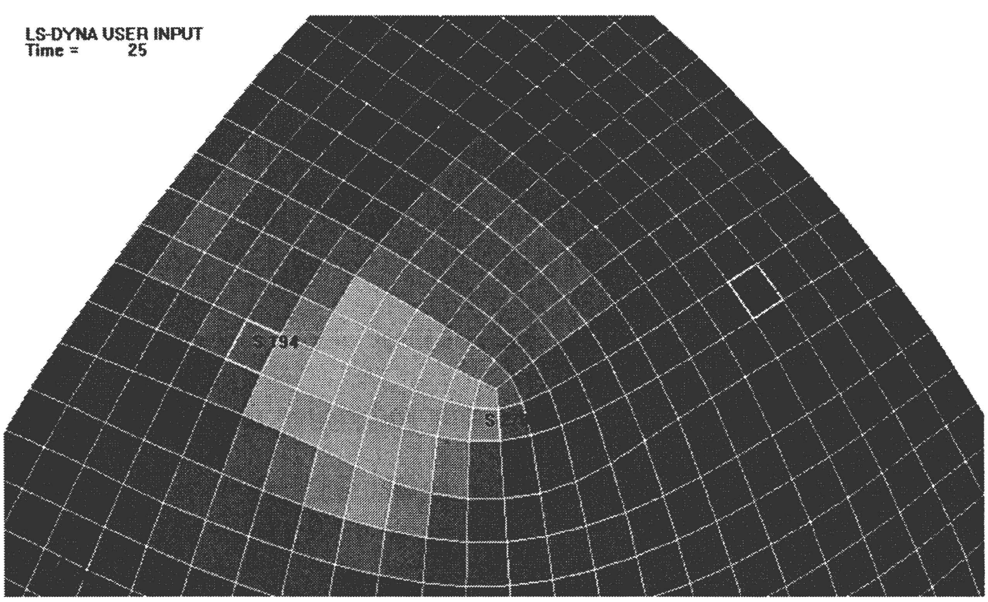

Figure 4.12: Location of the measuring elements in the biaxial state with $f_c = 0.05$

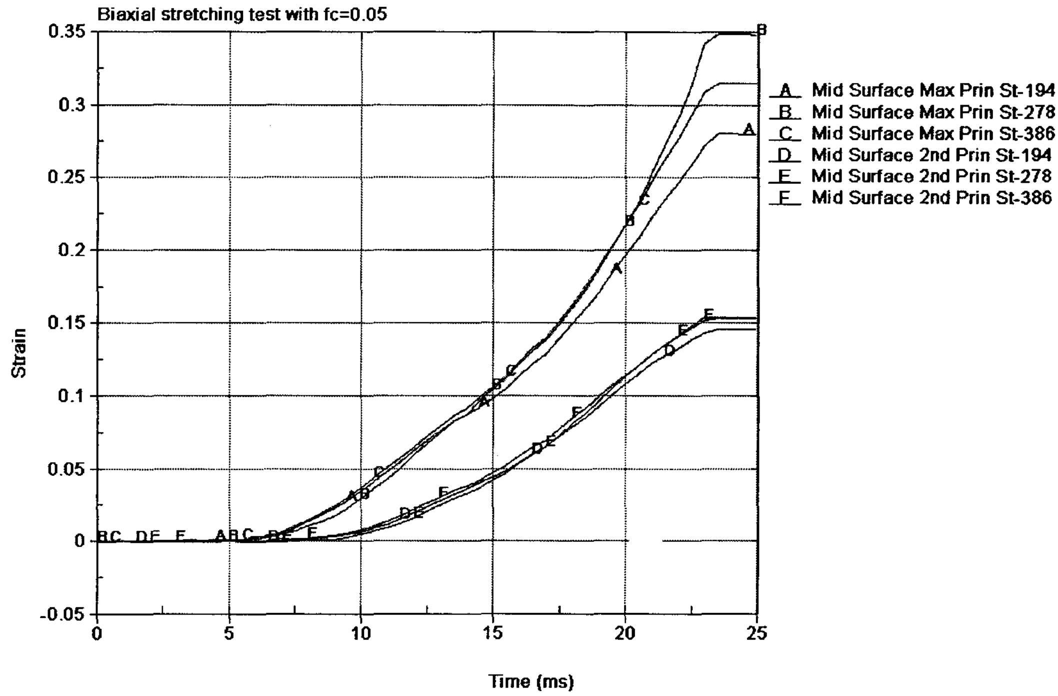

Figure 4.13: Minor and major strains of measuring elements in the biaxial state with $f_c = 0.05$

4.3.1.3 Friction condition with $f_c = 0.15$

In the biaxial stretching test with f_c = 0.15, the necking area is shown in Figure 4.14. Three elements, namely, No. 212, 284 and 428, are chosen as the measuring elements. The minor and major strains of these elements are shown in Figure 4.15. It can be found that the minor principal strain and major principle strain of all these three elements have no further increases after simulation time of 19.5 ms, which corresponds to the punch displacement of 31 mm. The values of ε_1 and ε_2 of the elements 212, 284 and 428 at 19.5ms were recorded and were used as the reference points in the biaxial side of FLD.

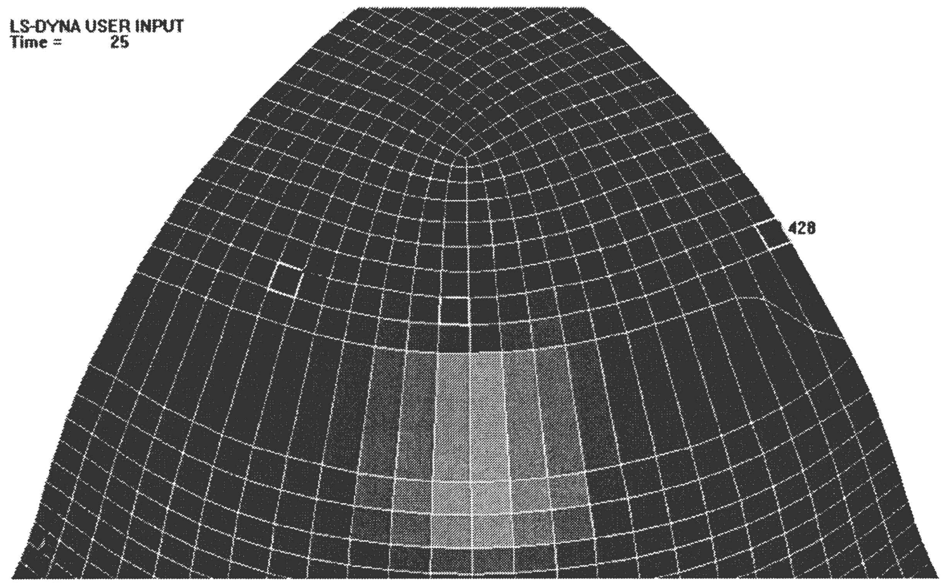

Figure 4.14: Location of the measuring elements in the biaxial state with $f_c = 0.15$

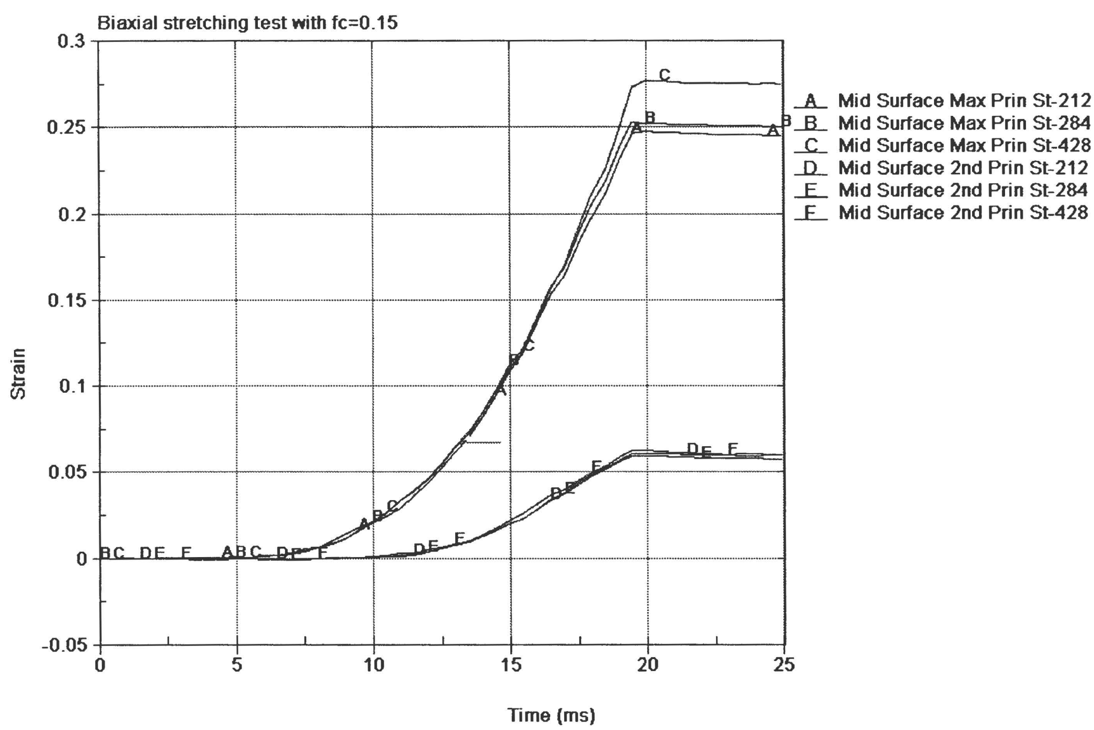

Figure 4.15: Minor and major strains of measuring elements in the biaxial state with $f_c = 0.15$

4.3.2 Forming Limits from the Uniaxial State

Figure 4.16 shows the profile of the simulation model for the uniaxial tension test. Figure 4.17 shows the necking area of blank under uniaxial tension at the different friction conditions.

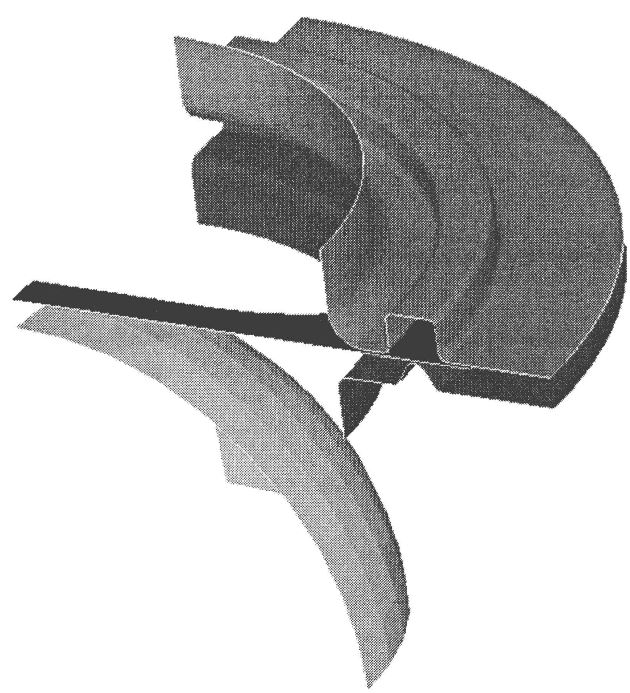

Figure 4.16: Simulation model for uniaxial tension test

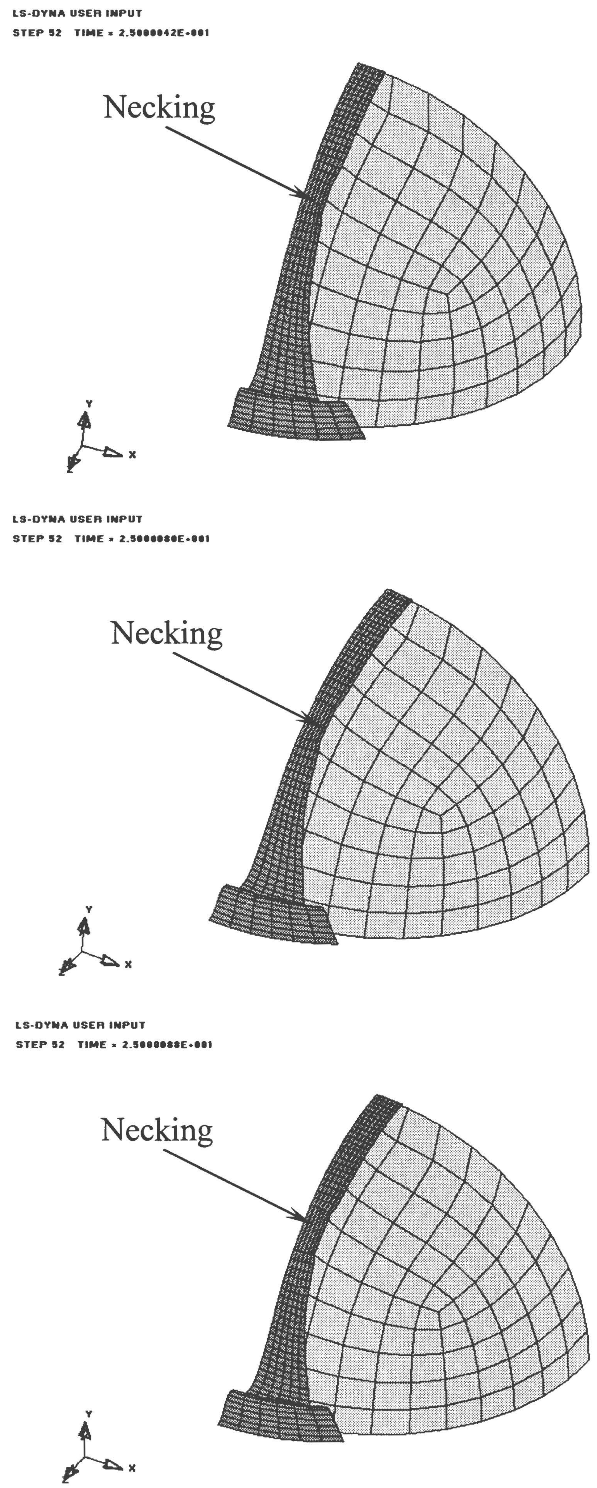

(a) $f_c = 0.01$

(b) $f_c = 0.05$

(c) $f_c = 0.15$

Figure 4.17: Deformation of the sheet with the punch displacement of 40 mm

4.3.2.1 Friction condition with $f_c = 0.01$

In the uniaxial tension test with f_c = 0.01, the necking area is shown in Figure 4.18. Three elements, namely, No. 114, 66 and 18, are chosen as the measuring elements. The minor and major strains of these elements are shown in Figure 4.19. It can be found that the minor principal strain and major principle strain of all these three elements have no further increase after simulation time of 21 ms, which corresponds to the punch displacement of 34 mm. The values of ε_1 and ε_2 of the elements No. 114, 66 and 18 at 21 ms were recorded and were used as the reference points in the draw side of FLD. Elements No. 19, 20 and 21 listed in Figure 4.18 are for the purpose of comparing with the Figure 4.20 and Figure 4.22 in the following sections to show the friction's effect on the necking location in the uniaxial tension.

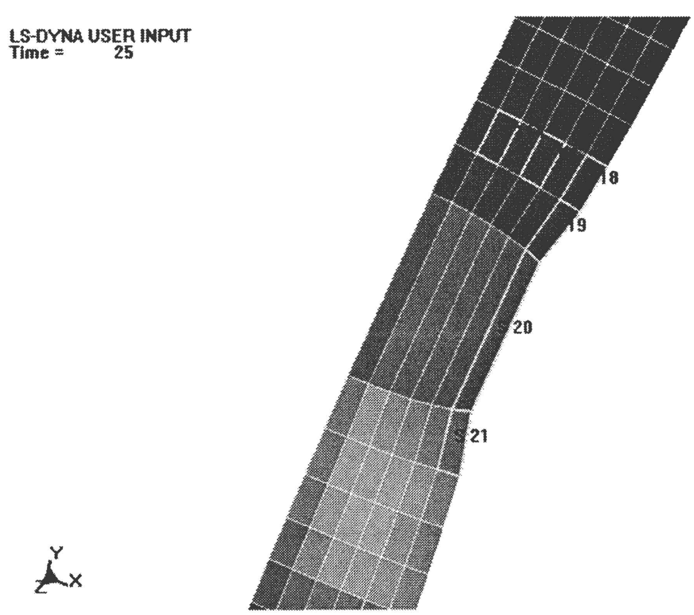

Figure 4.18: Location of the measuring elements in the uniaxial state with $f_c = 0.01$

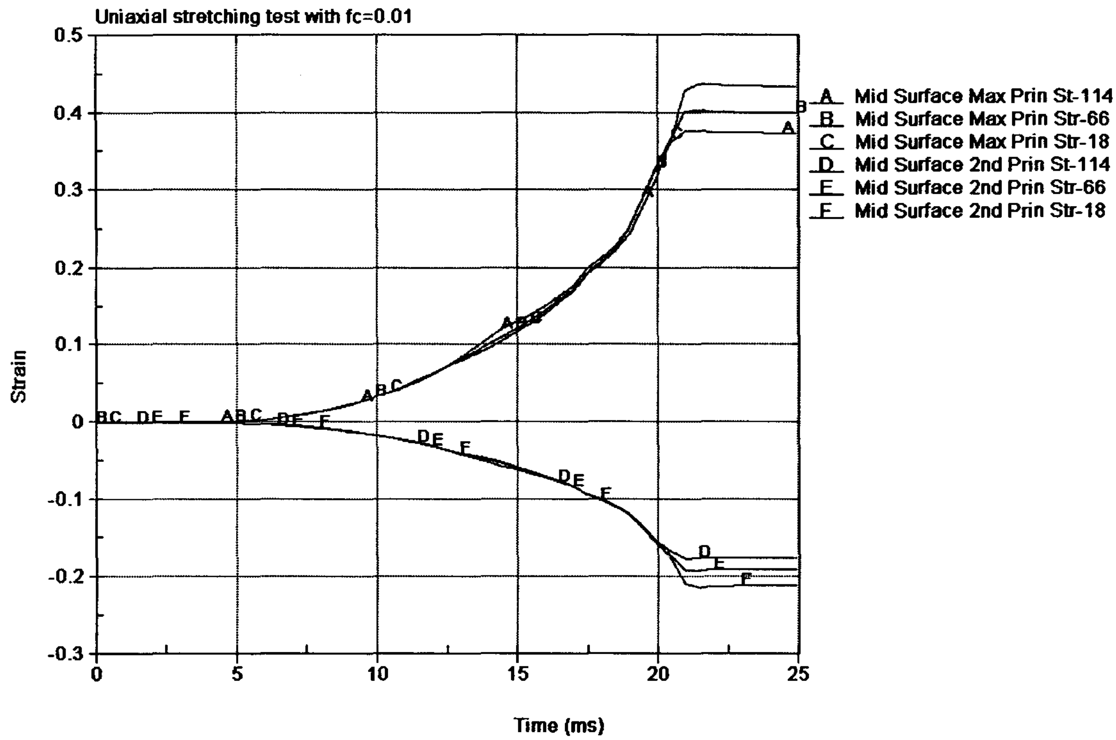

Figure 4.19: Minor and major strains of measuring elements in the uniaxial state with $f_c = 0.01$

4.3.2.2 Friction condition with $f_c = 0.05$

In the uniaxial tension test with f_c = 0.05, the necking area is shown in Figure 4.20. Three elements, namely, No. 116, 68 and 20, are chosen as the measuring elements. The minor and major strains of these elements are shown in Figure 4.21. It can be found that the minor principal strain and major principle strain of all these three elements have no further increase after simulation time of 20 ms, which corresponds to the punch displacement of 32 mm. The values of ε_1 and ε_2 of the elements116, 68 and 20 at 20 ms are recorded and are used as the reference points in the draw side of FLD.

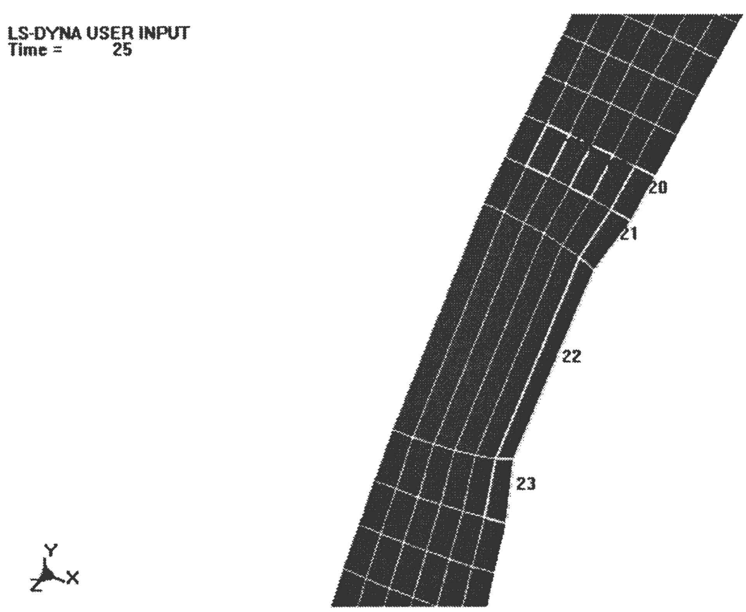

Figure 4.20: Location of the measuring elements in the uniaxial state with $f_c = 0.05$

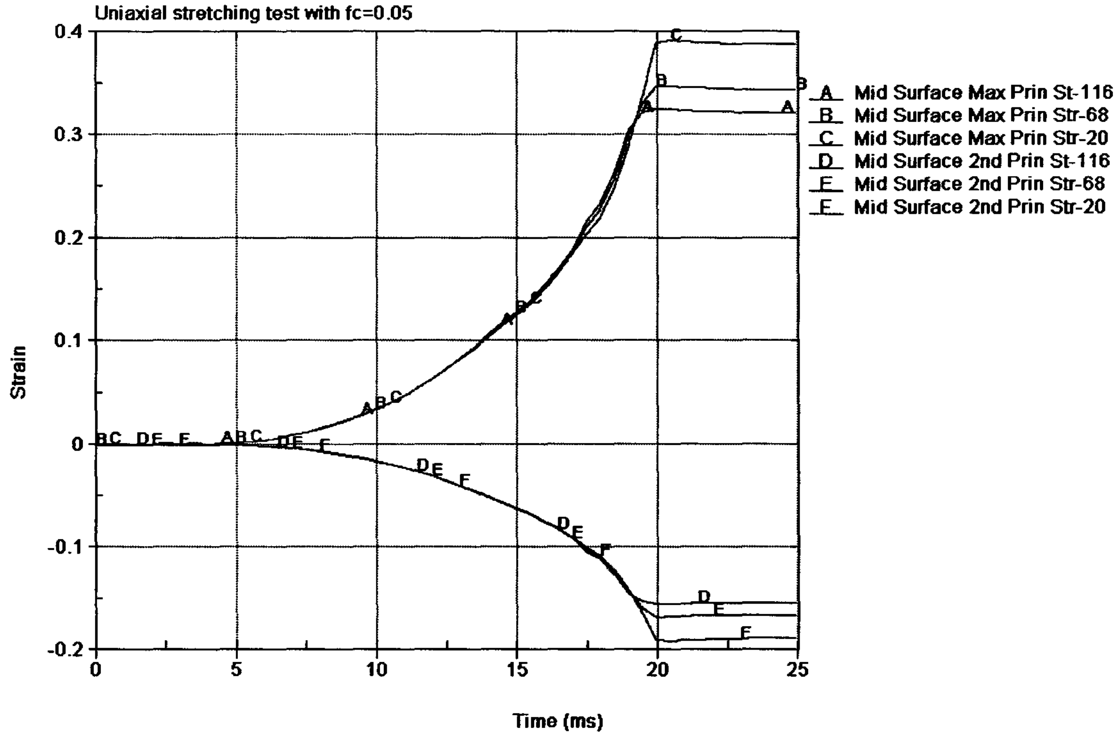

Figure 4.21: Minor and major strains of measuring elements in the uniaxial state with $f_c = 0.05$

4.3.2.3 Friction condition with $f_c = 0.15$

In the uniaxial tension test with $f_c = 0.15$, the necking area is shown in Figure 4.22. Three elements, namely, No. 117, 69 and 21, are chosen as the measuring elements. The minor and major strains of these elements are shown in Figure 4.23. It can be found that the minor principal strain and major principle strain of all these three elements have no further increase after simulation time of 19 ms, which corresponds to the punch displacement of 30 mm. The values of ε_1 and ε_2 of the elements 117, 69 and 21 at 19ms were recorded and were used as the reference points in the draw side of FLD. As mentioned earlier, elements No. 19, 20 and 21 in Figure 4.18, elements No. 21, 22 and 23 in Figure 4.20 and elements No. 22, 23 and 24 in Figure 4.22 are used to illustrate the relative necking location in the different friction conditions for uniaxial tension test. It can be seen that the effect of friction condition on the necking location in the uniaxial tension test is insignificant compared to its effect in the biaxial tension test. In the uniaxial tension test, the necking location just moves down a little (1 or 2 elements distance) when the friction coefficient increases. It is in reasonable agreement with the observation (Duan et al., 2006) that the friction's effect on the necking location in the uniaxial tension is negligible.

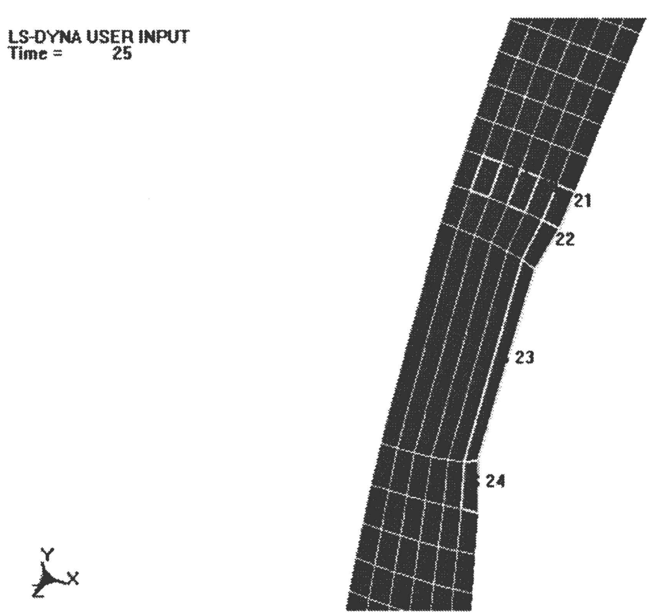

Figure 4.22: Location of the measuring elements in the uniaxial state with $f_c = 0.15$

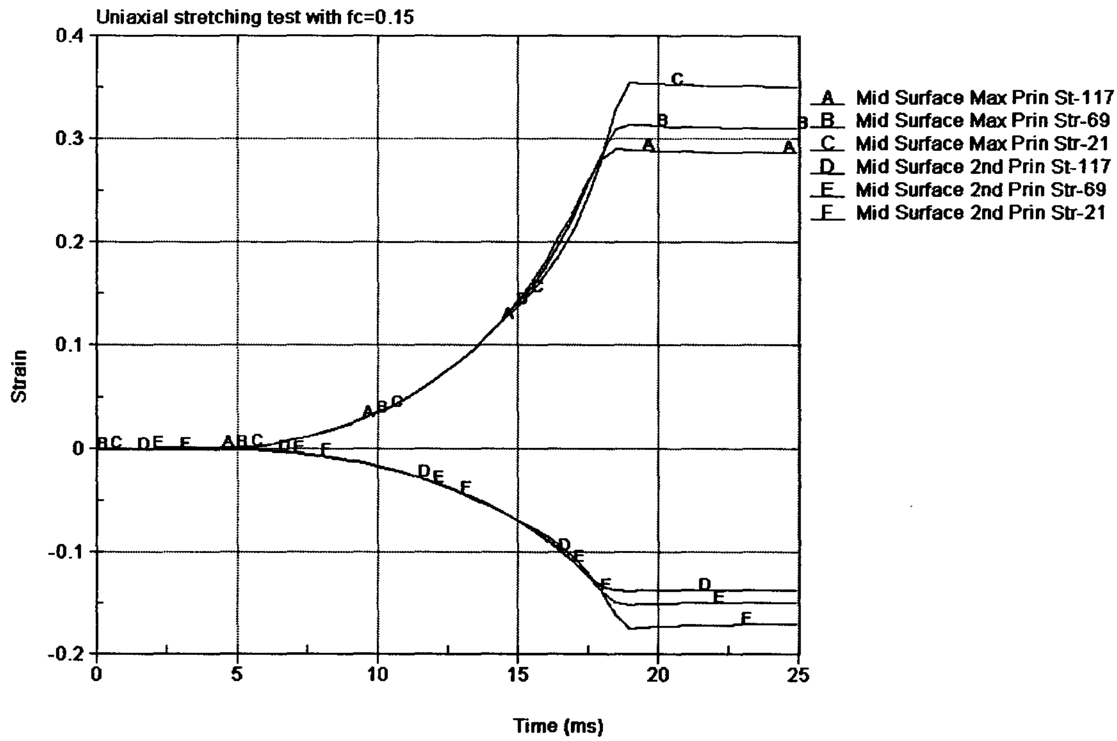

Figure 4.23: Minor and major strains of measuring elements in the uniaxial state with $f_c = 0.15$

4.3.3 Forming Limit at Plane Strain State

Figure 4.24 shows the profile of the simulation model for plane strain stretching test. Figure 4.25 shows the necking area of blank under the plane strain stretching at the different friction conditions.

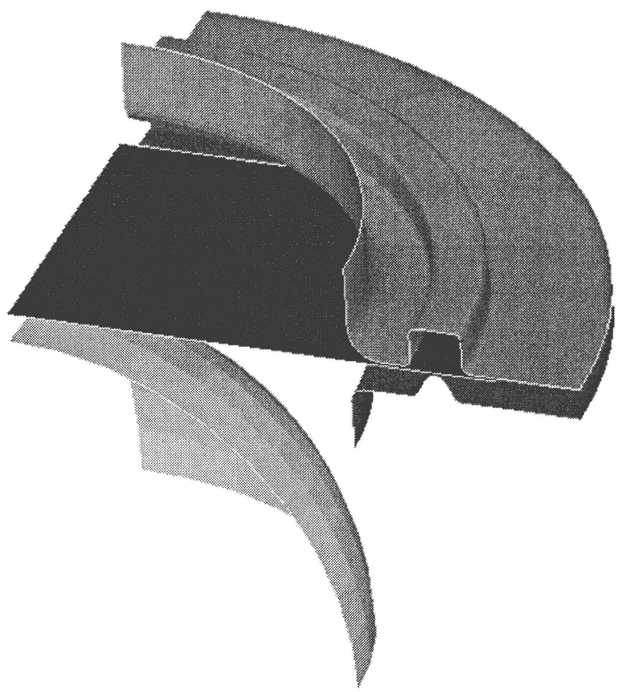

Figure 4.24: Simulation model for plane strain stretching test

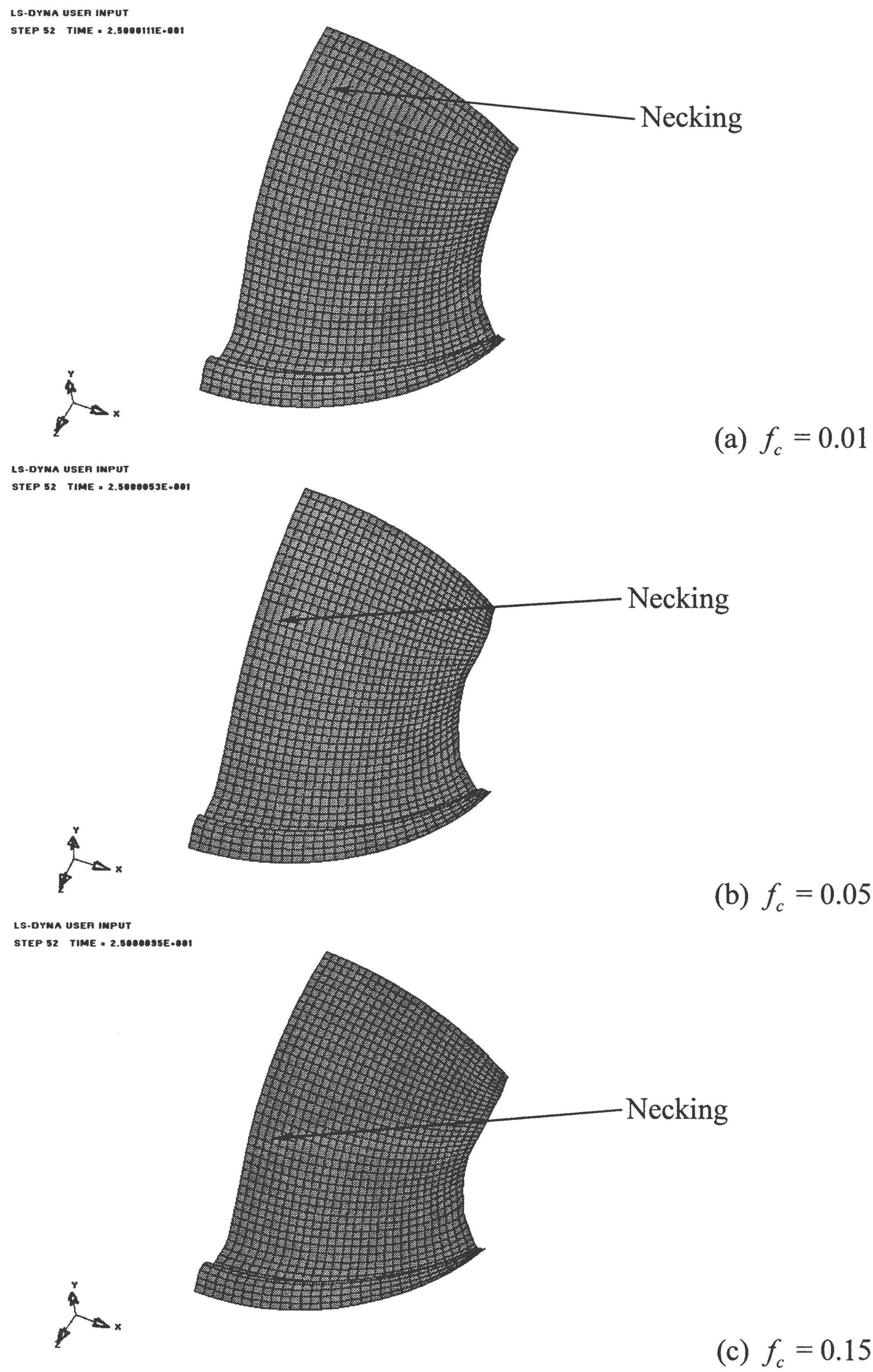

Figure 4.25: Deformation of the sheet with the punch displacement of 40 mm

4.3.3.1 Friction condition with $f_c = 0.01$

In the plane strain stretching test with $f_c = 0.01$, the necking area is shown in Figure 4.26. Three elements, namely, No. 50, 188 and 326, are chosen as the measuring elements. The minor and major strains of these elements are shown in Figure 4.27. It can be found that the minor principal strain and major principle strain of all these three elements have no further increase after simulation time of 21.5 ms, which corresponds to the punch displacement of 35 mm. The values of ε_1 and ε_2 of the elements 50, 188 and 326 at 21.5 ms were recorded and were used as the reference points for the plane strain state of FLD.

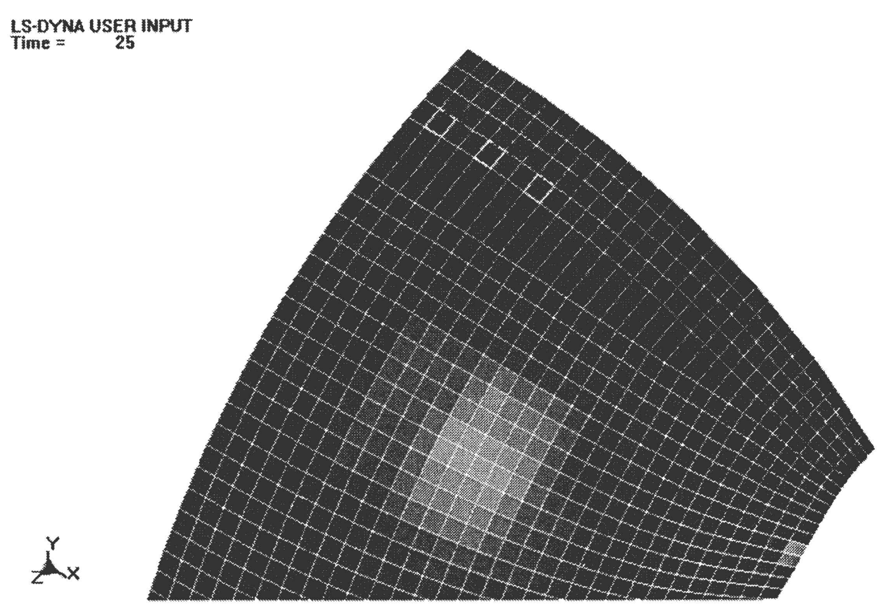

Figure 4.26: Location of the measuring elements in the plane strain state with $f_c = 0.01$

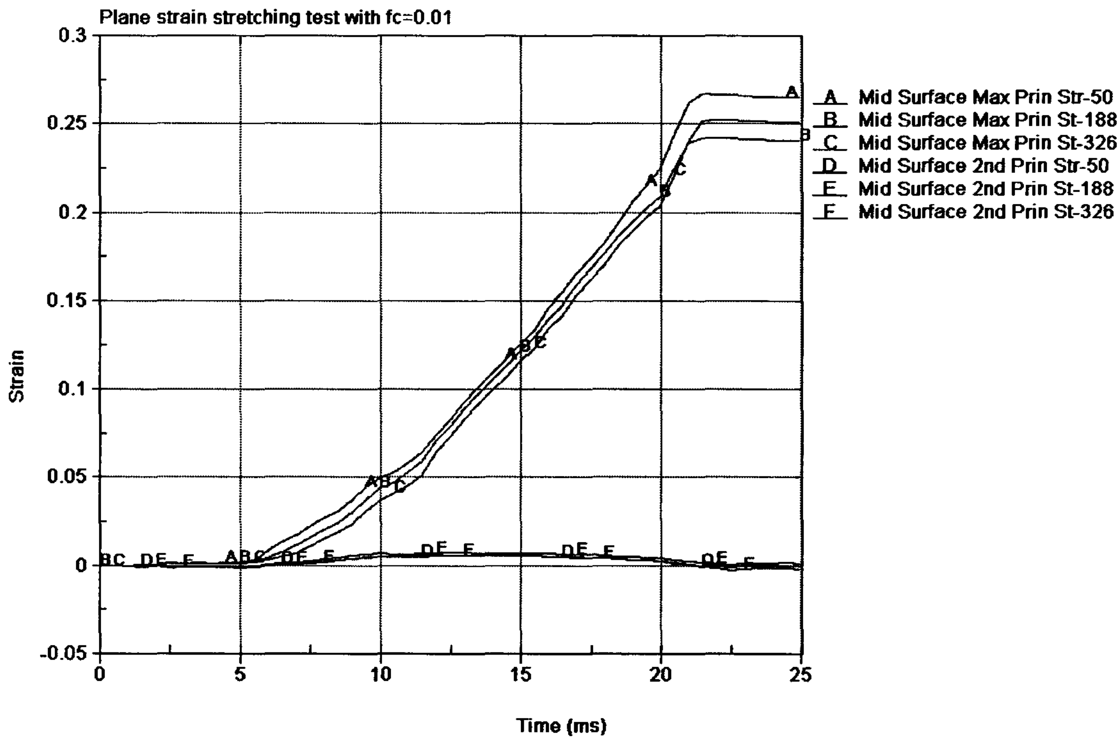

Figure 4.27: Minor and major strains of measuring elements in the plane strain state with $f_c = 0.01$

4.3.3.2 Friction condition with $f_c = 0.05$

In the plane strain stretching test with f_c = 0.05, the necking area is shown in Figure 4.28. Three elements, namely, No. 59, 197 and 335, are chosen as the measuring elements. The minor and major strains of these elements are shown in Figure 4.29. It can be found that the minor principal strain and major principle strain of all these three elements have no further increase after simulation time of 23 ms, which corresponds to the punch displacement of 38 mm. The values of ε_1 and ε_2 of the elements 59, 197 and

335 at 23 ms were recorded and were used as the reference points for the plane strain state of FLD.

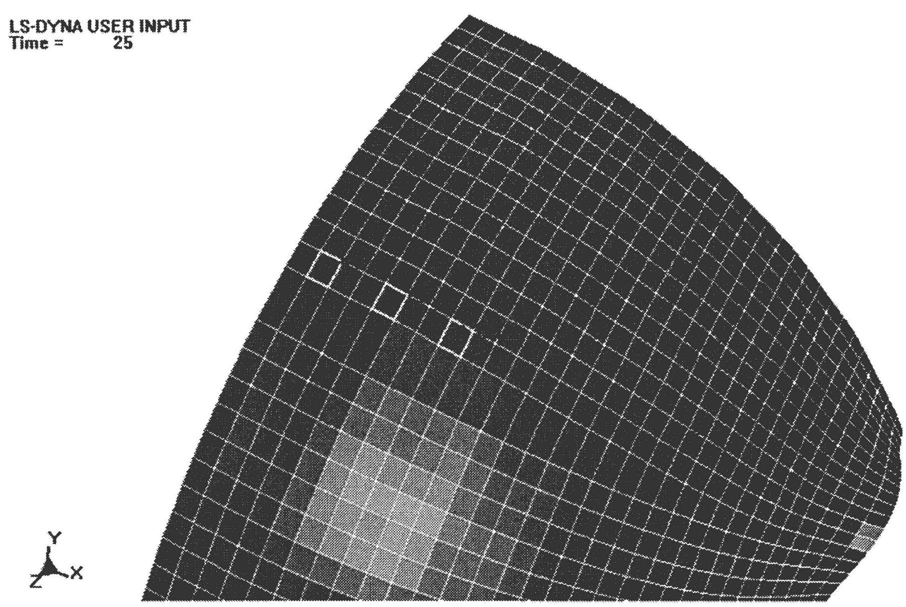

Figure 4.28: Location of the measuring elements in the plane strain state with $f_c = 0.05$

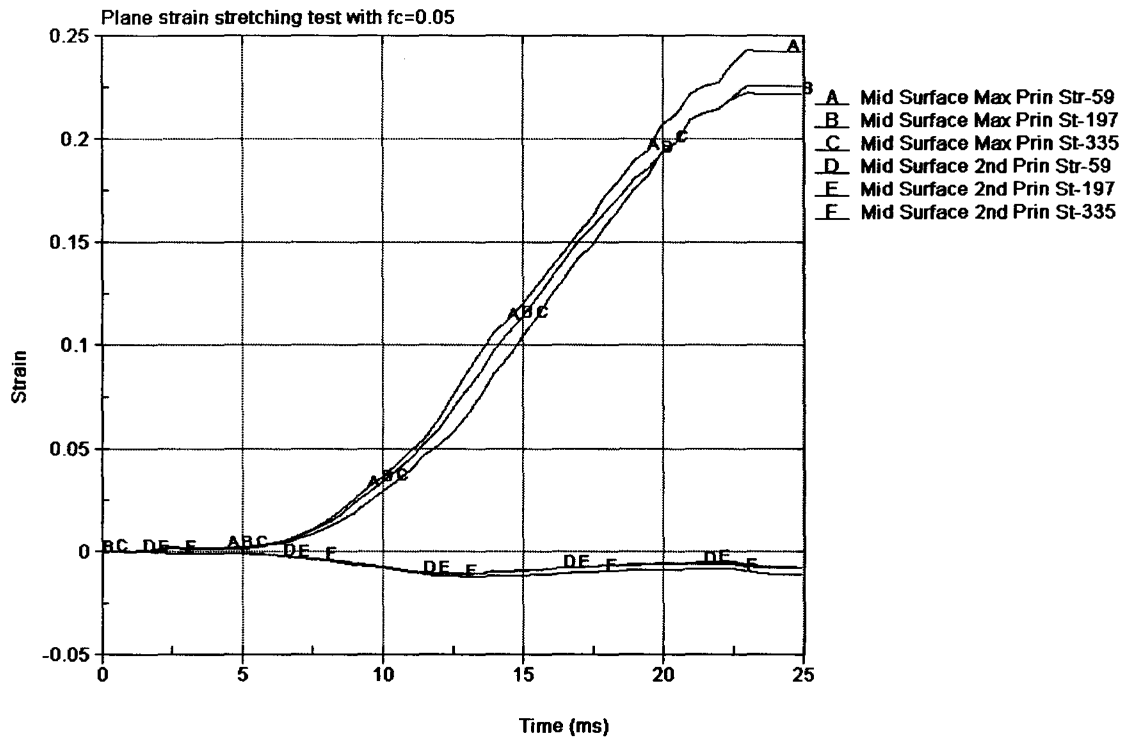

Figure 4.29: Minor and major strains of measuring elements in the plane strain state with $f_c = 0.05$

4.3.3.3 Friction condition with $f_c = 0.15$

In the plane strain stretching test with f_c = 0.15, the necking area is shown in Figure 4.30. Three elements, namely, No. 115, 207 and 299, are chosen as the measuring elements. The minor and major strains of these elements are shown in Figure 4.31. It can be found that the minor principal strain and major principle strain of all these three elements have no further increase after simulation time of 23.5 ms, which corresponds to the punch displacement of 38.875 mm. The values of ε_1 and ε_2 of the elements 115, 207 and 299 at 23.5ms were recorded and were used as the reference points for the plane strain state of FLD.

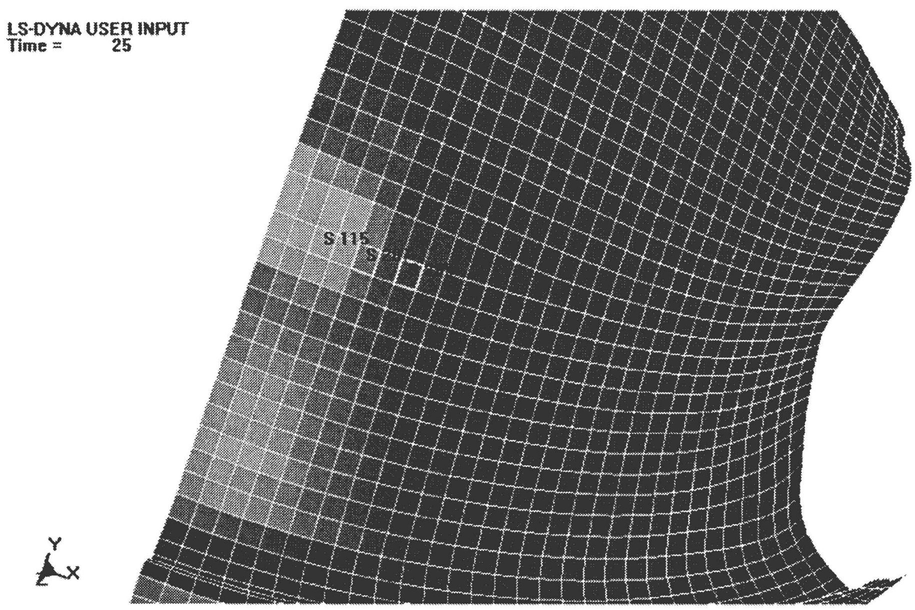

Figure 4.30: Location of the measuring elements in the plane strain state with f_c = 0.15

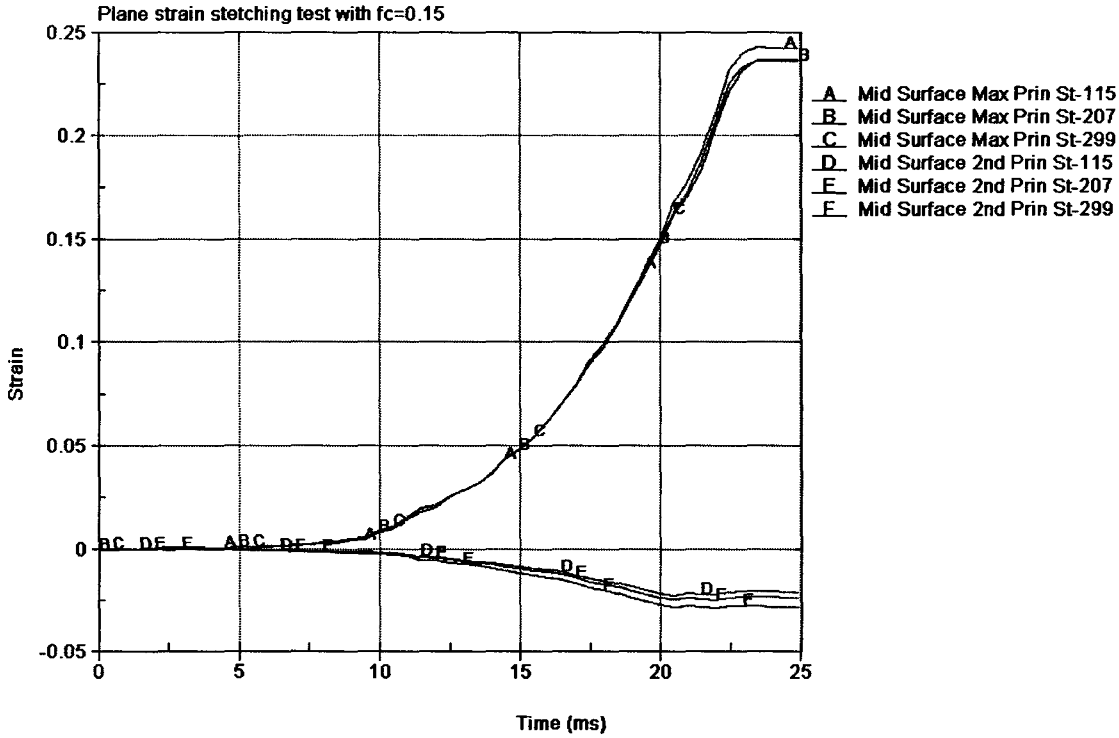

Figure 4.31: Minor and major strains of measuring elements in the plane strain state with $f_c = 0.15$

4.3.4 FE Predicted FLD

From the above simulations, 27 reference points at 9 different strain paths have been obtained. Based on these reference points corresponding to the unnecked elements closest to the necking area, the FLD of the AA 5182-O has been predicted as shown in Figure 4.32. The predicted FLC in Figure 4.32 is a trendline fitting the reference points with a cubic polynomial. It can be seen that a remarkable agreement has been achieved between the predicted FLD with the experimental FLD by Wu et al. (2003).

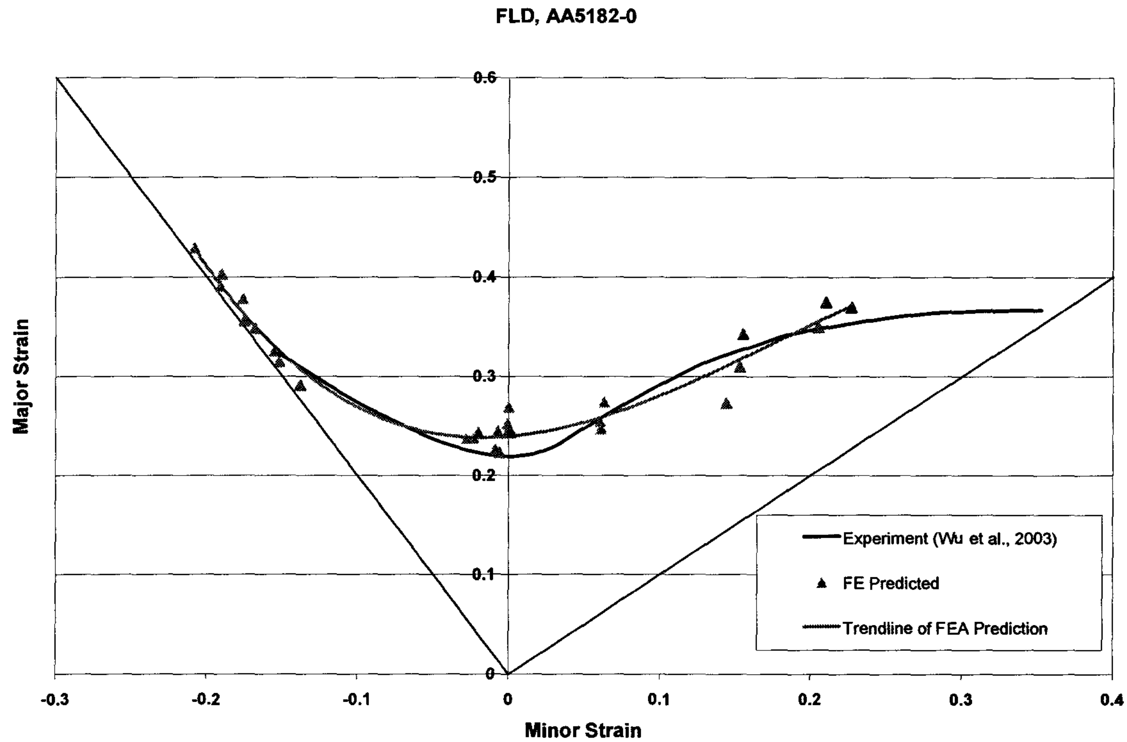

Figure 4.32: Comparison between FEA predicted FLD with the experimental one for AA5182-O

4.3.5 Uncertainty of Forming Limits

A significant scatter of forming limits has been observed during the experimental process for determination of FLD (Jain & Allin, 1994; Janssens et al., 2001). The uncertainty of the experimental determination of a FLD is a complex problem as it is caused by many sources. The experimentally determined FLD largely depends on the experimental procedure used to obtain the forming limit curve. Typically, the uncertainty of the shape of the FLC is attributed to the variability of material properties, specimen geometry, boundary conditions like friction at the punch sheet interface, number of samples used for the test, and so on (Van Minh et al., 1974; Jain & Allin, 1994; Janssens et al., 2001). Some other reasons for the uncertainty of experimentally determined FLD reported by Jain & Allin (1994) included the variability of specimen orientation, punch velocity and the subjective nature of FLD “line”. Hotz (2004) comprehensively analyzed the influencing factors on the scatter of the forming limit. In addition to the factors mentioned above, Hotz also took the following factors into account for the experimental determination of FLD including the grid type and grid application method, measurement system and software used, criterion used for definition of forming limit and regression approach for producing the FLC.

By summarizing all the potential sources for the uncertainty of the FLD, two categories are classified among these sources based on their intrinsic characteristics.

- Objective uncertainty sources that can be quantified through objective measurements: material properties, thickness of specimen for certain strain path and friction conditions.
- Subjective uncertainty sources that are affected by subjective decisions made by the experimenter: selection of specimen to obtain the different strain paths, selection of the measuring grids, number of strain paths, number of samples per strain path and method of producing the FLC.

In the following sections, the influences of these uncertainty sources are investigated through the FE simulations. It has to be recognized that the FE simulation itself also involves many numerical uncertainties in terms of predicting the FLD. These uncertainties could include, but are not limited to, the mesh size, element type, material hardening, yield criteria, contact algorithm and so on. Some of these numerical factors have been discussed on Section 4.2. However, in this part of study, our focus is to illustrate the experimental uncertainties numerically using finite element simulations.

4.3.5.1 Influence of the objective uncertainty sources

To determine the influence of objective sources of uncertainty, a simulation experiment is conducted. Seven objective parameters are considered including yield stress, hardening exponent, anisotropic parameters R_0, R_{45} and R_{90}, thickness of blank and friction coefficient between punch and blank. Three levels of each parameter are created by varying their nominal values over ±10%. In Table 4.4, "2" represents the nominal value of each parameter, "1" represents 10% less than the nominal value of each parameter and "3" represents 10% greater than the nominal value of each parameter.

After conducting a series of finite element simulations, 225 limit strain points are obtained as shown in Figure 4.33. The 225 points are collected through measuring 3 reference elements in 15 tests along 5 different strain paths, i.e., biaxial state with f_c = 0.01, f_c = 0.05 and f_c = 0.15, plane strain state with f_c = 0.05 and uniaxial state with f_c = 0.05. It can be seen that a large scatter of the forming limits appears at balanced biaxial state. The scatter of the forming limits in the uniaxial state is along the strain path and it has very small effect on the shape of FLC while the scatter of forming limit in the plane strain state along the strain path will greatly affect the FLD_0 value. These observations are in good agreement with the experimental results of Janssens et al., (2001) and Hotz (2004).

Figure 4.34 to Figure 4.41 show the effect of each objective parameter on the forming limit of AA 5182-O. It can be seen that the yield stress almost has no effect on the forming limit. Figure 4.35 shows that higher n will increase the level of FLD, and this result is in good agreement with experimental observations (Graf & Hosford, 1990; Zhao et al., 1996; Rees, 2001). For the anisotropic parameters R_0, R_{45} and R_{90}, it can be seen that R_{45} has very small effect on the forming limit compared with the effects of R_0 and R_{90}. By comparing Figure 4.37 with Figure 4.38, we can find that R_0 and R_{90} have the contrary effects on the shape of FLC. Usually just the average anisotropy parameter $\bar{R}$ ($\bar{R} = (R_0 + 2R_{45} + R_{90})/4$) is considered in industry. The effects of R_0 and R_{90} on the forming limit counteract with each other and R_{45}'s effect on the forming limit is negligible, so generally $\bar{R}'s$ effect on the shape of FLD is not significant. From Figure 4.39, higher forming limits are found for thicker sheet, especially at the right-hand side of FLD. This trend is consistent with the known improvement in formability attributed to thicker sheet material (Rees, 2001), even though the improvement is not significant in Figure 4.39 due to only a 10% difference of sheet thickness investigated in this study. Figure 4.40 shows that the friction coefficient has little influence on the shape of FLC. However, the friction coefficient does affect the strain path taken during the deformation, especially at the biaxial stretching strain state as shown in Figure 4.41. Friction makes material move away from the balanced biaxial state. The higher friction coefficient is, the closer strain path moves to the plane strain axis (Graf & Hosford, 1993).

Table 4.4: Layout of simulation with three levels of each parameter

Test No.	σ_y	n	R_0	R_{45}	R_{90}	Thickness	Friction coefficient
1	1	2	2	2	2	2	2
2	3	2	2	2	2	2	2
3	2	1	2	2	2	2	2
4	2	3	2	2	2	2	2
5	2	2	1	2	2	2	2
6	2	2	3	2	2	2	2
7	2	2	2	1	2	2	2
8	2	2	2	3	2	2	2
9	2	2	2	2	1	2	2
10	2	2	2	2	3	2	2
11	2	2	2	2	2	1	2
12	2	2	2	2	2	3	2
13	2	2	2	2	2	2	1
14	2	2	2	2	2	2	3
15	2	2	2	2	2	2	2

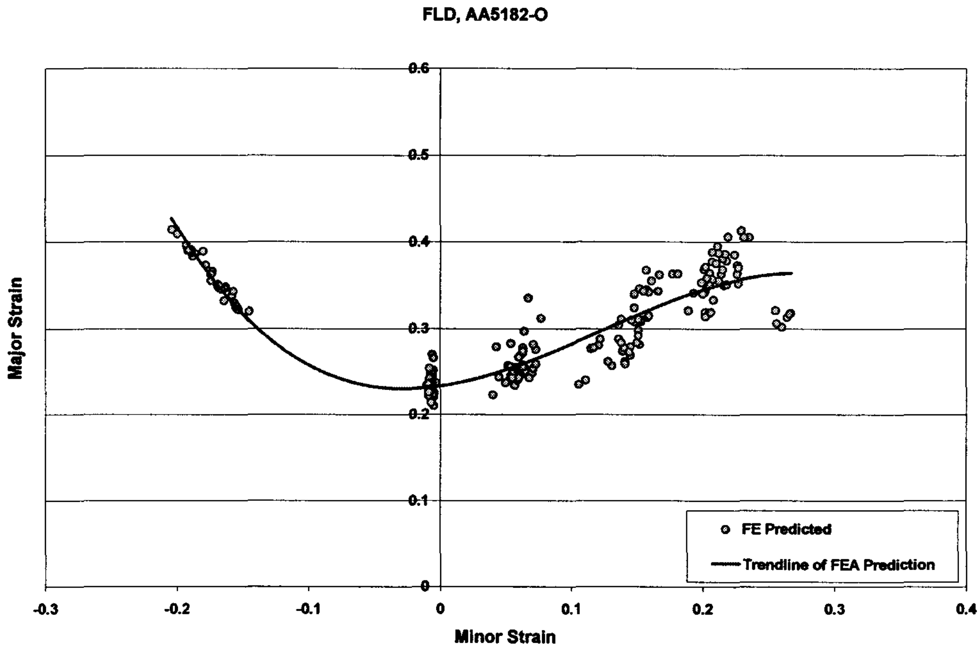

Figure 4.33: Reference limit strain points for FLD of AA5182-O

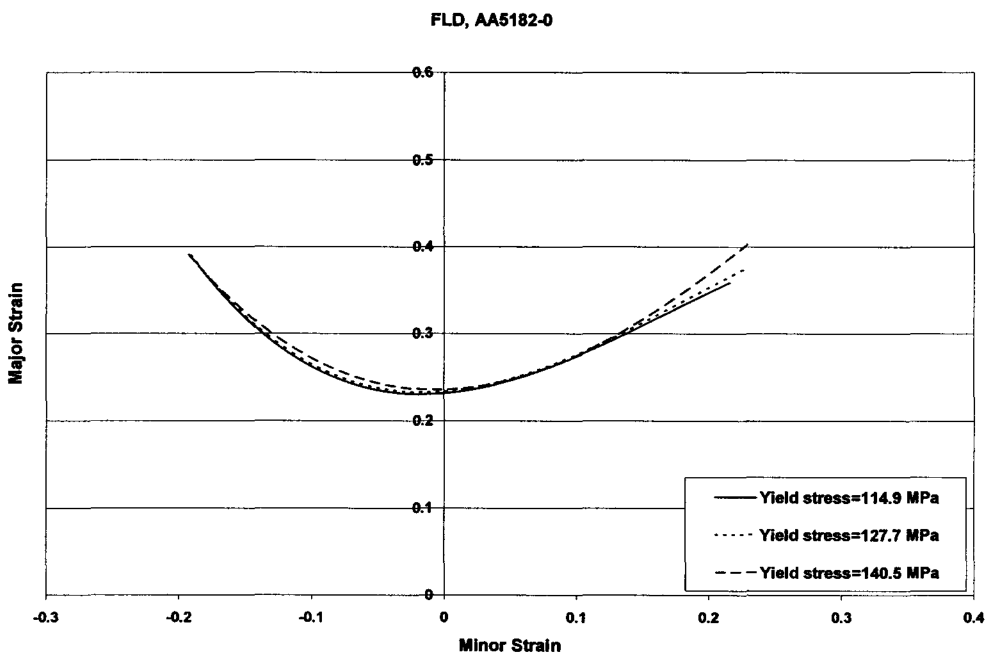

Figure 4.34: FLDs showing the effect of material yield stress

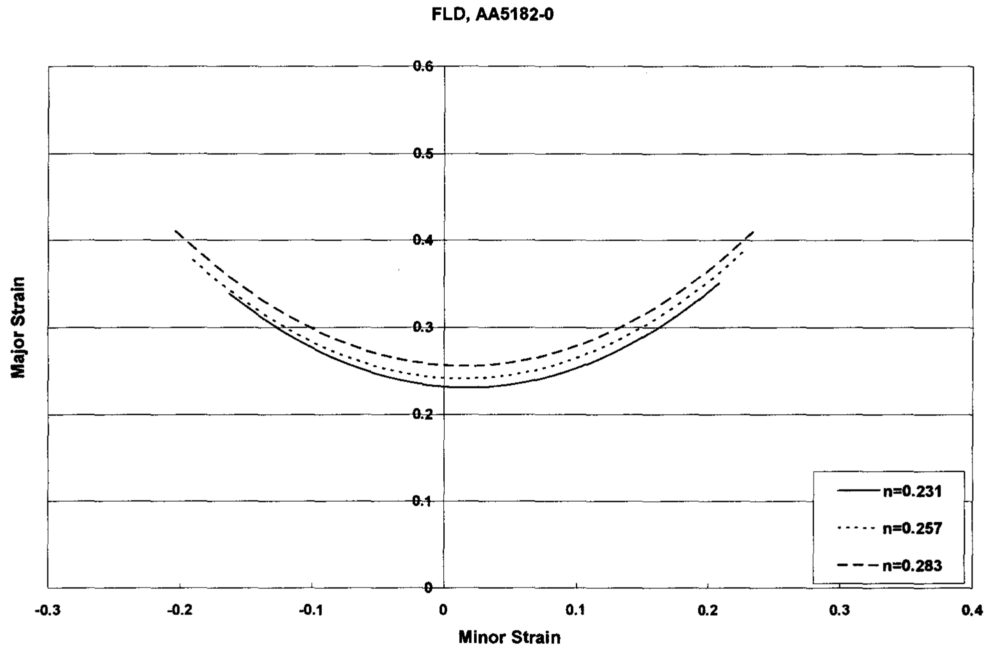

Figure 4.35: FLDs showing the effect of hardening exponent

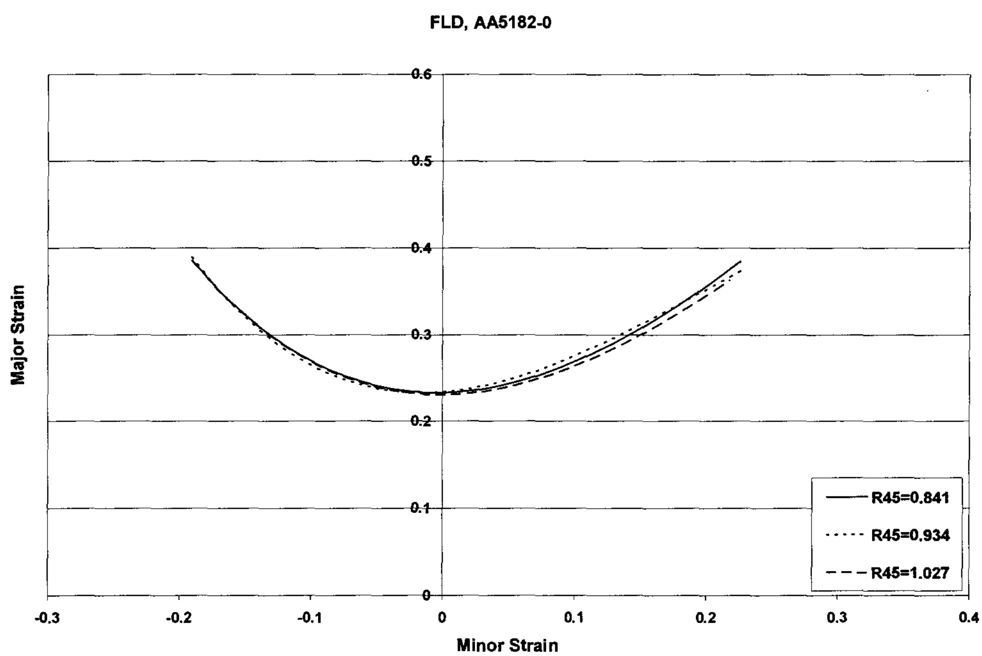

Figure 4.36: FLDs showing the effect of R_{45}

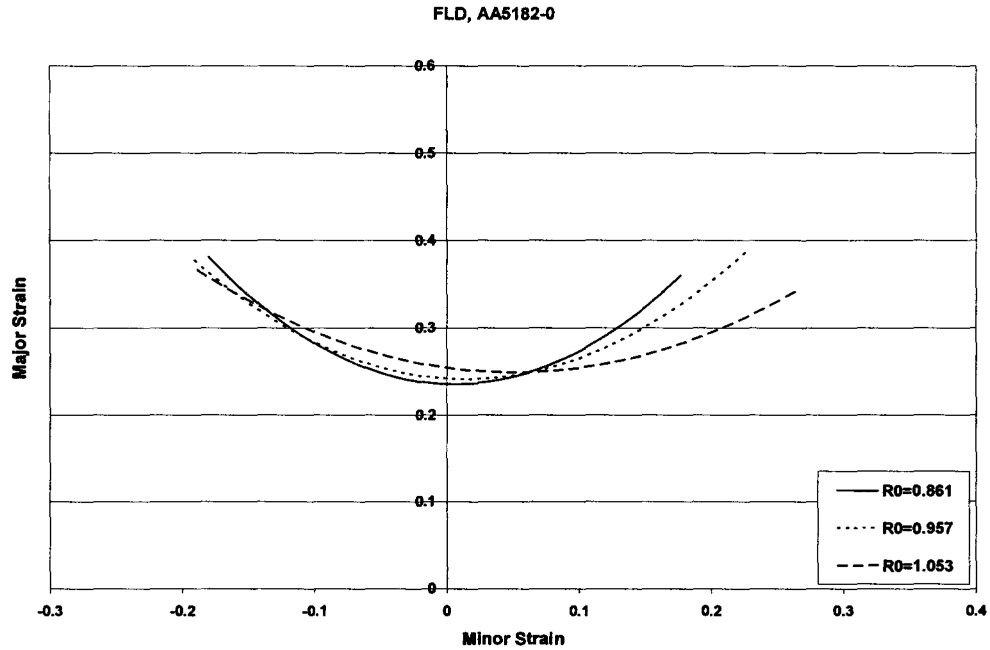

Figure 4.37: FLDs showing the effect of R_0

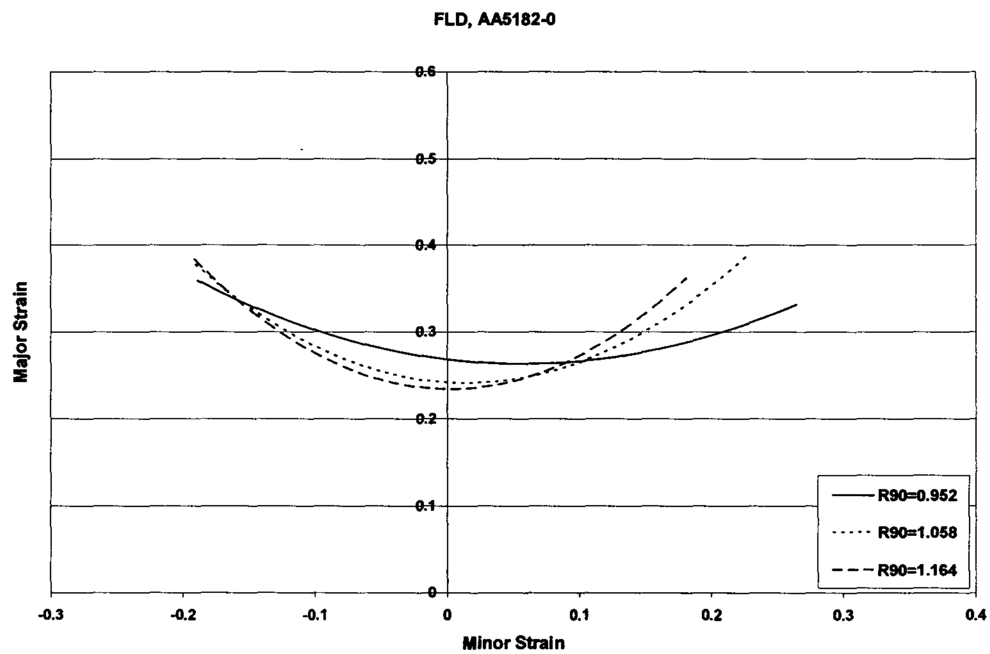

Figure 4.38: FLDs showing the effect of R_{90}

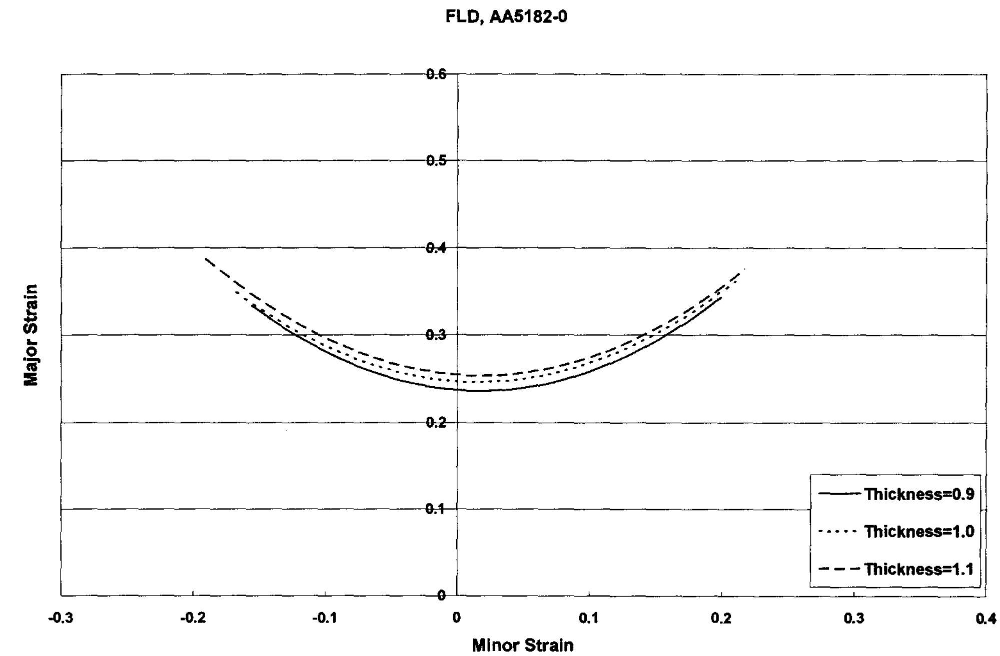

Figure 4.39: FLDs showing the effect of thickness

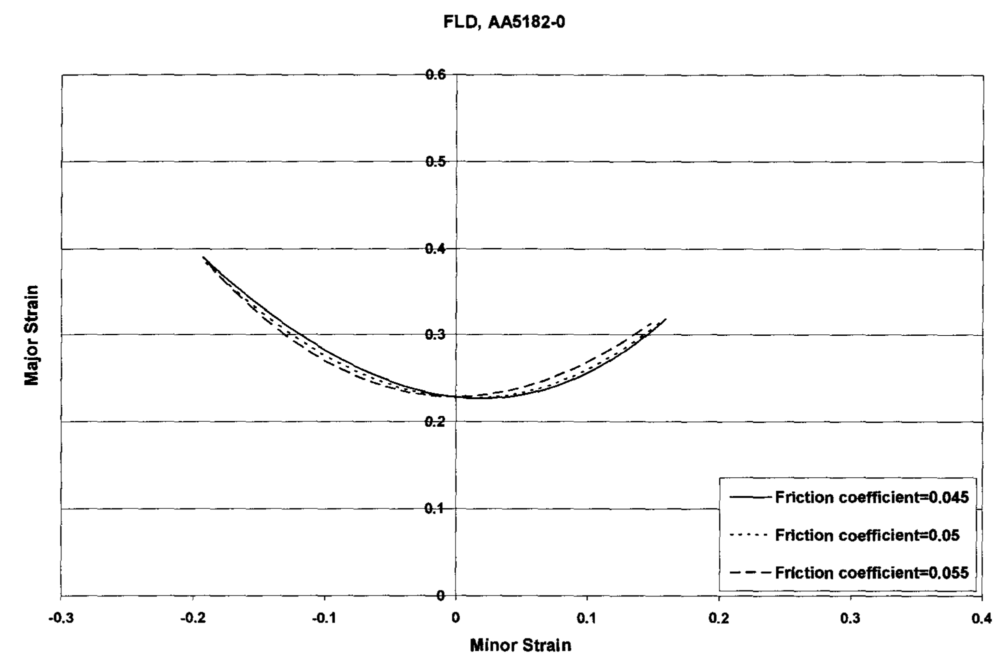

Figure 4.40: FLDs showing the effect of friction coefficient

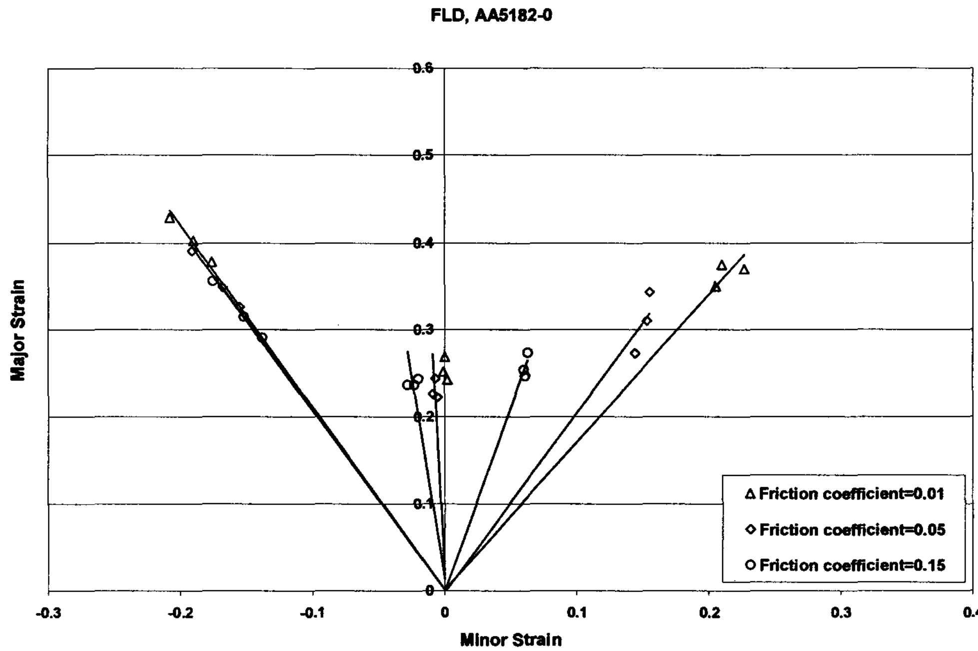

Figure 4.41: FLDs showing the strain paths obtained with different friction conditions

4.3.5.2 Influence of the subjective uncertainty sources

The following four subjective factors have been investigated to see their influence on the shape of FLC for AA 5182-O.

- Selection of measuring elements
- Number of strain paths
- Number of samples per strain path
- Polynomial order used to fit the FLC

(1) Selection of measuring elements

As introduced in the foregoing section, totally 225 forming limit strain points along 5 strain paths with 3 measuring elements in each path are obtained by finite element analysis. For each measuring element, 15 different limit strain values are obtained corresponding to 15 test cases. By randomly picking part of these 225 limit strain points to form three sets of measuring element samples for the purpose of generating the FLD, it can be found that the different set of measuring element sample from the same big pool give the different results of forming limit curve as shown in Figure 4.42.

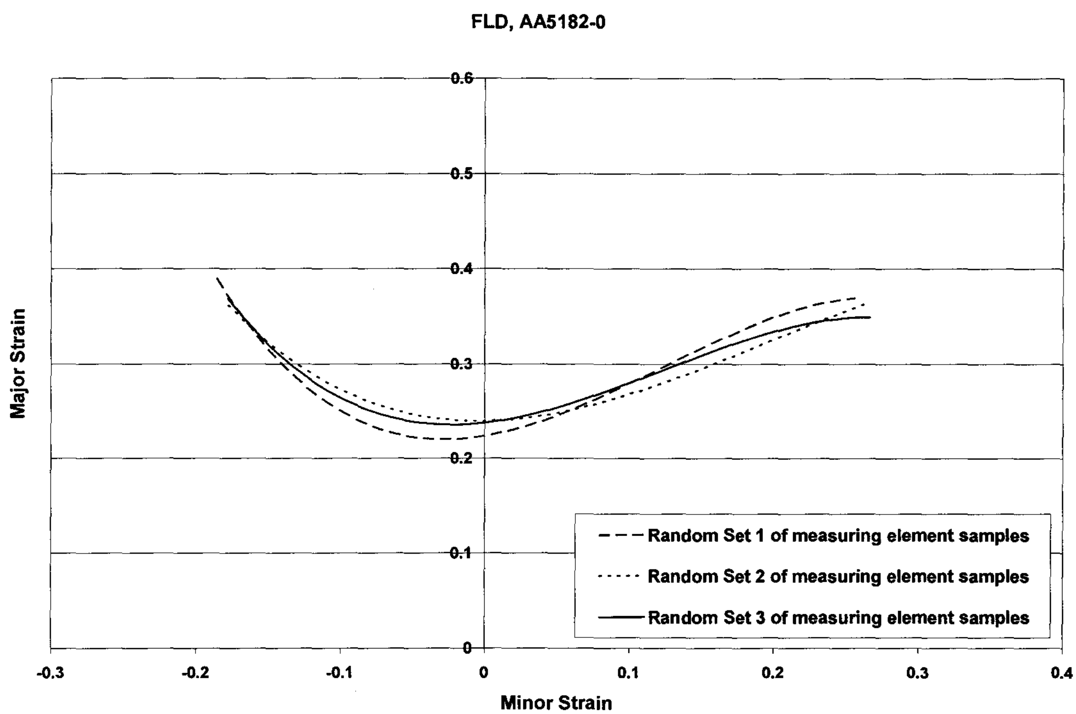

Figure 4.42: FLDs for different set of measuring element samples

(2) Number of strain paths

As discussed before, there are 5 strain paths used to analyze the uncertainty of forming limit in this study including 3 strain paths in biaxial state, 1 path in plane strain state and 1 path in uniaxial state. Figure 4.43 shows the effect of the number of strain paths on the shape of FLC. The curve representing "3 strain paths" is the curve using 1 path in uniaxial state, 1 path in plane strain state and 1 path in biaxial state for producing the FLC. The curve representing "4 strain paths" is the curve using 1 path in uniaxial state, 1 path in plane strain state and 2 paths in biaxial state for producing the FLC. The curve representing "5 strain paths" is the curve using 1 path in uniaxial state, 1 path in plane strain state and 3 paths in biaxial state for producing the FLC. It can be seen that different number of strain paths used in biaxial state for producing the FLC does affect the shape of FLC in the right hand side of FLD. Three FLCs in Figure 4.43 suppose to be identical in the left hand side of FLD. However, due to the polynomial curve fitting used for generating the trendlines, the three FLCs in left hand side are slightly offset.

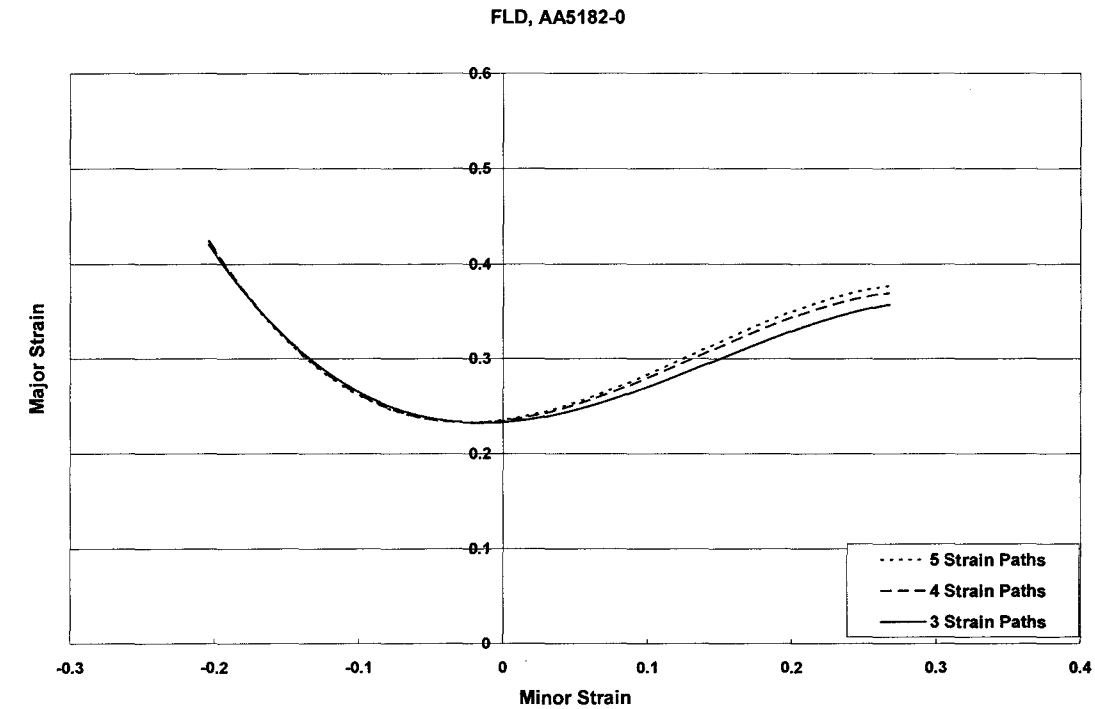

Figure 4.43: FLDs for different combinations of strain paths

(3) Number of samples per strain path

As discussed in the previous section, there are 15 test samples used in each strain path. From Figure 4.44, it can be seen that the predicted FLC based on one sample per strain path has certain different shape compared with the other predicted FLCs based on 5, 10 or 15 samples per strain path. The number of samples per strain path has very little effect on the shape of FLC except the tail of FLC at the balanced biaxial state when the number of samples per strain path is greater than five.

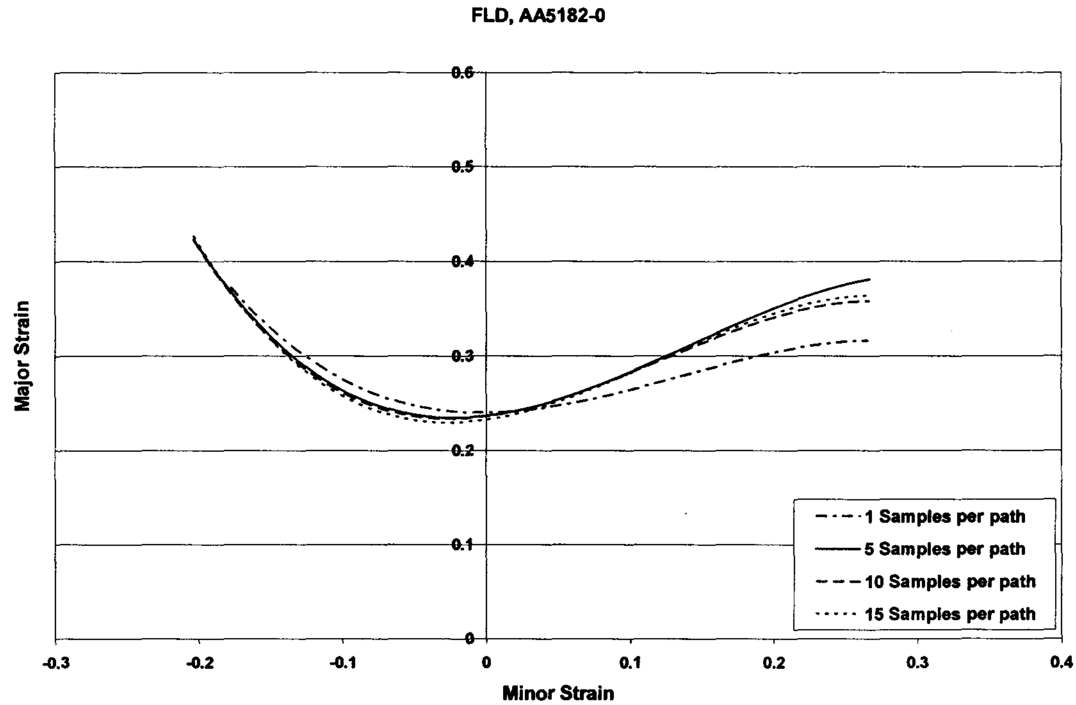

Figure 4.44: FLDs for different number of samples used in each strain path

(4) Polynomial order used to fit the FLC

In our study, the trendline of the strain limit points is treated as FLC. Trendline used for the study of regression analysis is a graphic representation of trends in data series. Mathematically, several equations can be used to calculate the trendline, such as linear equation, polynomial equation, logarithmic equation, exponential equation and so on. In this study, the polynomial equation is used to calculate the trendline for the strain limit points, it calculates the least squares fit through the data points by using the polynomial equation. The different order polynomial equation used will give different shape of curve. It can be seen in Figure 4.45.

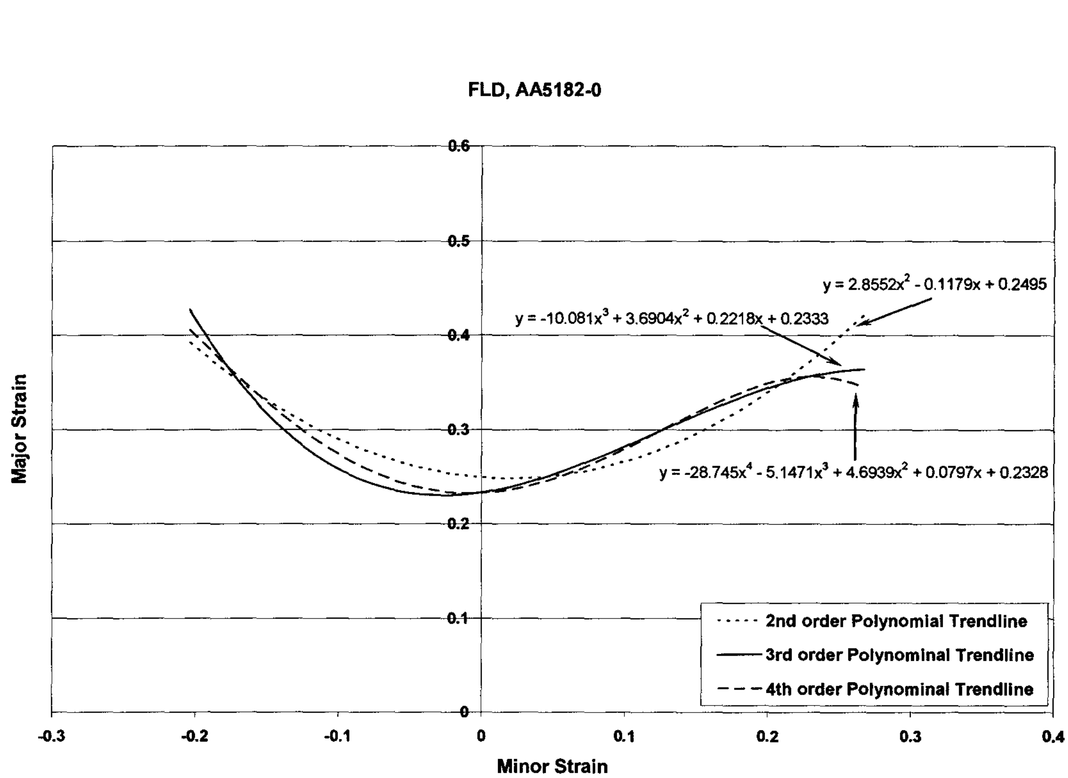

Figure 4.45: FLDs produced by different methods

From Figure 4.42 to Figure 4.45, it can be seen that how to select the measuring elements and what order of the polynomial to fit the FLC are the two most significant subjective factors influencing the shape of FLC. More strain paths used in the biaxial stretching state give relatively higher forming limits in the right-hand side of the FLD. The subjective effect of number of samples per strain path on the shape of FLC can be negligible if more than five samples are used in each path.

4.3.6 FLD Considering Objective and Subjective Uncertainties

As discussed in the above section, the significant scatter of forming limits is observed either in the experimentally determined FLD or in the finite element predicted FLD. Thus the forming limit of a sheet metal is more suitably represented by a forming limit band rather than a forming limit curve. By considering the objective and subjective uncertainties of forming limits, a FLD with the forming limit band for AA 5182-O is presented here.

In this research, five strain paths were used to study the effects of objective and subjective uncertainty sources on the shape of FLD. In each strain path, 15 samples are tested and the principal strains of 3 measuring elements are recorded as the reference points for predicting the FLD. Figure 4.46 shows 15 forming limit strain points of the measuring element No. 350 at the biaxial stretching state with $f_c = 0.01$. The ellipse in the FLD represents the region covering all possible forming limit strains for Element 350 with 99.9% confidence. The ellipse is produced using the software Mathematica by assuming minor strain and major strain following the multi-normal distribution. Figure 4.47 and Figure 4.48 give the 99.9% confidence regions of forming limit strains for the other two measuring elements at the biaxial stretching state with $f_c = 0.01$. By applying the same method, 99.9% confidence regions of forming limit strains for 3 measuring elements at 5 different strain paths are obtained as shown in Figure 4.49 through Figure 4.53.

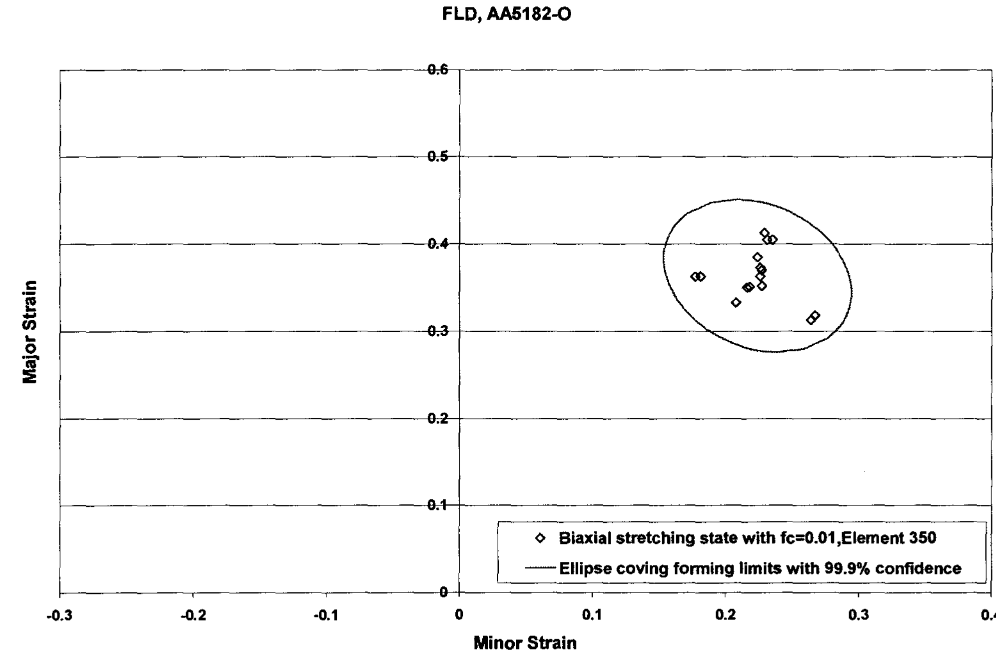

Figure 4.46: 99.9% confidence region of forming limits for element 350 under biaxial stretching state with $f_c = 0.01$

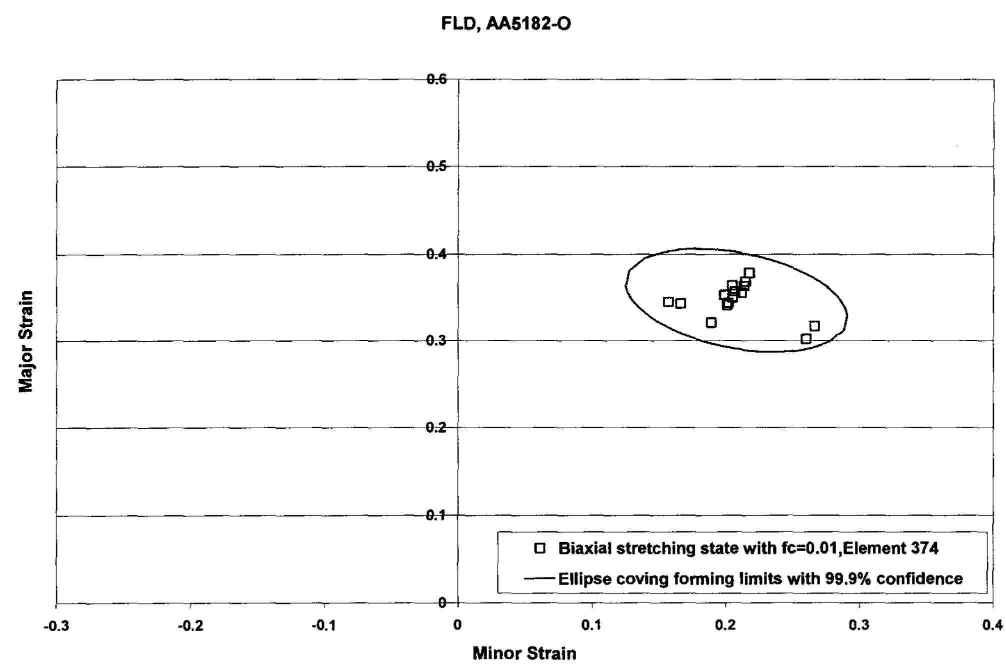

Figure 4.47: 99.9% confidence region of forming limits for element 374 under biaxial stretching state with $f_c = 0.01$

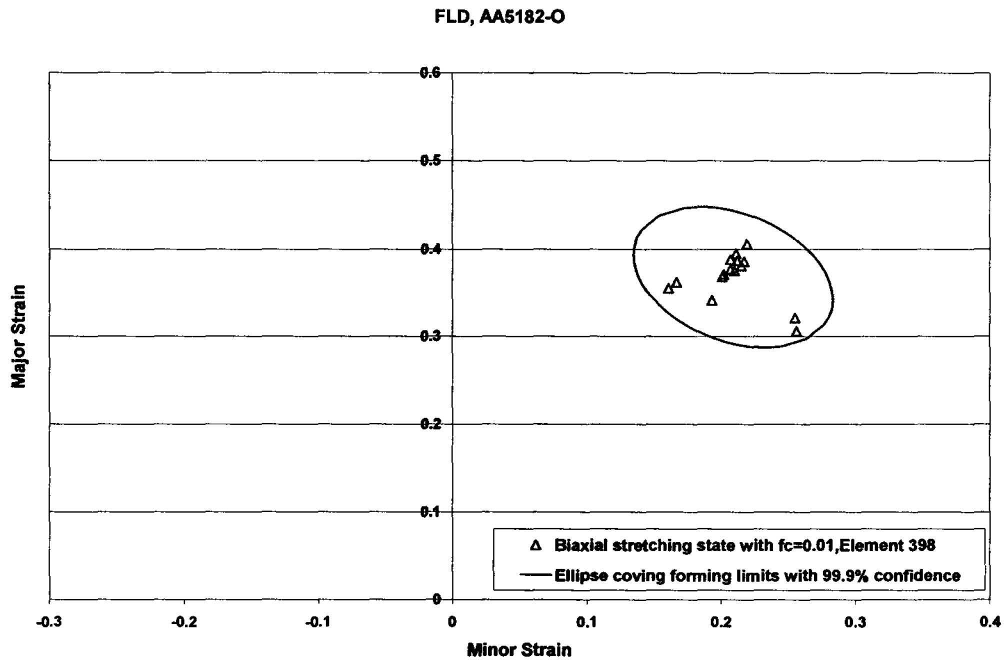

Figure 4.48: 99.9% confidence region of forming limits for element 398 under biaxial stretching state with $f_c = 0.01$

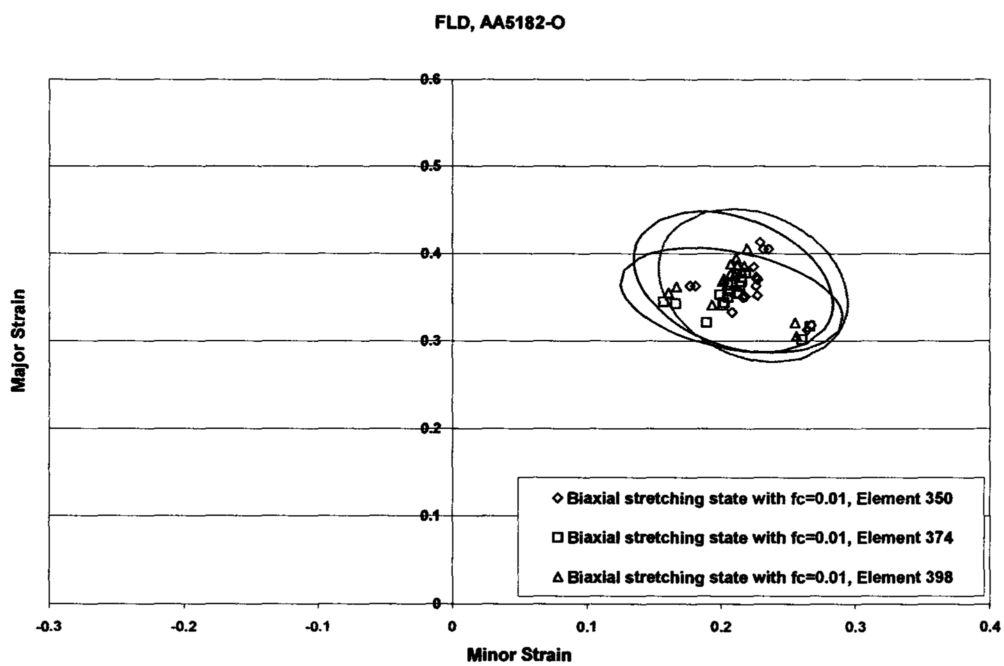

Figure 4.49: 99.9% confidence region of forming limits at biaxial stretching state with $f_c = 0.01$

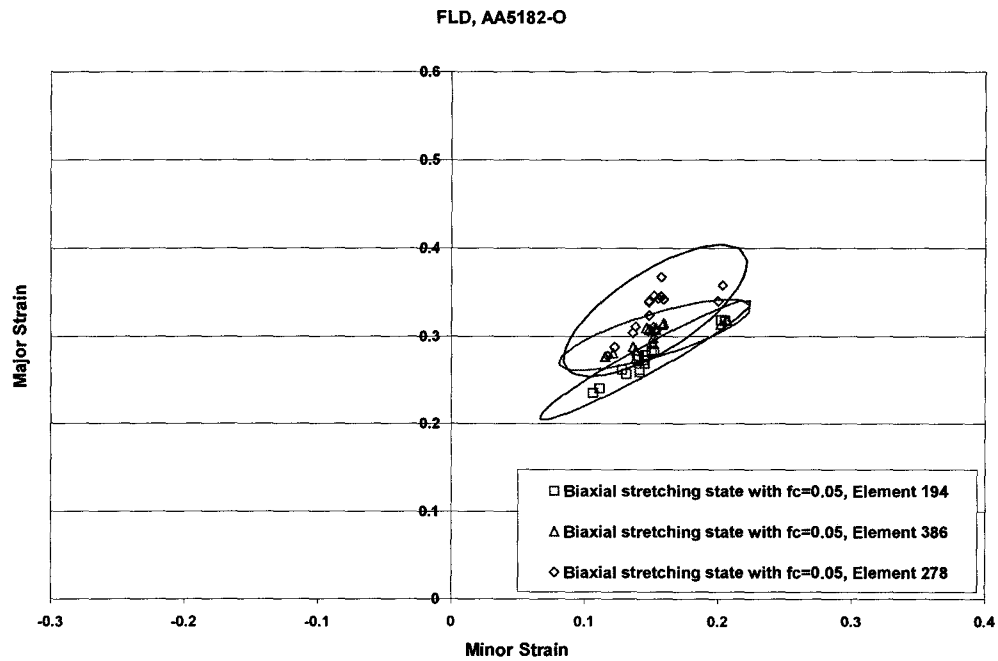

Figure 4.50: 99.9% confidence region of forming limits at biaxial stretching state with $f_c = 0.05$

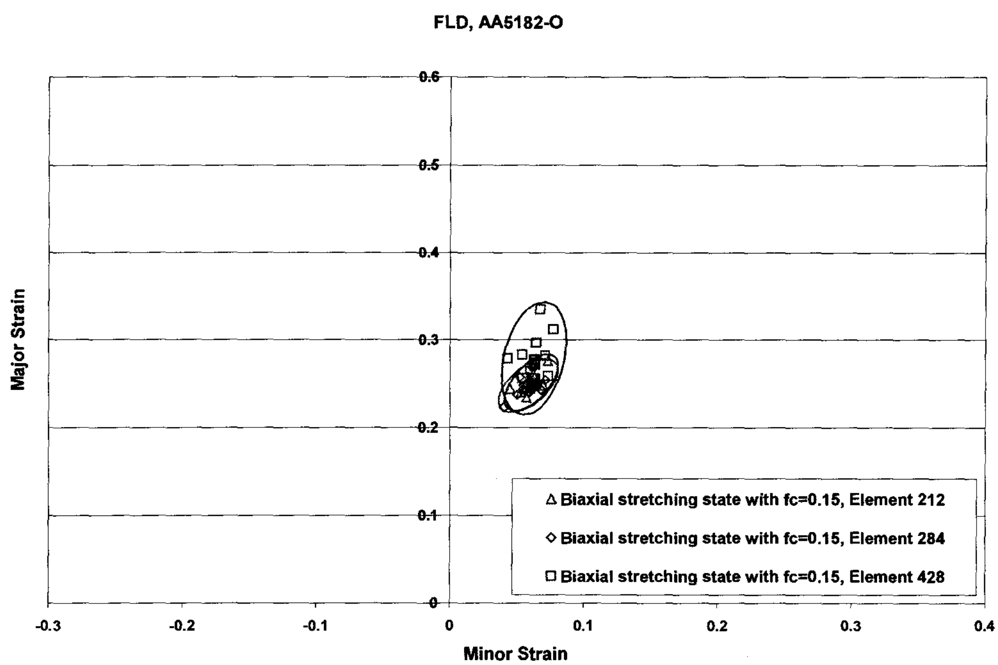

Figure 4.51: 99.9% confidence region of forming limits at biaxial stretching state with $f_c = 0.15$

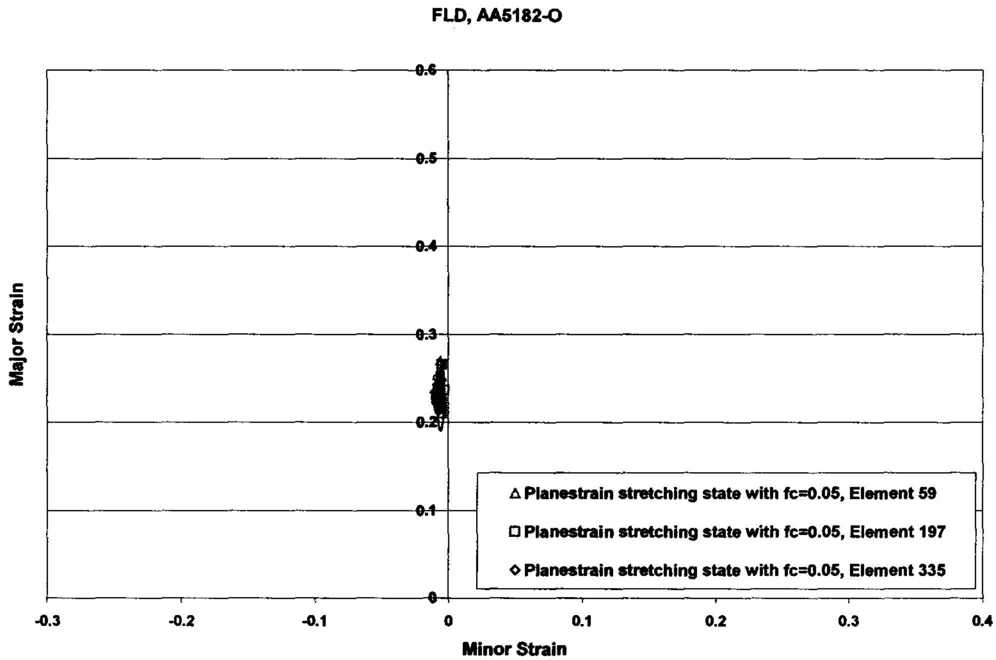

Figure 4.52: 99.9% confidence region of forming limits at plane strain stretching state with $f_c = 0.05$

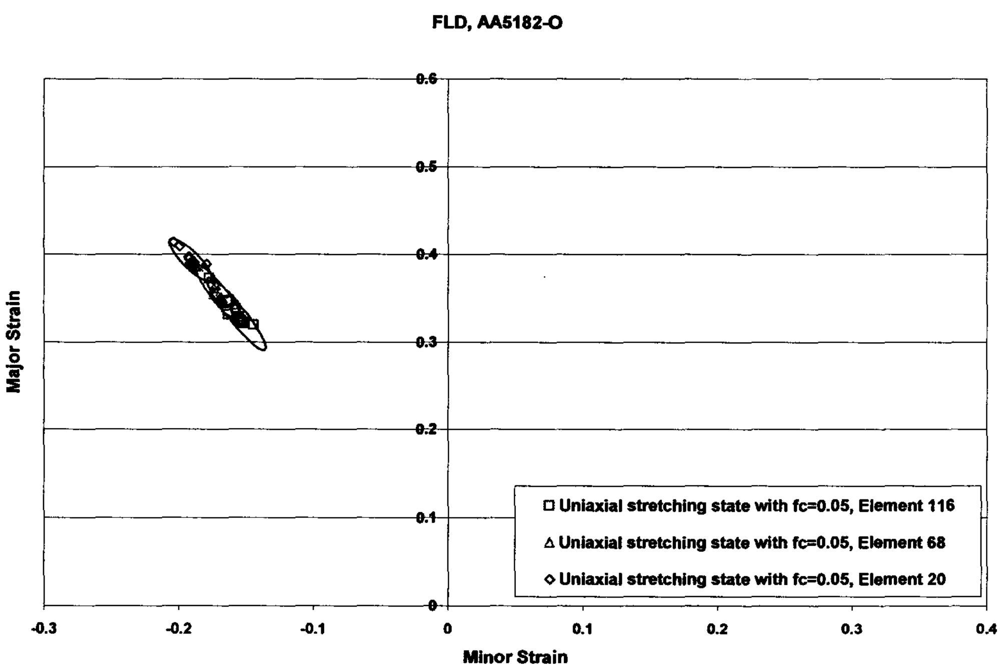

Figure 4.53: 99.9% confidence region of forming limits at uniaxial tension state with $f_c = 0.05$

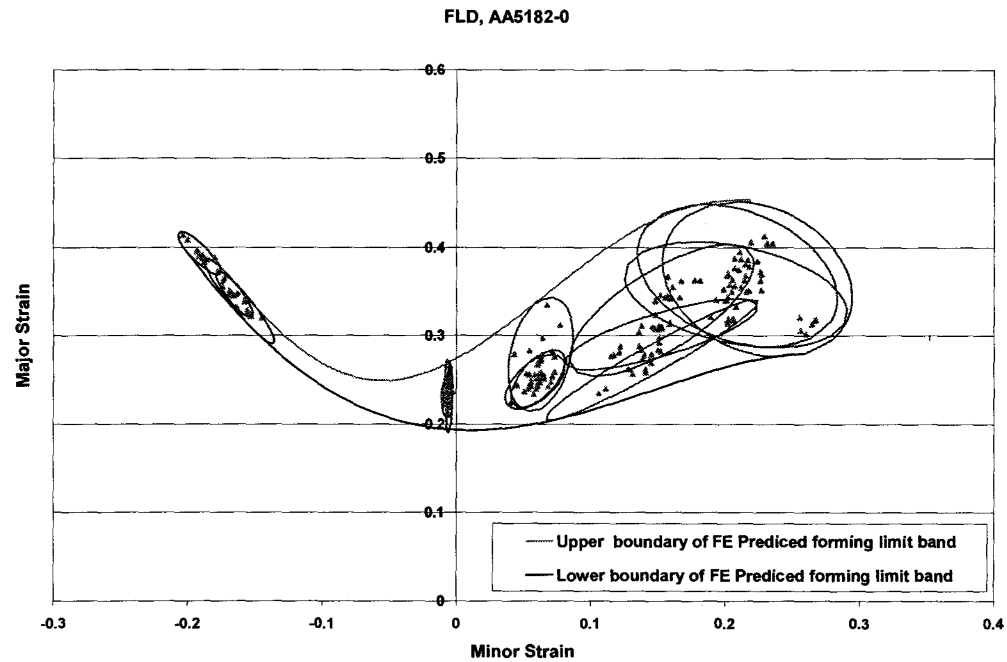

Figure 4.54: 99.9% confidence region of forming limit strains for AA 5182-O

Based on all the above ellipses obtained, a forming limit band covering all the forming limit strains of AA 5182-O with 99.9% confidence is presented as shown in Figure 4.54. From Figure 4.54, it can be seen that all the ellipses are apt to elongate along the specific strain paths than perpendicular to them at the different stretching states except the state closest to balanced biaxial stretching. Generally this observation is in good agreement with the experimental results of Van Minh et al. (1974). Basically the ellipse used in this study is to illustrate the scatter of the strain limits. The area and orientation of ellipse for the different strain paths is depending on the distribution of strain points. The ellipses coving the strain points at the biaxial state with $f_c = 0.01$ (most close to the balanced biaxial state) are kind of different in terms of elongation direction. This is because the larger scatter of strain points is found in this strain path compared to other strain paths. The ellipse is covering more area and oriented to fit all the strain points in. The observation of larger scatter of strain pints at balanced biaxial state can be supported by the experimental findings shown in Figure 12 for DC06 080 by Janssens et al., 2001.

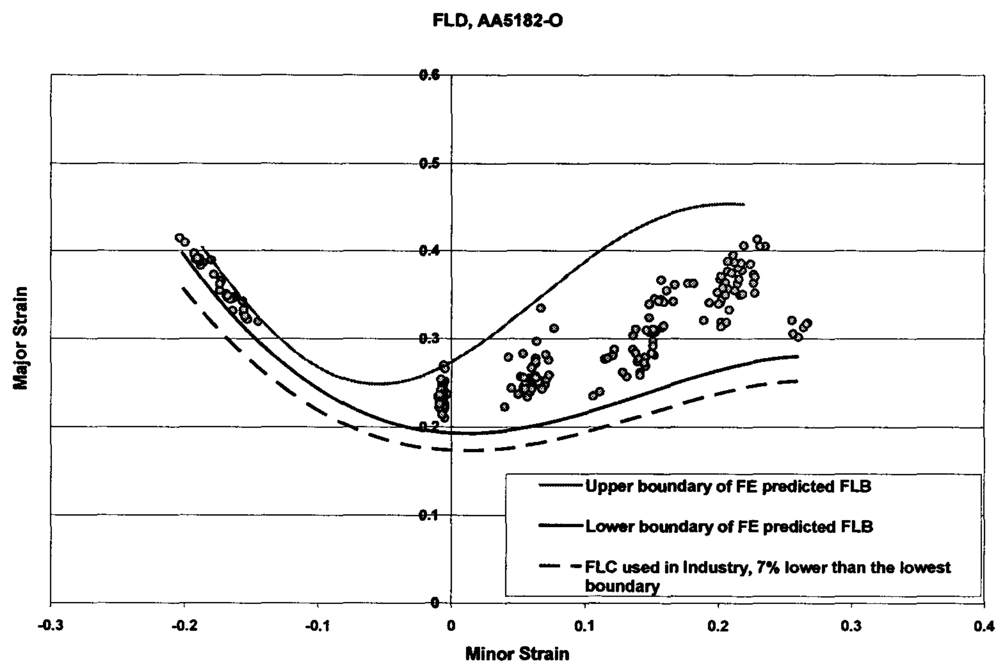

Figure 4.55: Comparison of FLDs of AA 5182-O

By comparing the FE predicted forming limit band with the experimentally derived FLC of AA5182-O (dash line in Figure 4.55), which is usually 7% lower than the lowest boundary (private communications with Jain, 2005), it can be found that our proposed FLD will not only be able to reflect the inherent uncertainty of the forming limit strain, but also will help the designer not be forced into an overly conservative design.

Chapter 5

Improving Reliability by the Taguchi Method

There are many criteria for evaluating the reliability of a tube hydroforming process, however, the thickness of the hydroformed tube is a common concern in industry (Rama et al., 2003), and so the corresponding thickness-thinning ratio can be used as a measure of forming reliability. In the hydroforming process, the values of the forming parameters are known to have a certain scatter around their nominal values, so the results of the process depend on these uncertain parameters. In order to improve the reliability, a set of design parameters that yield predicted performance, i.e., the thinning ratio, to be as insensitive to variation in parameter levels as possible needs to be determined at the design stage.

The Taguchi method, an experimental design method, is a proven tool for this task. It employs a set of orthogonal experimental design arrays to investigate the influence of the forming parameters on the resulting thinning ratio. This knowledge then allows the optimal combination of parameters to be determined. In addition, by incorporating 'noise' parameters into the experiment, knowledge is gained on how the forming parameter levels affect not only the average value of thinning ratio, but also the variance of the thinning ratio. It is shown in this research that the reliability of the process can be improved both by modifying mean process output and by reducing process output variance.

Finite element simulation is used to conduct virtual experiments according to designs developed with Taguchi orthogonal arrays. Results of the experiments are analyzed statistically following the Taguchi approach to determine output mean and variance sensitivity to input parameter values. A tube hydroforming process of expanding a circular tube into a square die is used to illustrate the proposed approach.

5.1 Reliability Analysis Based on Thinning Ratio

Similar to the stress-strength interference model in traditional reliability theory, a resulting thinning ratio-limit thinning ratio interference model is presented in this study. The term "resulting thinning ratio", denoted *rtr*, represents the critical thickness thinning ratio of the hydroformed tube and the term "limit thinning ratio", denoted *ltr*, represents the acceptable interval limits of the thinning ratio which is set by the tube product designers.

In this research, we assume the resulting thinning ratio obeys the normal distribution. The probability density function of the resulting thinning ratio $f_{rtr}(x)$ can then be expressed as:

$$f_{rtr}(x)=\frac{1}{\sigma_{rtr}\sqrt{2\pi}}\exp[-\frac{1}{2}(\frac{x-\mu_{rtr}}{\sigma_{rtr}})^2] \tag{5.1}$$

where μ_{rtr} is the mean value of the resulting thinning ratio and σ_{rtr} is the standard deviation of the resulting thinning ratio.

Usually the permissible thinning ratio for a specific part is given as tolerance interval limits, such as $[m-n/2, m+n/2]$, in industry (Hopperstad et al., 1999). So the limit thinning ratio can be defined as a random variable following the symmetric triangular distribution. Then probability density function of the limit thinning ratio $f_{ltr}(x)$ can be expressed as

$$f_{ltr}(x)=\begin{cases}\dfrac{(x-m+n)}{n^2} & m-n\le x\le m\\ \dfrac{(m+n-x)}{n^2} & m<x\le m+n\end{cases} \tag{5.2}$$

where m is the mean value of the limit thinning ratio and n is the width of the limit thinning ratio. Figure 5.1 shows the resulting thinning ratio-limit thinning ratio interference model. An overlap existing between the two distributions means that failure may occur, with the area of the overlap representing the probability of failure.

The failure state of the part is defined by the limit thinning ratio less than the resulting thinning ratio. So the failure probability, F, of the forming process can be calculated by

$$F = P(ltr - rtr < 0) = \int f_{rtr}(x) f_{ltr}(x) dx \tag{5.3}$$

The reliability of the process, R, is then given by

$$R = 1 - F \tag{5.4}$$

When Eqs. (5.1) and (5.2) are substituted into Eq. (5.3), the failure probability of the process can be expressed as

$$F = \left(\frac{n+m-\mu_{rtr}}{n^2}\right) \times \Phi\left(\frac{m+n-\mu_{rtr}}{\sigma_{rtr}}\right) - \left(\frac{n-m+\mu_{rtr}}{n^2}\right) \times \Phi\left(\frac{m-n-\mu_{rtr}}{\sigma_{rtr}}\right) - 2\times\left(\frac{m+\mu_{rtr}}{n^2}\right) \times \Phi\left(\frac{m-\mu_{rtr}}{\sigma_{rtr}}\right) + \frac{\sigma_{rtr}}{\sqrt{2\pi}n^2} \times \left\{ \begin{array}{l} \exp\left[-\dfrac{(m+n-\mu_{rtr})^2}{2\sigma_{rtr}^2}\right] + \\ \exp\left[-\dfrac{(m-n-\mu_{rtr})^2}{2\sigma_{rtr}^2}\right] - \\ 2\exp\left[-\dfrac{(m-\mu_{rtr})^2}{2\sigma_{rtr}^2}\right] \end{array} \right\} \tag{5.5}$$

where $\Phi(x) = \frac{1}{\sqrt{2\pi}} \int_x^{+\infty} \exp(-\frac{t^2}{2}) dt$.

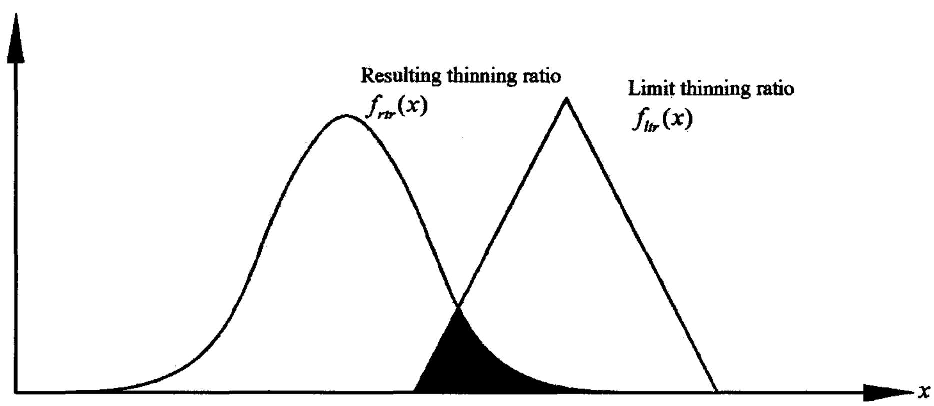

Figure 5.1: Resulting thinning ratio-Limit thinning ratio interference model

5.2 Finite Element Simulation

A typical hydroforming process, in which the tubular blank is expanded into a square die as shown in Figure 5.2, is used as the illustrative example in this Chapter. The material of the tube is assumed to be isotropic elastic-plastic steel obeying the power law stress-strain relationship, $\sigma = k\varepsilon^n$.

Due to symmetry, one-quarter of die and tubular blank was modeled for the simulation. The die was modeled as a rigid body with 2 rigid shell elements and the straight tube consisted of 256 solid elements. The master surface-slave surface contact algorithm was used in all simulations. Friction between the die and the outer surface of tube was taken into account. Figure 5.3 shows the finite element mesh and the effective strain contour after the forming operation. The finite element simulations were performed using the explicit FEM code H3DMAP.

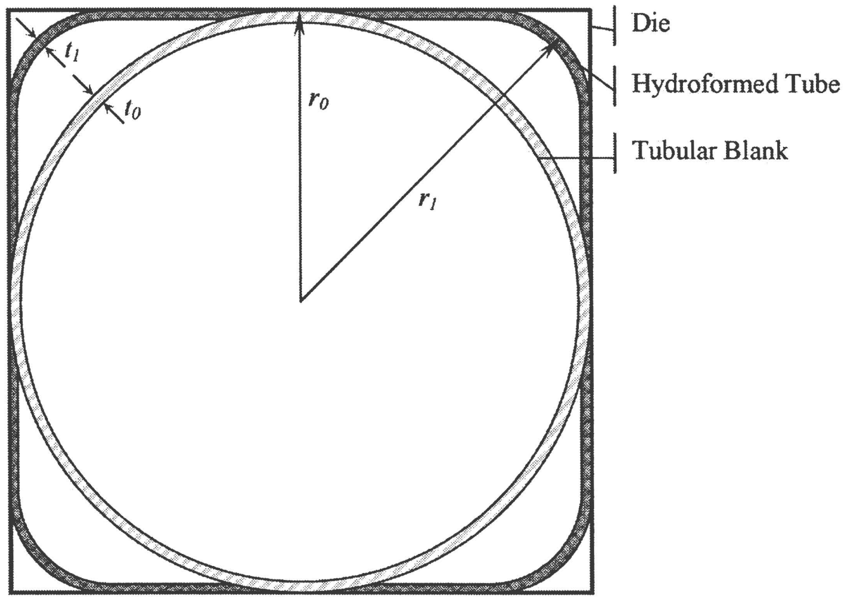

Figure 5.2: Schematic view of the tube hydroforming process

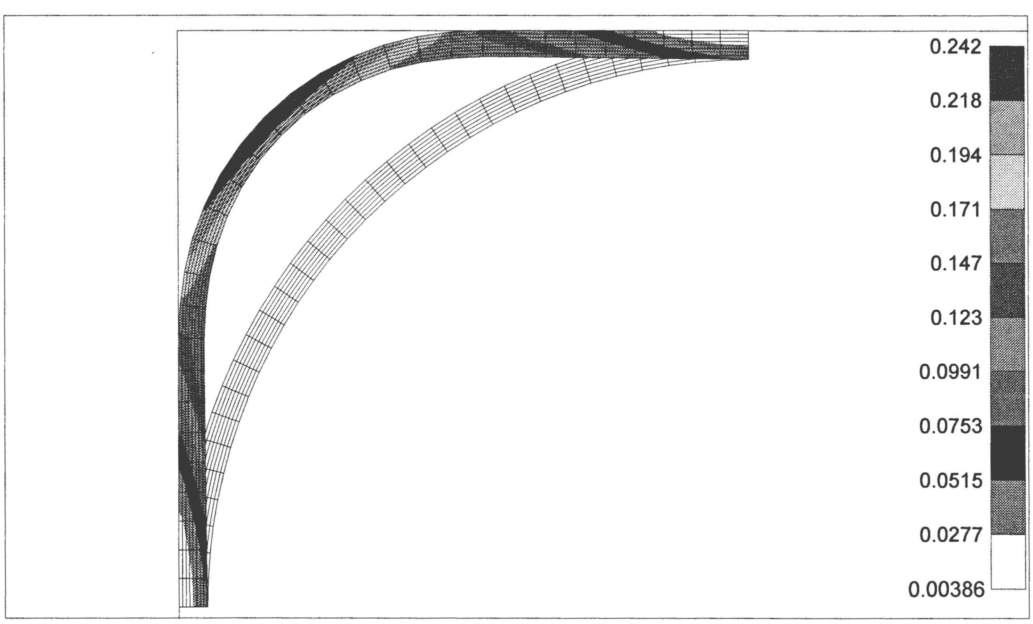

Figure 5.3: Finite element mesh and effective strain contour

5.3 Taguchi Method

Taguchi (1999) believed that the best opportunity to eliminate variation is during design of a product and its manufacturing process. He suggested that the design process should be seen as three stages, i.e., system design, parameter design and tolerance design. System design determines the general specifications, functions and physical envelope of the product. Parameter design determines levels of product and manufacturing process parameters that lead to these general specifications for the product. Finally, tolerance design selects manufacturing tolerance values for each of these parameters. The first two design stages offer the greatest opportunity to maximize product reliability and minimize costs, while the last stage is far less effective at achieving these goals.

Parameter design typically uses designed experiments employing orthogonal arrays to study a large parameter space using only a small number of experiments. In the Taguchi approach, two sets of arrays are used in each experiment, the 'inner' array, in which the factors are the design parameters of the product or process, and the 'outer' array, in which the factors are the 'noise' factors the product or process is exposed to. Noise factors are those uncontrollable (or expensive to control) parameters that can affect process output. For example, in hydroforming, material properties will vary slightly from part to part. By including the variability of such factors in the experimental design, the sensitivity of the process output to such variability can be determined and minimized. In the context of this work, reduced output variability will lead to improved process reliability.

5.3.1 Choice of Quality Characteristic

As discussed in a previous section, the tube wall thickness thinning ratio is used as a measure of reliability of the tube hydroforming process. Therefore, the thinning ratio can be chosen as the quality characteristic for minimization. The thinning ratio is defined by

$$\mathit{Thinning\ ratio}(\%) = \frac{t_0 - t_1}{t_0} \times 100 \tag{5.6}$$

where t_0 is the original thickness of the tube as shown in Figure 5.2 and t_1 is the minimum thickness of the hydroformed tube.

Typically, the final size of the hydroformed tube is a product design parameter. This final size is determined from the 'bulge ratio' defined by

$$\mathit{Bulge\ ratio}(\%) = \frac{r_1}{r_0} \times 100 \tag{5.7}$$

where r_1 is the maximum radius of the hydroformed tube and r_0 is the original radius of the tube as shown in Figure 5.2. In order to investigate the influence of the forming parameters on the thinning ratio, a specific bulge ratio is set for all the simulation cases.

5.3.2 Construction of Orthogonal Arrays

Three kinds of forming parameters influence the hydroformability, i.e., geometric parameters, material parameters and process parameters. Variations of these parameters directly affect the forming quality. Two controllable forming parameters selected as the design parameters in this study are thickness of tube and the material grade. To evaluate these factors, three levels are chosen for each parameter as shown in Table 5.1. Different material grades lead to different yield strength values. Two uncontrollable parameters selected as the noise factors are the friction coefficient and the material hardening exponent. Two levels for each noise factor are considered, as shown in Table 5.2. The design parameters are allocated to the inner array using a Taguchi 'L_9' orthogonal array (i.e., an array with 9 runs allowing three levels of each factor), and the noise factors are allocated to the outer array in a 'L_4' orthogonal array (i.e., an array with 4 runs allowing two levels of each factor), as shown in Table 5.3. By combining both these arrays into an experimental design, 36 combinations of the forming and noise parameters are evaluated in separate experimental runs.

Table 5.1: Level of design parameters

Designation	Design parameters	Level 1	Level 2	Level 3
A	Thickness of Tube (mm)	1.5	2	2.5
B	Yield Strength (MPa)	345	414	483

Table 5.2: Level of noise factors

Designation	Noise factors	Level 1	Level 2
C	Friction coefficient	0.9	1.1
D	Hardening Exponent	0.12	0.14

Table 5.3 Orthogonal array, critical thinning ratios and S/N ratios

						Thinning ratio (%)						
	Inner array: Design parameters					Outer array: Noise factors						
					C	1	1	2	2			
					D	1	2	1	2			
					$C \times D$	1	2	2	1			
Run No.	A	B	$A \times B$	$A \times B$		N_1	N_2	N_3	N_4	Average	Standard Deviation	S/N
1	1	1	1	1		13.29	13.09	13.22	13.13	13.18	0.0900	-22.40
2	1	2	2	2		13.46	13.46	13.25	13.44	13.40	0.1021	-22.54
3	1	3	3	3		14.00	14.36	13.94	14.26	14.14	0.2020	-23.01
4	2	1	2	3		15.91	15.56	15.11	15.42	15.50	0.3318	-23.81
5	2	2	3	1		16.03	15.29	15.71	15.30	15.58	0.3568	-23.85
6	2	3	1	2		18.38	20.64	18.41	20.91	19.59	1.3786	-25.85
7	3	1	3	2		14.97	14.42	14.94	14.47	14.70	0.2954	-23.35
8	3	2	1	3		14.62	14.19	14.62	14.15	14.40	0.2603	-23.17
9	3	3	2	1		16.11	18.85	16.06	18.41	17.36	1.4804	-24.81

5.4 Results and Discussion

The virtual experiments were conducted using the finite element simulation according to the array in Table 5.3. The bulge ratio was set as 120% for all the forming cases so that the simulation stopped when the maximum radius of the hydroformed tube reached 1.2 times the original radius. The minimum tube thickness, leading to the critical thickness thinning ratio, occurred at the 45° corner position, as shown in Figure 5.2, in all the cases. The critical thinning ratio in each of the 36 experimental runs is given in Table 5.3.

5.4.1 Mean Value Analyses

The resulting thinning ratio is assumed to follow the normal distribution, so the mean value of the response over different noise levels can be determined as the average value, that is

$$\mu_{rtr} = \frac{1}{n}\sum_{i=1}^{n} y_i \tag{5.8}$$

where n is the number of the trial conditions, y_i is the value of the corresponding critical thinning ratio. The mean values of thinning ratio at each run of inner array are shown in Table 5.3.

The mean values of the thinning ratio for each design parameter at levels 1 to 3 are shown in Table 5.4. Thinning ratio values are plotted in Figure 5.4 for noise factor values N_1 to N_4, along with the mean response value at each factor level and the total average for all experimental runs. The large difference in response for different noise factor values when design parameter *B* (i.e., material yield strength) is at level 3 shows that a strong interaction exists between these factors. Thus, selection of suitable values of the design parameters can reduce the sensitivity of the process output to noise factors.

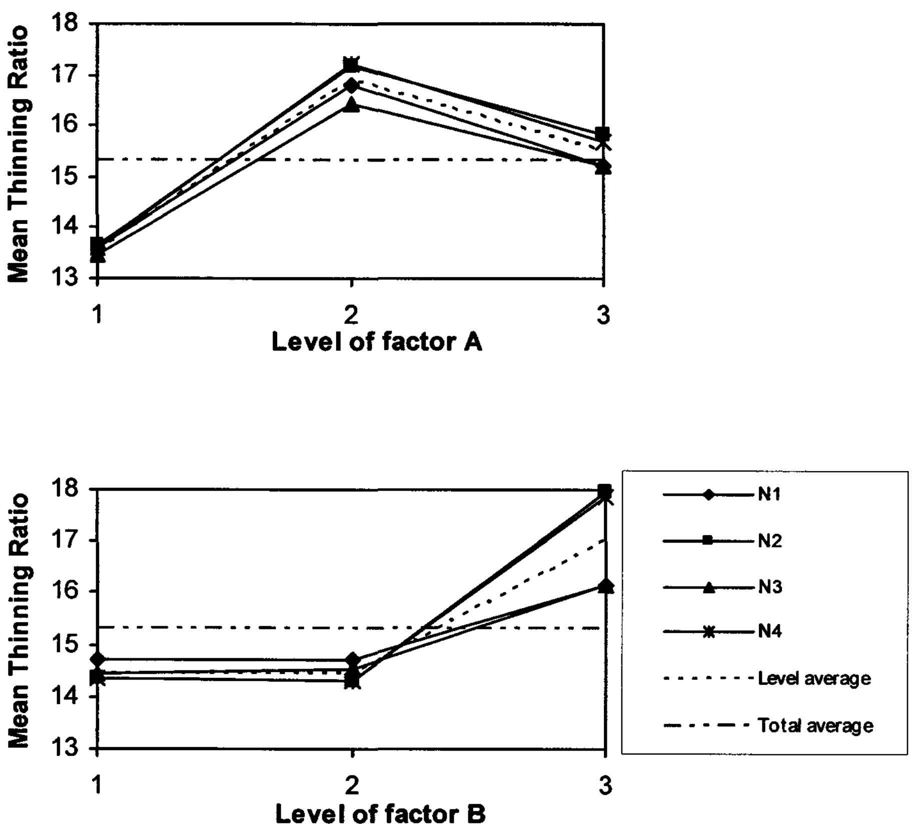

Figure 5.4: Mean values of thinning ratio for each design parameter

Table 5.4: Design parameters' effects on mean values

	Average value of thinning ratio (%)									
	A (Thickness of tube)					B (Yield strength)				
Level	N1	N2	N3	N4	Level average	N1	N2	N3	N4	Level average
1	13.58	13.64	13.47	13.61	13.58	14.72	14.36	14.42	14.34	14.46
2	16.77	17.16	16.41	17.21	16.89	14.70	14.31	14.53	14.30	14.46
3	15.23	15.82	15.21	15.68	15.48	16.16	17.95	16.14	17.86	17.03

Note: Total average value of the thinning ratio is 15.32%.

5.4.2 Variance Analysis

The variance of the thinning ratio is approximated as

$$\sigma_{rtr}^2 = \frac{1}{n-1}\sum (y_i - \mu_{rtr})^2 \tag{5.9}$$

The standard deviation of thinning ratio is then the square root of the variance. The value at each run of the inner array is shown in Table 5.3.

The standard deviations of the responses of the thinning ratio for each design parameter levels 1 to 3 are shown in Table 5.5 and are plotted in Figure 5.5. Figure 5.5 shows that the process variance is minimized by setting Factor A to level 1 and Factor B to level 1 or 2. If this is practical, selecting these levels will minimize process variation and improve robustness to changes in the noise factor levels.

Table 5.5: Design parameters' effects on standard deviation

	Standard deviation of thinning ratio (%)	
Level	A (Thickness of tube)	B (Yield strength)
1	0.1313	0.2390
2	0.6890	0.2397
3	0.6787	1.0203

Note: Total average standard deviation of the thinning ratio is 0.4997%

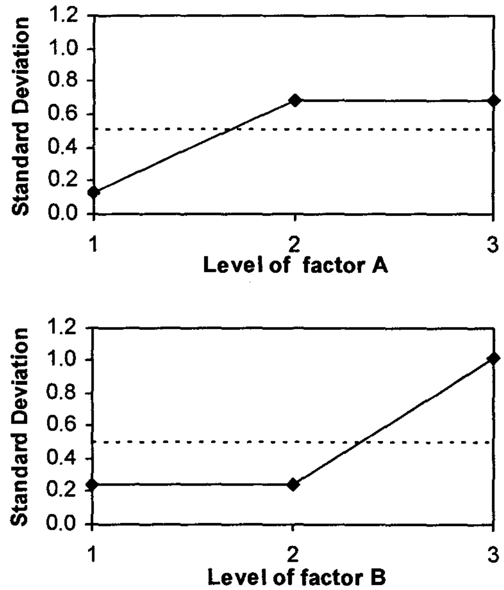

Figure 5.5: Standard deviation of thinning ratio for each design parameter

5.4.3 S/N Analyses

The Taguchi method uses the signal-to-noise (S/N) ratio instead of the average response value to analyze the quality characteristic because the S/N ratio can reflect changes in both the average and variation of the quality characteristic. The thinning ratio quality characteristic used in this study is to be minimized, thus the "lower is better" mean square deviation should be used.

The S/N ratios of the thinning ratio in the 9 trial conditions of inner array are shown in Table 5.3. The average S/N ratio of the thinning ratio for each design parameter at levels 1 to 3 are shown in Table 5.6 and plotted in Figure 5.6.

Table 5.6: Design parameters' effects on S/N ratio

	Average S/N ratio		
	Level 1	Level 2	Level 3
A (Thickness of tube)	-22.6512	-24.5057	-23.7754
B (Yield strength)	-23.1853	-23.1879	-24.5592

Note: Total average S/N ratio is -23.6311

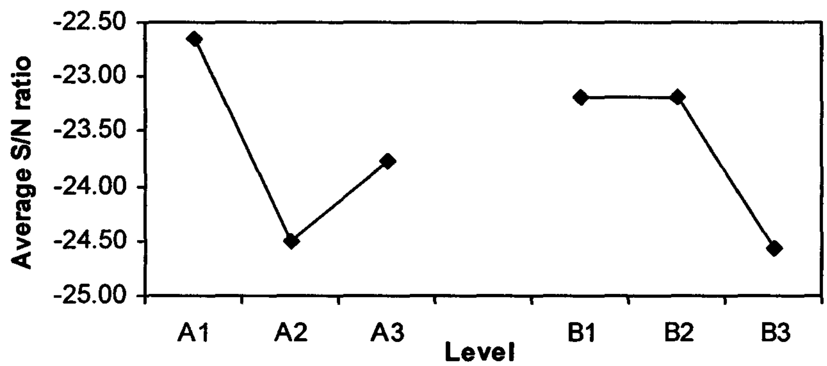

Figure 5.6: S/N ratio graph for the thinning ratio

From Table 5.6 and Figure 5.6, it can be concluded that *A*1*B*1 is the optimal combination of the design parameters for the minimization of the thinning ratio. This conclusion is consistent with the results obtained on the analyses of the mean value and standard deviation of the thinning ratio. It confirms that S/N ratio analyses of Taguchi method can optimize the lower-is-better quality characteristic not only by minimizing the average value, but also by minimizing the variation.

5.4.4 ANOVA Analyses

Analysis of variance (ANOVA) is used to quantitatively investigate the effects of the parameters on the quality characteristic. It uses the sum of squares to partition the overall variation from the average S/N ratio into the contribution by each of the parameters and the error. The percentage contribution by each parameter in the total sum of the squared deviations can be used to evaluate the importance of the parameters change on the process performance.

The results of an ANOVA for the thinning ratio are shown in Table 5.7. The tube thickness is the most significant parameter influencing the thinning ratio. The effect of the yield strength is relatively smaller than that of thickness. The interaction of thickness and yield strength exists but is mild. This is also seen in interaction plot shown in Figure 5.7. The three curves are mostly, but not exactly, parallel with each other indicating some interaction between the factor levels.

Table 5.7: Analysis of variance for thinning ratio

	DOF	Sum of squares	Contribution
A (Thickness of tube)	2	5.24	53.42%
B (Yield strength)	2	3.77	38.44%
$A \times B$	4	0.80	8.14%
Total	8	9.80	100%

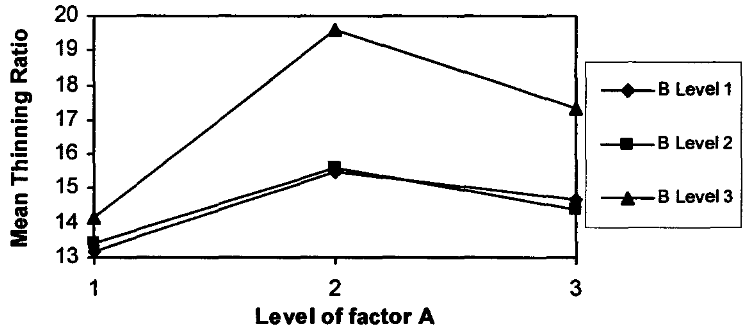

Figure 5.7: Interaction analysis of parameters A and B

5.4.5 Improvement of Reliability

The example hydroforming case was assumed to start with the two design parameters, tube thickness and yield strength, having nominal values of 2 mm and 414 MPa, respectively. From Table 5.3, at this initial condition, the mean value of the resulting thinning ratio would be 15.58% and the standard deviation would be 0.3568% (Run #5). The Taguchi S/N analysis showed that an improved combination of the design parameters was a thickness of 1.5 mm and strength of 345 MPa, i.e. factor levels $A1B1$. This combination improves both the mean thinning ratio to 13.18% and the standard deviation to 0.09% (Run #1).

The acceptable thinning ratio for the tube hydroforming process discussed in this research is set as the interval limits [15.5%, 16.5%]. A triangular distribution is used to describe the limit thinning ratio, as shown in Figure 5.8, the mean value of the limit thinning ratio is 16% and the width is 0.5%.

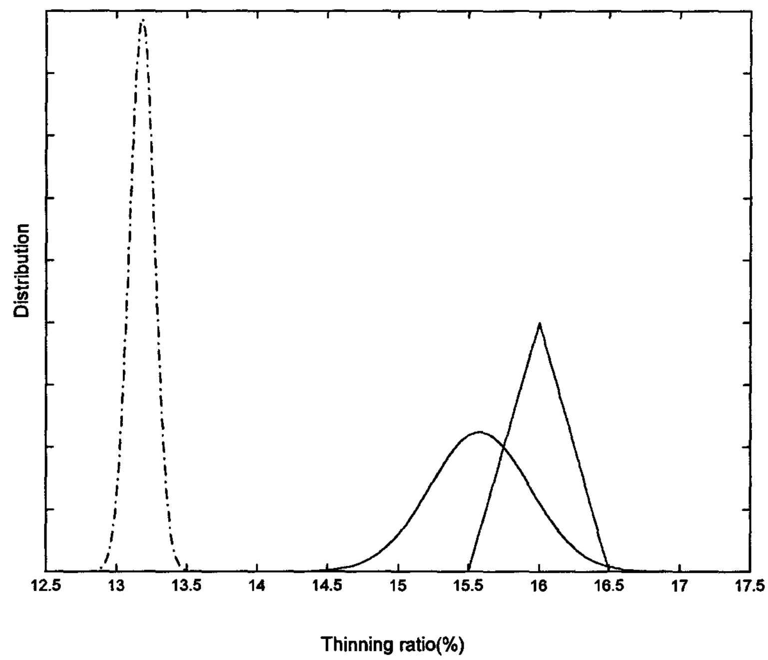

Figure 5.8: Reliability of the process with the initial and optimal forming parameters

According to Eqs. (5.4) and (5.5), the initial reliability of the tube hydroforming process would be 42.19%. The dashed line in Figure 5.8 shows the distribution of the thinning ratio after applying Taguchi S/N optimization. Not only has the thinning ratio distribution shifted substantially away from the maximum acceptable thinning ratio, but also the variance due to noise factors has decreased significantly. The reliability of the process now approaches 100%, and is less likely to be affected by normal process variation than in the base case.

Chapter 6

Multi-objective Optimization Based on Taguchi Method

Problems related to the improvement of product quality and production efficiency can always be associated with optimization procedures. The Taguchi method can optimize quality characteristics through the setting of design parameters, and can reduce the sensitivity of the system performance to sources of variation (Yang & Tarng, 1998; Huh et al., 2003; Anastasiou, 2002). But, if more than one quality characteristic is simultaneously considered for the same process, the Taguchi Method may not give a unique optimal combination of parameters, especially when these quality characteristics compete with each other. Attempting to optimize more than one objective makes the optimization problem a multi-objective one (Shabeer & Wang, 2000).

Mathematically, there are many methods to solve the multi-objective problem. Objectives usually conflict, so that the conditions leading to an optimal value of one objective gives non-optimal values of the others. Under such circumstances, a state (i.e., a particular realization of problem parameter values) is preferred to another state if at least one objective is improved while none of the other objectives are worsened. If a state is found such that no other state is preferred in this way, it has the quality of being Pareto optimal. A given problem may have many Pareto optimal solutions, the collection of which forms the Pareto set, or Pareto front, of the problem.

Common multi-objective solution methods are the weighted sum method, the ε-constraint method and the goal attainment method. The weighted sum method has a deficiency in that the Pareto optimal set is not available on non-convex portions in the criterion space. A difficulty of the ε-constraint method is to select a suitable ε to ensure a feasible solution, and a further disadvantage of this approach is that the use of hard constraints is rarely adequate for expressing true design objectives. The goal attainment method provides a convenient intuitive interpretation of the design problem which is solvable using standard optimization procedures, and there is always at least one Pareto optimal solution, also called the non-dominated solution, which balances the objectives in a unique and optimal way (Marler & Arora, 2003). In this chapter, a multi-objective optimization approach is proposed by integrating the classical mathematical optimization method with the Taguchi method, and the optimization problem is solved by the goal attainment method.

A free bulging tube hydroforming process is a common test case in the research on tube hydroformability because it has many forming parameters involved in affecting its hydroformability. The objective of the free bulging process is to get a high bulge ratio while no necking failure happens. Obtaining an optimal combination of the forming parameters for satisfying these objectives is discussed in the following sections.

6.1 Methodology

The objective here is to investigate the influence of forming parameters on hydroformability to improve the hydroformed tube quality. The basic steps for achieving the above target are shown in Figure 6.1. First, the quality characteristics and the forming parameters are selected, and the appropriate orthogonal array is constructed. Finite element simulations are performed based on the arrangement of the orthogonal array, and the results are then transformed into Taguchi signal-to-noise (S/N) ratios. Statistical analysis of variance (ANOVA) is performed to see which parameters are significant. After eliminating the insignificant parameters, the remaining significant parameters are analyzed to obtain more information of their effects on the quality characteristics. Empirical models are then built through regression of the significant parameters, and the multi-objective optimization is performed to maximize these S/N ratios. Finally, a confirmation experiment is conducted to verify the optimal parameter levels selected.

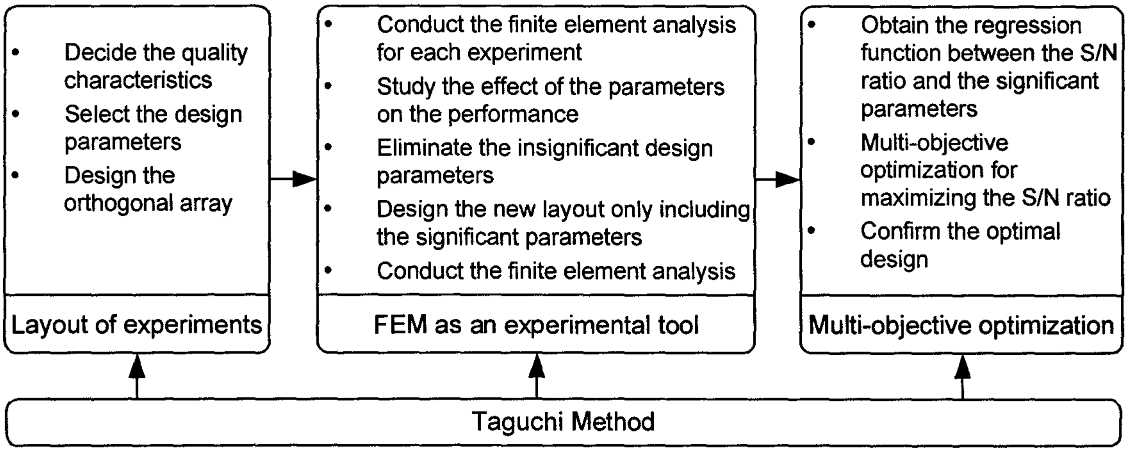

Figure 6.1: Multi-objective optimization using Taguchi Method

6.2 Free Bulging Tube Hydroforming Process

6.2.1 FEM Simulation

Finite element simulation is used as a numerical experimental tool. The hydroforming process of free bulging used in Chapter 3 is employed again as an example in this study (See Figure 3.3). Table 6.1 shows the nominal values of the process parameters, geometries of the tube and tooling, and the material properties of the tubular blank for the finite element simulation. The explicit FEM code H3DMAP is used for the analysis of the tube hydroforming process of free bulging.

Table 6.1: Parameters used in the FEM simulation

Material parameters	Value
Density ρ (kg/m^3)	7850
Young's Modulus E (GPa)	205
Hardening coefficient K (MPa)	537
Hardening exponent n	0.227
Poisson's ratio ν	0.3
Yield strength σ_y (MPa)	240
Ultimate tensile strength σ_u (MPa)	350
Geometry parameters	
Length of tube L_0 (mm)	200
Outer radius of tube r_0 (mm)	30
Thickness of tube t_0 (mm)	1.5
Die entry radius r_e (mm)	10
Bulge width W (mm)	100
Process parameters	
Internal pressure P_f (MPa)	40
Nominal stress ratio m	0.4
Friction coefficient μ (Coulomb)	0.06

6.2.2 Decision of Quality Characteristics and Objective Function

In the free bulging tube hydroforming process, the primary objective is to get the bulge ratio as high as possible without any failure happening. Among the three main failure modes involved in tube hydroforming, bursting failure is irrevocable while other failure modes like buckling and wrinkling are recoverable. Bursting is a consequence of necking, which causes fracture eventually. Although there are many different proposed criteria for predicting fracture in metal forming processes, there is no clearly preferred approach. Therefore, the commonly used thinning ratio criteria is used here as a measure of forming quality.

The thinning ratio as well as the bulge ratio is selected as the quality characteristics. The thinning ratio is defined as

$$Thinning\ ratio(\%) = \frac{t_0 - t_1}{t_0} \times 100 \tag{6.1}$$

where t_0 is the original thickness of the tube as shown in Figure 3.3, t_1 is the critical thickness of the hydroformed tube. The bulge ratio is defined as

$$Bulge\ ratio(\%) = \frac{r_1}{r_0} \times 100 \tag{6.2}$$

where r_1 is the maximum radius of the hydroformed tube and r_0 is the original radius of the tube as shown in Figure 3.3.

Two objective functions are chosen for this process. One is to obtain the minimum value of the thinning ratio, and the other is to obtain the maximum value of the bulge ratio.

6.2.3 Selection of Parameters and Construction of Orthogonal Array

Generally, there are three categories of parameters influencing hydroformability, i.e., geometry parameters, material parameters and process parameters Table 6.1). The eight forming parameters to be evaluated are shown in Table 6.2. To evaluate these factors, three levels are chosen for each. For eight factors with three levels for each, the experimental layout of a L_{18} orthogonal array is selected according to Taguchi's suggestion. Table 6.3 shows the L_{18} orthogonal array in which the eighteen runs are carried out to investigate the effects of the eight factors.

Table 6.2: Level of forming parameters

Designation	Forming parameters	Level 1	Level 2	Level 3
A	Length of the tube (mm)	180	200	220
B	Thickness of Tube (mm)	1.35	1.5	1.65
C	Die entry radius (mm)	8	10	12
D	Bulge width (mm)	90	100	110
E	Hardening Exponent	0.207	0.227	0.247
F	Internal Pressure (MPa)	36	40	44
G	Nominal Stress Ratio	0.2	0.4	0.6
H	Friction coefficient (Coulomb)	0.02	0.06	0.1

Table 6.3: Taguchi's L_{18} orthogonal array

Run No.	Forming Parameters							
	A	*B*	*C*	*D*	*E*	*F*	*G*	*H*
1	1	1	1	1	1	1	1	1
2	1	1	2	2	2	2	2	2
3	1	1	3	3	3	3	3	3
4	1	2	1	1	2	2	3	3
5	1	2	2	2	3	3	1	1
6	1	2	3	3	1	1	2	2
7	1	3	1	2	1	3	2	3
8	1	3	2	3	2	1	3	1
9	1	3	3	1	3	2	1	2
10	2	1	1	3	3	2	2	1
11	2	1	2	1	1	3	3	2
12	2	1	3	2	2	1	1	3
13	2	2	1	2	3	1	3	2
14	2	2	2	3	1	2	1	3
15	2	2	3	1	2	3	1	3
16	2	3	1	3	2	3	2	1
17	2	3	2	1	3	1	2	3
18	2	3	3	2	1	2	3	1

6.3 Results and Discussion

6.3.1 Effects of Forming Parameters on Hydroformability

Two different quality characteristics are analyzed by using the S/N and ANOVA analyses based on the results of the FEM simulation corresponding to the above orthogonal array.

6.3.1.1 S/N Analyses

In the Taguchi Method, the signal-to-noise (S/N) ratio is used to measure the quality characteristic deviation from the desired value. Thinning ratio is a quality characteristic with the objective "the lower the better". Bulge ratio is a quality characteristic with the objective "the higher the better". After conducting the FEM simulations and applying the S/N ratio calculation according to Eq. (2.4), the results of the bugle ratio and its S/N ratio in the 18 trial conditions are shown in Table 6.4. The average S/N ratio of the bulge ratio for each parameter at levels 1 to 3 are shown in Table 6.5 and plotted in Figure 6.2. Table 6.6 shows the FEM results of the thinning ratio and its S/N ratio calculated according to Eq. (2.3) in the 18 trial conditions. The average S/N ratio of the thinning ratio for each parameter at levels 1 to 3 are shown in Table 6.7 and plotted in Figure 6.3.

Table 6.4: Bulge ratio values and its S/N ratio

Run No.	Bulge ratio	S/N ratio
1	1.448	3.215
2	1.982	5.942
3	1.923	5.679
4	1.596	4.060
5	2.029	6.145
6	1.449	3.221
7	1.691	4.564
8	1.439	3.162
9	1.590	4.030
10	1.678	4.498
11	1.719	4.704
12	1.640	4.297
13	1.498	3.510
14	1.639	4.293
15	1.853	5.358
16	1.744	4.828
17	1.492	3.473
18	1.597	4.065

Table 6.5: Average S/N ratio of the bulge ratio for each parameter

Designation	Forming parameters	Average S/N ratio		
		Level 1	Level 2	Level 3
A	Length of the tube	4.446	4.336	
B	Thickness of Tube	4.723	4.431	4.020
C	Die entry radius	4.113	4.620	4.442
D	Bulge width	4.140	4.754	4.280
E	Hardening Exponent	4.010	4.608	4.556
F	Internal Pressure	3.480	4.481	5.213
G	Nominal Stress Ratio	4.556	4.421	4.197
H	Friction coefficient	4.319	3.568	5.287

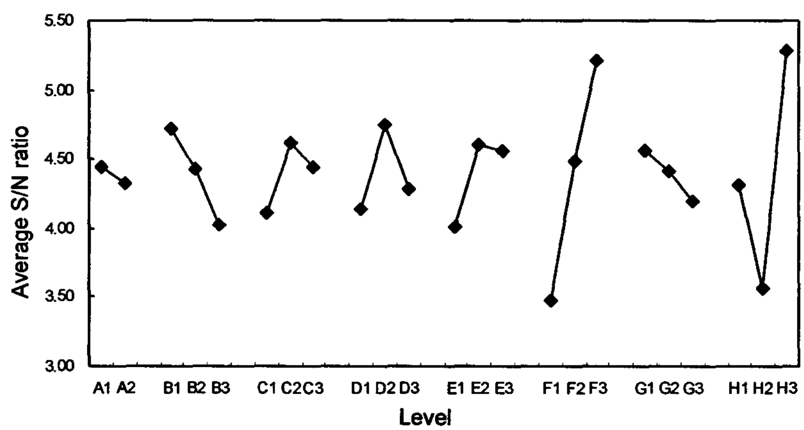

Figure 6.2: Average effect diagram of forming parameter on the bulge ratio

Table 6.6: Thinning ratio values and its S/N ratio

Run No.	Thinning ratio	S/N ratio
1	0.284	10.934
2	0.497	6.067
3	0.477	6.436
4	0.407	7.815
5	0.559	5.047
6	0.304	10.343
7	0.483	6.315
8	0.315	10.025
9	0.429	7.358
10	0.386	8.268
11	0.423	7.480
12	0.385	8.298
13	0.345	9.252
14	0.417	7.604
15	0.530	5.514
16	0.493	6.149
17	0.384	8.313
18	0.416	7.618

Table 6.7: Average S/N ratio of the thinning ratio for each parameter

Designation	Forming parameters	Average S/N ratio		
		Level 1	Level 2	Level 3
A	Length of the tube	7.815	7.611	
B	Thickness of Tube	7.914	7.596	7.630
C	Die entry radius	8.122	7.423	7.594
D	Bulge width	7.902	7.100	8.137
E	Hardening Exponent	8.382	7.311	7.446
F	Internal Pressure	9.527	7.455	6.157
G	Nominal Stress Ratio	7.459	7.576	8.104
H	Friction coefficient	8.007	6.750	8.383

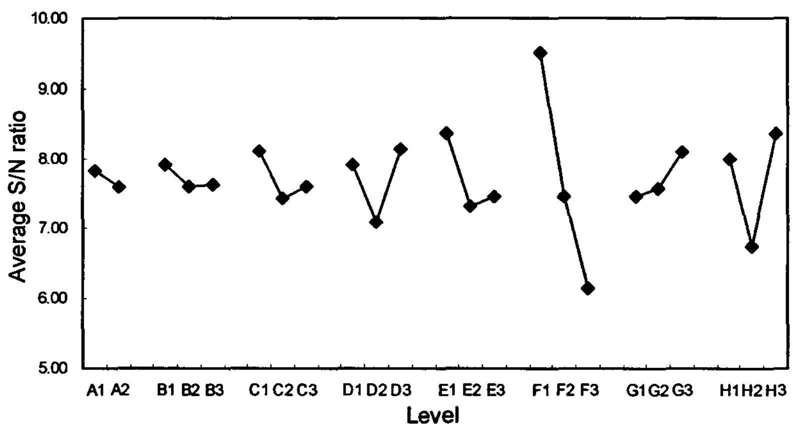

Figure 6.3: Average effect diagram of forming parameter on the thinning ratio

6.3.1.2 ANOVA Analyses

In order to investigate the effects of the forming parameters quantitatively, analysis of variance (ANOVA) is carried out. The results of ANOVA for the bulge ratio and thinning ratio are shown in Table 6.8 and Table 6.9. From Table 6.8, it can be seen that the significant parameters influencing the bulge ratio are internal pressure, friction coefficient and hardening exponent. The effect of length, thickness, die entry radius, bulge width, and nominal stress ratio are relatively small compared to that of internal pressure, friction coefficient and hardening exponent. These results are in good agreement with the results reported in the literature (Manabe & Amino, 2002; Koç & Altan, 2002). Table 6.9 shows the internal pressure is the most significant forming parameter affecting the thinning ratio, the friction coefficient is the next most significant parameter and the hardening exponent is the third one.

The forming parameters except internal pressure, friction coefficient and hardening exponent do not contribute much to the hydroformability, so they are eliminated from the optimization of the tube hydroforming process as discussed in the next section.

Table 6.8: Analysis of variance for bulge ratio

Parameters	Degree of freedom	Sum of squares	Contribution (%)
Length of the tube	1	0.055	0.37
Thickness of tube	2	0.747	5.10
Die entry radius	2	0.398	2.71
Bulge width	2	0.621	4.24
Hardening exponent	2	0.658	4.49
Internal pressure	2	4.543	31.00
Nominal stress ratio	2	0.198	1.35
Friction coefficient	2	4.458	30.42
Error	2	2.978	
Total	17	14.654	

Table 6.9: Analysis of variance for thinning ratio

Parameters	Degree of freedom	Sum of squares	Contribution (%)
Length of the tube	1	0.188	0.40
Thickness of tube	2	0.183	0.39
Die entry radius	2	0.797	1.70
Bulge width	2	1.777	3.79
Hardening exponent	2	2.042	4.35
Internal pressure	2	17.341	36.97
Nominal stress ratio	2	0.709	1.51
Friction coefficient	2	4.387	9.35
Error	2	19.482	
Total	17	46.907	

6.3.2 Multi-objective Optimization of Tube Hydroforming Process

After eliminating the insignificant forming parameters, the analyses of S/N ratio are conducted again with only the significant parameters, i.e., internal pressure, fiction coefficient and hardening exponent.

The same three levels of the internal pressure, fiction coefficient and hardening exponent as shown in Table 6.2 are chosen. A full factorial array is selected for the three factors with three levels, as shown in Table 6.10. Table 6.11 shows the FEM results of the bugle ratio calculated according to Eq. (6.2) and its S/N ratio calculated according to Eq. (2.4) in the 27 trial conditions, and Table 6.12 shows the FEM results of the thinning ratio calculated according to Eq. (6.1) and its S/N ratio calculated according to Eq. (2.3). These tables show that increased internal pressure, increased friction coefficient and increased hardening exponent each give higher bulge ratios, along with higher thinning ratios.

As mentioned earlier, the objectives of this study are to minimize the thinning ratio and maximize the bulge ratio. These two objectives conflict in the free bulge process since higher bulge ratio is highly correlated with higher thinning ratio, and vice versa. However, the use of the Taguchi S/N ratio assists in discriminating better quality characteristics, so the objectives in this study can be converted to simultaneously maximize the S/N ratio of bulge ratio and thinning ratio.

Table 6.10: A full factorial array for three parameters with three levels

Run No.	Internal pressure (A')	Friction coefficient (B')	Hardening exponent (C')
1	1	1	1
2	1	1	2
3	1	1	3
4	1	2	1
5	1	2	2
6	1	2	3
7	1	3	1
8	1	3	2
9	1	3	3
10	2	1	1
11	2	1	2
12	2	1	3
13	2	2	1
14	2	2	2
15	2	2	3
16	2	3	1
17	2	3	2
18	2	3	3
19	3	1	1
20	3	1	2
21	3	1	3
22	3	2	1
23	3	2	2
24	3	2	3
25	3	3	1
26	3	3	2
27	3	3	3

Table 6.11: Bulge ratio and its S/N ratio

Run No.	Internal pressure (MPa) (*A'*)	Friction coefficient (Coulomb) (*B'*)	Hardening exponent (*C'*)	Bulge ratio	S/N ratio
1	36	0.02	0.207	1.391	2.868
2	36	0.02	0.227	1.412	2.999
3	36	0.02	0.247	1.436	3.144
4	36	0.06	0.207	1.389	2.854
5	36	0.06	0.227	1.419	3.038
6	36	0.06	0.247	1.440	3.165
7	36	0.1	0.207	1.407	2.965
8	36	0.1	0.227	1.424	3.070
9	36	0.1	0.247	1.438	3.155
10	40	0.02	0.207	1.561	3.867
11	40	0.02	0.227	1.591	4.036
12	40	0.02	0.247	1.619	4.185
13	40	0.06	0.207	1.578	3.960
14	40	0.06	0.227	1.603	4.100
15	40	0.06	0.247	1.629	4.241
16	40	0.1	0.207	1.612	4.148
17	40	0.1	0.227	1.638	4.286
18	40	0.1	0.247	1.676	4.485
19	44	0.02	0.207	1.724	4.728
20	44	0.02	0.227	1.767	4.945
21	44	0.02	0.247	1.785	5.035
22	44	0.06	0.207	1.744	4.831
23	44	0.06	0.227	1.787	5.043
24	44	0.06	0.247	1.810	5.151
25	44	0.1	0.207	1.802	5.116
26	44	0.1	0.227	1.831	5.255
27	44	0.1	0.247	1.857	5.374

Table 6.12: Thinning ratio and its S/N ratio

Run No.	Internal pressure (MPa) (A')	Friction coefficient (Coulomb) (B')	Hardening exponent (C')	Thinning ratio	S/N ratio
1	36	0.02	0.207	0.279	11.078
2	36	0.02	0.227	0.297	10.535
3	36	0.02	0.247	0.308	10.229
4	36	0.06	0.207	0.283	10.954
5	36	0.06	0.227	0.303	10.381
6	36	0.06	0.247	0.315	10.025
7	36	0.1	0.207	0.300	10.458
8	36	0.1	0.227	0.311	10.135
9	36	0.1	0.247	0.319	9.915
10	40	0.02	0.207	0.383	8.344
11	40	0.02	0.227	0.399	7.973
12	40	0.02	0.247	0.413	7.688
13	40	0.06	0.207	0.397	8.017
14	40	0.06	0.227	0.411	7.730
15	40	0.06	0.247	0.423	7.466
16	40	0.1	0.207	0.421	7.521
17	40	0.1	0.227	0.433	7.264
18	40	0.1	0.247	0.451	6.910
19	44	0.02	0.207	0.461	6.732
20	44	0.02	0.227	0.479	6.399
21	44	0.02	0.247	0.487	6.255
22	44	0.06	0.207	0.475	6.460
23	44	0.06	0.227	0.493	6.137
24	44	0.06	0.247	0.502	5.986
25	44	0.1	0.207	0.505	5.940
26	44	0.1	0.227	0.516	5.747
27	44	0.1	0.247	0.525	5.591

Regression analyses are performed on the data in Table 6.11 and Table 6.12 to get the relationship of the S/N ratios of bulge ratio and thinning ratio with the forming parameters. The regression equations of S/N ratio of bulge ratio ($(S/N)_{BR}$) and S/N ratio of thinning ratio ($(S/N)_{TR}$) are given in Eqs. (6.3) and (6.4).

$$\begin{aligned}(S/N)_{BR} = &-6.71 + 0.22A' + 0.83B' + 6.91C' + 0.12A'B' - 69.9B'C' \\ &+ 0.03A'C' + 1.45A'B'C'\end{aligned} \tag{6.3}$$

$$\begin{aligned}(S/N)_{TR} = &\,46.5 - 0.85A' - 66.32B' - 77.33C' + 1.18A'B' + 328.02B'C' \\ &+ 1.48A'C' - 6.95A'B'C'\end{aligned} \tag{6.4}$$

Although enough degrees of freedom are available in the data to estimate the main second order effect terms (i.e., $A'^2, B'^2, C'^2 \cdots$), the coefficients of these terms are found to be not statistically significantly different from zero. The objective function for the optimization can now be formulated as follows:

$$\begin{aligned}&Max: && \begin{bmatrix}(S/N)_{BR} \\ (S/N)_{TR}\end{bmatrix} \\ &Subject\ to: && 36 \le Internal\ pressure \le 44 \\ & && 0.02 \le Friction\ coefficient \le 0.1 \\ & && 0.207 \le Hardening\ \exp onent \le 0.247\end{aligned} \tag{6.5}$$

The solution to the above objective function will lead to a combination of minimum thinning ratio together with a maximum bulge ratio, which is a Pareto optimal.

The goal attainment method (Gembicki, 1974) is used to solve the above multi-objective optimization problem. Applying the method to Eq. (6.5) transforms it to following formulation:

$$\begin{aligned} &Min: && \gamma \\ &Subject\ to: && (S/N)_{BR} + w_1\gamma \geq (S/N)_{BR}^{\ominus} \\ & && (S/N)_{TR} + w_2\gamma \geq (S/N)_{TR}^{\ominus} \\ & && 36 \leq Internal\ pressure \leq 44 \\ & && 0.02 \leq Friction\ coefficient \leq 0.1 \\ & && 0.207 \leq Hardening\ \exp onent \leq 0.247 \end{aligned} \tag{6.6}$$

where γ is a an unrestricted scalar, $(S/N)_{BR}^{\ominus}$ is the maximum S/N ratio of bulge ratio in Table 6.11, $(S/N)_{TR}^{\ominus}$ is the maximum S/N ratio of thinning ratio on Table 6.12, $[(S/N)_{BR}^{\ominus}, (S/N)_{TR}^{\ominus}]$ is the goal of the set of objectives $[(S/N)_{BR}, (S/N)_{TR}]$, the weighting vector $[w_1, w_2]$ controls the relative degree of under- or over-achievement of the goals. In this study, the weighting vector w is made equal to the goal, so that the same percentage under- or over-attainment of the goals is achieved (Gembicki, 1974). Solution of Eq. (6.6) gives the optimal combination of internal pressure, friction coefficient and hardening exponent as shown in Table 6.13, along with the estimated S/N ratios of bulge ratio $(S/N)_{BR}^{*}$ and thinning ratio $(S/N)_{TR}^{*}$. From the Table 6.11, Table 6.12 and Table 6.13, it can be seen that this Pareto optimal combination of the forming parameters comes as trade-off between the two objectives.

Table 6.13: Optimal combination of parameters and estimated S/N ratio

Internal Pressure (MPa)	Friction coefficient (Coulomb)	Hardening exponent	$(S/N)_{BR}^{*}$	$(S/N)_{TR}^{*}$
40.65	0.02	0.207	3.985	8.214

6.3.3 Confirmation Experiments

Confirmation is carried out at the optimal setting of the significant forming parameters while keeping the remaining parameters at the nominal values. The comparison between the optimal case and the nominal case is shown in Table 6.14. It can be found that the bulge ratio is increased from 1.580 to 1.587 and the thinning ratio is decreased from 0.393 to 0.383. As mentioned before, the objectives of this study are to minimize the thinning ratio and maximize the bulge ratio. It shows both bulge ratio and thinning ratio are improved by applying the optimal setting of the forming parameters determined by the approach presented in this study. Table 6.14 shows a higher internal pressure, a lower friction coefficient and a smaller hardening exponent are obtained in the optimal case. As shown in Table 6.11 and Table 6.12, for a free bulge hydroforming process, a higher internal pressure will usually give a higher bulge ratio and a higher thinning ratio (more thinning in thickness), while a lower friction coefficient and a smaller hardening exponent which means the material is less ductile, will usually give a lower bulge ratio and a lower thinning ratio (less thinning in thickness). It confirms that the optimal combination of forming parameters in Table 6.14 is a trade-off between the two objectives.

Table 6.14: Comparison between the optimal case and nominal case

	Internal Pressure (MPa)	Friction coefficient (Coulomb)	Hardening exponent	Bulge ratio	Thinning ratio
Optimal case	40.65	0.02	0.207	1.587	0.383
Nominal case	40	0.06	0.227	1.580	0.393

6.3.4 Pareto Set

As discussed before, if there are many Pareto optimal solutions for a given multi-objective optimization problem, the collection of these Pareto optimal solutions will form the Pareto set of this problem. In the above example, the weighting vector was set equal to the goal, and a Pareto optimal combination of internal pressure, friction coefficient and hardening exponent was obtained and the improvement of the bulge ratio as well as the thinning ratio was confirmed. By varying the values of weights w_1 and w_2, a series of Pareto optimal combinations of internal pressure, friction coefficient and hardening exponent can be obtained. These Pareto optimal combinations of internal pressure, friction coefficient and hardening exponent will form the Pareto set for the given free bulging tube hydroforming process. By choosing a series of values between 0 and 1 as the weight w_1, the weight w_2 is found as being equal to one minus w_1. Based on these different weight vectors, a series of corresponding Pareto optimal solutions are obtained by solving the Eq. (6.6) using the goal attainment method. A series of corresponding bulge ratios and thinning ratios according to the different combination of internal pressure, friction coefficient and hardening exponent are obtained by the finite element analyses. The resulting Pareto optimal set is plotted in Figure 6.4.

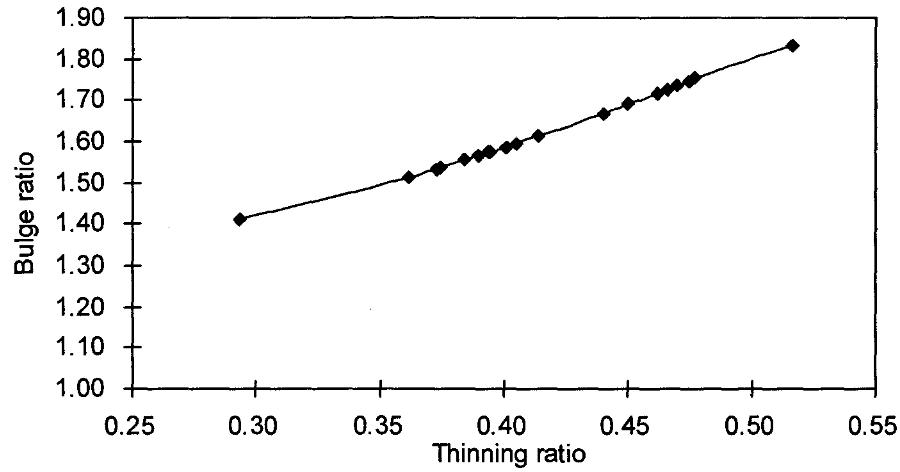

Figure 6.4: Pareto optimal combinations of thinning ratio and bulge ratio

The curve in Figure 6.4 is the Pareto optimal front of the combination of thinning ratio and bulge ratio for this free bulge hydroforming process. All possible combinations of the thinning ratio and bulge ratio are located on or below the Pareto front. If a specific bulge ratio is required for this process, the obtainable optimal thinning ratio will be the projected point of this bulge ratio from this Pareto optimal front. Conversely, if a given thinning ratio is deemed acceptable, the Pareto optimal front gives the maximum bulge ratio achievable.

Chapter 7

Conclusions

The principal objective of this dissertation is to provide effective tools for engineers to design a reliable and robust metal forming process before any tooling is constructed. Chapter 3 presented the study of reliability analysis of metal forming process based on forming limit diagram. Chapter 4 presented the study of prediction of forming limit diagram using finite element simulation and the uncertainty of forming limit is analyzed. A study of improving the reliability of metal forming process using a robust design method is presented in Chapter 5. Chapter 6 investigated the effects of forming parameters on the quality performance of process based on the Taguchi method and a multi-objective optimization for a tube hydroforming process is studied based on the Taguchi method. This chapter summarizes the results of the research, draws conclusions and offers some recommendations for the future research works.

7.1 Summary of Conclusions

Based on the research results detailed in Chapter 3-6. The following conclusions have been drawn for this research:

(1) Traditional reliability theory can be applied to the task of evaluating metal forming process quality and used to predict the probability of part failure during forming process. The forming limit, which is widely used for evaluating the formability of materials, can be used as the failure criteria for reliability analysis of metal forming process. By considering the inherent scatter of forming limit, a probability distribution such as the normal distribution can be used to evaluate the failure probability of a forming process.

(2) Two improvements have been made on the reliability analysis of the metal forming operation based on the forming limit diagram as compared to the previous study conducted by Kleiber et al. (2002). First, the limit strain is defined as the distance from the origin to certain strain point along a particular strain path, such definition is conformable with the statistical experimental observation that the strain points tend to spread more along the particular strain path than perpendicular to the estimated curve (Van Minh et al., 1974). Second, the forming limit band offsetting the forming limit curve with the same upper and lower percentage is used to present the uncertainty of the strain limits, such presentation reflects the actual practice better than the marginal zone below the FLC as the FLC constructed from the experimental results usually represent the average strain limit of a material (Janssens et al., 2001).

(3) The uncertainty sources which cause the scatter of forming limits are classified into two categories based on their intrinsic characteristics including the objective uncertainty sources and the subjective uncertainty sources. The effects of these objective and subjective uncertainty sources on the shape and location of FLC are investigated respectively using the finite element simulation. The resultant effects of these uncertainty sources on FLD from the FE simulations are in reasonable agreement with the experimental findings reported in the literature. Use of the FE predicted FLD considering both objective and subjective uncertainty sources is more time and cost effective when generating FLDs for new materials as compared to the current experimental approach.

(4) The Taguchi method is used as a systematic approach to design a robust metal forming process in this research. A major benefit of the Taguchi method is that not only does it determine levels of controllable factors that improve mean reliability performance, but it also determines levels of controllable factors that minimize variation of the process output as the uncontrollable factors vary. Another benefit of the Taguchi approach is that it determines the relative contribution of each factor to process reliability. This allows design efforts to be concentrated on the most sensitive factors.

(5) A new method of optimizing the forming parameters for metal forming processes is presented based on the finite element analysis and the Taguchi method. The significant forming parameters affecting the formability are identified by performing the experiments designed according to the Taguchi orthogonal array. By eliminating the

insignificant parameters from the optimization of the forming parameters, it results in significant saving of computational time.

(6) Optimization of conflicting objectives for a forming process is achieved by converting the conflicting objectives to simultaneously maximize the Taguchi S/N ratios of the conflicting objectives in this research. An example of maximizing the bulge ratio and minimizing the thinning ratio for a given free bulge tube hydroforming process is used to illustrate the method. The results show that this approach is very effective.

7.2 Contributions

There are five Journal/Conference papers based on this research have been accepted for publication. Each chapter from Chapter 3 to chapter 6 has one paper associated with it. A paper based on the study of Chapter 3 entitled "Reliability Analysis of the Tube Hydroforming Process Based on Forming Limit Diagram" has been published at the ASME Journal of Pressure Vessel Technology. A paper partially based on the study of Chapter 4 entitled "Prediction of Forming Limit Diagrams for Aluminum Alloy Sheet Using Finite Element Analysis" has been presented at 2006 ASME Pressure Vessels and Piping Conference. A paper based on the study of Chapter 5 entitled "Improving the Reliability of Tube Hydroforming Process by the Taguchi Method" has been published at the ASME Journal of Pressure Vessel Technology. A paper based on the study of Chapter 6 entitled "Multi-objective Optimization of Forming Parameters for Tube Hydroforming Process Based on the Taguchi Method" has been published at the

International Journal of Advanced Manufacturing Technology. A paper based on the study of Appendix A entitled "Reliability Analysis of the Tube Hydroforming Process Using Fuzzy Sets Theory" has been presented at 2004 ASME Pressure Vessels and Piping Conference.

7.3 Recommendations for Future Work

The methodologies proposed in this research have significant potential to be extended and some improvements of this research can also be made in future works.

(1) In this research, two failure criteria are used to evaluate the reliability of metal forming process, one is forming limit of material and another is stress-strength interference model. In industry, the fracture of deformed part is a common concern for forming quality. In most fracture criteria for a ductile material, there is a critical limit value which is usually treated as a material constant. Actually this critical value has certain scatter and it should be treated as a random variable. Doing so would allow the fracture criteria to be used as the failure criteria for reliability analysis of metal forming processes.

(2) A study of prediction of FLD using finite element simulation is presented in this research. Some objective and subjective uncertainty sources have been investigated to see their effects on the forming limit. These uncertainty sources can be extended in the future to cover all the potential factors such as hardening rule, yield criteria, finite element code and so on.

(3) In the appendix of this research, the stress of deformed part is treated as a fuzzy variable due to the incomplete and vague statistical information of its relative parameters. The membership function of fuzzy stress is obtained by using fuzzy linear regression method. An alternative method, i.e. neural network, can be considered in the future to obtain statistical information on the stress. The relationship between the stress of a deformed part and its relative parameters can be obtained by training a neural network with the sample data obtained from finite element simulation.

References

Ahmetoglu, M., Altan, T. Tube hydroforming: state-of-the-art and future trends. *Journal of Materials Processing Technology* 98, No. 1: 25-33, 2000.

Ahmetoglu, M., Sutter, K. Tube hydroforming: current research, applications and need for training. *Journal of Materials Processing Technology* 98, No. 2: 224-231, 2000.

Anastasiou, K. S. Optimization of the aluminium die casting process based on the Taguchi method. *Proceedings of the Institution of Mechanical Engineers Part B-Journal of Engineering Manufacture* 216: 969-977, 2002.

Antony, J. Simultaneous Optimisation of Multiple Quality Characteristics in Manufacturing Processes Using Taguchi's Quality Loss Function. *International Journal of Advanced Manufacturing Technology* 17: 134-138, 2001.

Aretz, H. Numerical restrictions of the modified maximum force criterion for prediction of forming limits in sheet metal forming. *Modelling and Simulation in Materials Science and Engineering* 12: 677-692, 2004.

Arrieux, R., Bedrin, C., Boivin, M. Determination of an intrinsic forming limit stress diagram for isotropic metal sheets. The 12th Biennial Congress of the International Deep Drawing Research Group, 1982.

Arwashan, N. Reliability Analysis of Sheet Metal Forming. TMS Annual Meeting & Exhibition, San Diego, CA, Feb 28 ~ March 4, 1999.

Asnafi, N., Skogsgardh, A. Theoretical and experimental analysis of stroke-controlled tube hydroforming. *Materials science & engineering* 279: 95-110, 2000.

Aven, T. Reliability evaluation of multistate systems with multistate components. *IEEE Transactions on Reliability* R-34: 473-479, 1985.

Bammann, D. J. Modelling temperature and strain rate dependent large deformations of metals. *Applied Mechanics Reviews* 43: S312-S319, 1990.

Banabic, D., Bunge, H.-J., Pőhlandt, K., Tekkaya. A.E. Formability of Metallic Materials - Plastic Anisotropy, Formability Testing, Forming Limits. Berlin: Springer-Verlag, 2000.

Barata da Rocha, A., Jalinier, J. M. Plastic instability of sheet metals under simple and complex strain paths. *Transactions of the Iron and Steel Institute of Japan* 24: 132-140, 1984.

Barlat, F., Lian, J. Plastic behavior and stretchability of sheet metals. Part I: A yield function for orthotropic sheets under plane stress conditions. *International Journal of Plasticity* 5: 51-66, 1989.

Bastani, F. B. On the uncertainty in the correctness of computer programs. *IEEE Transactions on Software Engineering* SE-11: 857-864, 1985.

Beaudoin, A. J., Koya, T., Smith, P.E., Wiese, J.W. Experiences in the Use of an Evolutionary Damage Model with LS-DYNA3D. SAE 950915, 1995.

Belytschko, T., Chiang, H.Y., Plaskacz, E.J. Two Dimensional Shear Band Computations and the Effects of Imperfections. The Third International Congress of Computational Plasticity, 1992.

Billinton, R., Allan, R. N. *Reliability evaluation of engineering systems - concepts and techniques*. 2nd ed. New York: Plenum Press, 1992.

Bodsberg, L., Hokstad, P. A system approach to reliability and life-cycle cost of process safety systems. *IEEE Transactions on Reliability* R-44: 179-186, 1985.

Boudeau, N., Lejeune, A., Gelin, J. C. Influence of material and process parameters on the development of necking and bursting in flange and tube hydroforming. *Journal Of Materials Processing Technology* 125-126: 849-855, 2002.

Brown, C. B., Yao, J. T. P. Fuzzy Sets and Structural Engineering. *Journal of Structure Engineering* 109: 1211-1225, 1983.

Bullough, R., Green, V. R., Tomkins, B., Wilson, R., Wintle, J. B. A review of methods and applications of reliability analysis for structural integrity assessment of UK nuclear plant. *International Journal of Pressure Vessels and Piping* 76: 909-919, 1999.

Cai, K. Y. System failure engineering and fuzzy methodology: An introductory overview. *Fuzzy Sets and Systems* 83: 113-133, 1996.

Cao, J., Liu, W. K., Cheng, H. S., Lu, H. S. A multi-scale approach for predicting wrinkling and its experimental verification. NSF Design, Service and Manufacturing Grantees and Research Conference, Birmingham, Alabama, Jan 6-9, 2003.

Cao, J., Yao, H., Karafillis, A., Boyce, M. C. Prediction of localized thinning in sheet metal using a general anisotropic yield criterion. *International Journal of Plasticity* 16: 1105-1129, 2000.

Carleer, B., van der Kevie, G., de Winter, L., van Veldhuizen, B. Analysis of the Effect of Material Properties on the Hydroforming Process of Tubes. *Journal Of Materials Processing Technology* 104: 158-166, 2000.

Celmins, A. Least-squares model fitting to fuzzy vector data. *Fuzzy Sets and Systems* 22: 245-269, 1987.

Cen, Y. Fuzzy quality and analysis on fuzzy probability. *Fuzzy Sets and Systems* 83: 283-290, 1996.

Chang, N. B., Chen, Y. L., Yang, H. H. A fuzzy goal regression model for the construction cost estimation of municipal waste incinerators. *International journal of systems science* 27: 433-445, 1996.

Chang, P. T., Lee, E. S. A generalized fuzzy weighted least-squares regression. *Fuzzy Sets and Systems* 82: 289-298, 1996.

Choquet, G. Theory of Capacities. *Annales De L'Institut Fourier* 5: 131-295, 1954.

Chow, C. L., Yang, X. J., Chu, E. Viscoplastic constitutive modeling of anisotropic damage under nonproportional loading. *ASME Journal of Engineering Materials and Technology* 123: 403-408, 2001.

Collins, J. D. Risk analysis methodologies developed for the US Department of Defense. *Reliability Engineering & System Safety* 20, No. 2: 87-115, 1988.

Davis, E. A. Yield and fracture of medium-carbon steel under combined stress. *ASME Journal of Applied Mechanics* 67: A13-A24, 1945.

Dhavlikar, M. N., Kulkarni, M. S., Mariappan, V. Combined Taguchi and dual response method for optimization of a centerless grinding operation. *Journal of Materials Processing Technology* 132: 90-94, 2003.

Diamond, P. Fuzzy least squares. *Information Science* 46: 141-157, 1988.

Dohmann, F., Hartl, C. Hydroforming - A method to manufacture light-weight parts. *Journal of Materials Processing Technology* 60, No. 1-4: 669-676, 1996.

Duan, X., Sheppard, T. Influence of forming parameters on the final subgrain size during hot rolling of aluminium alloys. *Journal Of Materials Processing Technology* 130-131: 245-249, 2002.

Duan, X., Jain, M., Metzger, D., Kang, J., Wilkinson, D. S., Embury, J. D. Prediction of shear localization during large deformation of a continuous cast Al–Mg sheet. *Materials Science and Engineering A* 394, No. 1-2: 192-203, 2005.

Duan, X., Jain, M., Wilkinson, D. S. Development of a Heterogeneous Microstructurally Based Finite Element Model for the Prediction of Forming Limit Diagram for Sheet Material. *Metallurgical and Materials Transactions A* 37, No. 12: 3489-3501, 2006.

Dubois, D., Prade, H. *Possibility Theory*. New York: Plenum Press, 1988.

Dupow, H., Blount, G. A review of reliability prediction. *Aircraft Engineering and Aerospace Technology* 69: 342-356, 1997.

Ebert, C. Rule-based fuzzy classification for software quality control. *Fuzzy Sets and Systems* 63: 349-358, 1993.

Fisher, R. A. *Statistical Methods for Research Workers*. London: Oliver and Boyd, 1925.

Gembicki, F. W. Vector Optimization for Control with Performance and Parameter Sensitivity Indices. Ph.D. Thesis, Case Western Reserve University, 1974.

Gharpuray, M. M., Tanaka, H. Fuzzy Linear Regression Analysis of Cellulose Hydrolysis. *Chemical Engineering Communications* 41: 299-314, 1986.

Ghosh, A. K., Hecker, S. S. Stretching limits in sheet metals: In-plane versus out-of-plane deformation. *Metallurgical Transactions A* 5: 2161-2164, 1974.

Goodwin, G. M. Application of strain analysis to sheet metal forming problems in the press shop. *SAE 680093*, 1968.

Graf, A., Hosford, W. Calculation of forming limit diagrams. *Metallurgical Transactions A* 21: 87-94, 1990.

Graf, A., Hosford, W.F. Effect of changing strain paths of forming limit diagrams of Al 2008-T4. *Metallurgical Transactions A* 24: 2503-2512, 1993.

Graf, A., Hosford, W.F. The influence of strain path changes on forming limit diagram of Al 6111-T4. *International Journal of Mechanical Sciences* 36: 897-910, 1994.

Harris, J. Fuzzy logic methods in fatigue and creep. *Journal of Strain Analysis for Engineering Design* 36: 411-420, 2001.

Hayashi, H. Experimental Determination of Forming Limit Diagram (FLD) of Steel Sheets. SAE 982374, 1998.

Hecker, S. S. Experimental studies of sheet stretchability, Formability: Analysis, Modeling and Experimentation. AIME/ASM Symposium, New York, 1978.

Hecker, S. S. Simple technique for determining forming limit curves. *Sheet Metal Industries* 52: 671-676, 1975.

Henkind, S. J., Harrison, M. C. An analysis of four uncertainty calculi. *IEEE Transactions on Systems, Man and Cybernetics* 18: 700-714, 1988.

Heshmaty, B., Kandel, A. Fuzzy Linear Regression and its Applications to Forecasting in Uncertain Environment. *Fuzzy Sets and Systems* 15: 159-191, 1985.

Hill, R. On discontinuous plastic states, with special reference to localized necking in thin sheets. *Journal of the Mechanics And Physics of Solids* 1: 19-30, 1952.

Hill, R. A theory of the yielding and plastic flow of anisotropic metals. *Proceedings of the Royal Society of London. Series A, Mathematical and Physical Sciences* 193: 281-297, 1948.

Hopperstad, O. S., Leira, B. J., Remseth, S., Tromborg, E. Reliability-based analysis of a stretch-bending process for aluminium extrusions. *Computers and Structures* 71: 63-75, 1999.

Horstemeyer, M. F. A Numerical Parametric Investigation of Localization and Forming Limits. *International Journal of Damage Mechanics* 9: 255-285, 2000.

Hosford, W. F., Duncan, J. L. Sheet Metal Forming: A Review. *JOM* 51: 39-44, 1999.

Hotz, W. Update proposal of ISO 12004 for the measurement of forming limit diagrams. GOM User Meeting, Braunschweig, Germany, April 10, 2004.

Hu, Q. G., Zhu, R. C. *Multiple Data Analysis Method.* Tianjing, China: Nankai University Press, 1990.

Huang, H. M., Pan, J., Tang, S. C. Failure prediction in anisotropic sheet metals under forming operations with consideration of rotating principal stretch directions. *International Journal of Plasticity* 16: 611-633, 2000.

Huh, H., Heo, J. H., Lee, H. W. Optimization of a roller levelling process for Al7001T9 pipes with finite element analysis and Taguchi method. *International Journal of Machine Tools & Manufacture* 43: 345-350, 2003.

Hutchinson, J. W., Neale, K. W. "Sheet necking—II: time-independent behavior." In *Mechanism of Sheet Metal Forming*, edited by Koistinen, D. P., Wang, N. M., 111-126. New York: Plenum Press, 1978.

Hutchinson, J. W., Neale, K. W. "Sheet necking—III: strain-rate effects." In *Mechanism of Sheet Metal Forming*, edited by Koistinen, D. P., Wang, N. M., 269-283. New York: Plenum Press, 1978.

Hwang, Y. M., Lin, Y. K. Analysis and Finite Element Simulation of the Tube Bulge Hydroforming Process. *Journal Of Materials Processing Technology* 125-126: 821-825, 2002.

Ip, K. W., Kwong, C. K., Wong, Y. W. Fuzzy regression approach to modelling transfer moulding for microchip encapsulation. *Journal of Materials Processing Technology* 140: 147-151, 2003.

Jain, M., Allin, J. Analysis of Experimental Variability of Forming Limit Diagrams. 39th International SAMPE Symposium, Anaheim, CA, April 11-14, 1994.

Jain, M. Private communications from Dr. Mukesh Jain, Department of Mechanical Engineering, McMaster University, 2005.

Jain, M., Allin, J., Duan, X., Lloyd, D. J. Effect of reverse dome stretching on dome height and forming limits of sheet materials. *Materials Science and Engineering A* 390: 210-216, 2005.

Janssens, K., Lambert, F. Statistical Evaluation of the Uncertainty of Experimentally Characterised Forming Limits of Sheet Steel. *Journal of Materials Processing Technology* 112: 174-184, 2001.

Jozsef, S. On the effect of linear data transformations in possibilistic fuzzy linear regression. *Fuzzy Sets and Systems* 45: 185-188, 1992.

Kapur, K. C., Lamberson, L. R. *Reliability in Engineering Design*. New York: John Wiley, 1977.

Karwowski, W., Mital, A. Potential applications of fuzzy sets in industrial safety engineering. *Fuzzy Sets and Systems* 19: 105-120, 1986.

Kaufmann, A. *Introduction to the Theory of Fuzzy Subsets*. Vol. 1. New York: Academic Press, 1975.

Kaufmann, A., Gupta, M. M. *Fuzzy Mathematical models in Engineering and Management science*. Netherlands: Elsevier Science Publishers, 1988.

Keeler, S. P. Circular grid system — A valuable aid for evaluating sheet metal formability. *SAE 680092*, 1968.

Keeler, S. P. Determination of forming limits in automotive stampings. *Sheet Metal Industries* 42: 683-691, 1967.

Keeler, S. P. "On the origins of the FLD." In *Forming Limit Diagram: Concepts, Methods and Applications*, edited by Wagoner, R. H., et al. Warrendale, USA: The Minerals, Metals and Materials Society, 1989.

Keeler, S. P., Backofen, W. A. Plastic instability and fracture in sheets stretched over rigid punches. *ASM Transactions* 56: 25-48, 1964.

Kim, B., Bishu, R. R. Evaluation of fuzzy linear regression models by comparing membership functions. *Fuzzy Sets and Systems* 100: 342-352, 1998.

Kim, B., Bishu, R. R. On Assessing Operator Response Time in Human Reliability Analysis (HRA) Using a Possibilistic Fuzzy Regression Model. *Reliability Engineering & System Safety* 52: 27-34, 1996.

Kim, S. J., Kim, K. S., Jang, H. Optimization of manufacturing parameters for a brake lining using Taguchi method. *Journal of Materials Processing Technology* 136: 202-208, 2003.

Kleemola, H. J., Pelkkikangas, M. T. Effect of predeformation and strain path on the forming limits of steel, copper and brass. *Sheet Metal Industries* 63: 559-591, 1977.

Kleiber, M., Rojek, J., Stocki, R. Reliability assessment for sheet metal forming operations. *Computer Methods in Applied Mechanics and Engineering* 191: 4511-4532, 2002.

Klir, G. J., Yuan, B. *Fuzzy Sets and Fuzzy Logic: Theory and Applications*. Upper Saddle River, NJ: Prentice Hall, PTR, 1995.

Ko, D., Kim, D., Kim, B. Application of artificial neural network and Taguchi method to preform design in metal forming considering workability. *International Journal of Machine Tools & Manufacture* 39: 771-785, 1999.

Kobayashi, T., Ishigaki, H., Abe, T. Effect of strain ratios on the deforming limit of sheet steel and its application to actual press forming. The Seventh Biennial Congress of the International Deep Drawing Research Group, Amsterdam, Netherlands, 1972.

Koç, M., Altan, T. Application of Two Dimensional (2D) FEA for the Tube Hydroforming Process. *International Journal of Machine Tools & Manufacture* 42: 1285-1295, 2002.

Koç, M., Aue-u-lan, Y. On the characteristics of tubular materials for hydroforming - experimentation and analysis. *International Journal of Machine Tools & Manufacture* 41, No. 5: 761-772, 2001.

Kutz, M. *Handbook of materials Selection*. New York: John Wily & Sons, 2002.

Kwakernaak, H. Fuzzy random variables: definitions and theorems. *Information Science* 15: 1-29, 1978.

Laukonis, J. V., Ghosh, A. K. Effects of strain path changes on the formability of sheet metals. *Metallurgical Transactions A* 9: 1849-1856, 1978.

Lee, S. W. Study on the forming parameters of the metal bellows. *Journal of Materials Processing Technology* 130-131: 47-53, 2002.

Li, B., Zhu, M. A Fuzzy Linear Regression Method for the Performance Evaluation of I.C. Engines. *Journal of Huazhong University of Science & Technology* 5: 61-63, 1998.

Li, B., Zhang, Y., Zhu, M. A Study on the Structure Design and Reliability of Cylinder Head for Vehicle Engines. *SAE 1999-01-0828*, 1999.

Li, B., Zhu, M., Xu, K. A Practical engineering method for fuzzy reliability analysis of mechanical structures. *Reliability Engineering and System Safety* 67: 311-315, 2000.

Li, B., Metzger, D.R., Nye, T.J. Reliability Analysis of the Tube Hydroforming Process Using Fuzzy Sets Theory. 2004 ASME Pressure Vessels and Piping Conference, San Diego, USA, July 25-29, 2004.

Li, B., Metzger, D. R., Nye, T. J. Reliability Analysis of the Tube Hydroforming Process Based on Forming Limit Diagram. ASME *Journal of Pressure Vessel Technology* 128: 1-6, 2006.

Li, B., Nye, T. J. Prediction of Forming Limit Diagrams for Aluminium Alloy Sheet Using Finite Element Analysis. 2006 ASME Pressure Vessels and Piping Conference, Vancouver, Canada, July 23-27, 2006.

Li, B., Nye, T. J., Metzger, D. R. Multi-objective Optimization of Forming Parameters for Tube Hydroforming Process Based on the Taguchi Method. *International Journal of Advanced Manufacturing Technology* 28: 23-30, 2006.

Li, B., Nye, T. J., Metzger, D.R. Improving the Reliability of Tube Hydroforming Process by the Taguchi Method. ASME *Journal of Pressure Vessel Technology* 129: 242-247, 2007.

Lin, J. L., Wang, K. S., Yan, B. H., Tarng, Y. S. Optimization of the electrical discharge machining process based on the Taguchi method with fuzzy logics. *Journal of Materials Processing Technology* 102: 48-55, 2000.

Liu, Y., Qiao, Z., Wang, G. Fuzzy random reliability of structure based on fuzzy random variables. *Fuzzy Sets and Systems* 86: 345-355, 1997.

Lloyd, D. J., Sang, H. The influence of strain path on subsequent mechanical properties—orthogonal tensile paths. *Metallurgical Transactions A* 10: 1767-1772, 1979.

LSTC. *LS-DYNA Keyword User's Manual*: Livermore Software Technology Corporation, January 2007.

Lu, Z. H., Lee, D. Prediction of history-dependent forming limits by applying different hardening models. *International Journal of Mechanical Sciences* 29: 123-137, 1987.

Lücke, U., Hartl, C. Hydroforming. *Journal Of Materials Processing Technology* 115: 87-91, 2001.

Maker, B. N., Zhu, X. Input Parameters forMetal Forming Simulation Using LS-DYNA. The 6th International LS-DYNA Users Conference, Dearborn, Michigan, April 9-11, 2000.

Manabe, K., Amino, M. Effects of process parameters and material properties on deformation process in tube hydroforming. *Journal of Materials Processing Technology* 123: 285-291, 2002.

Marciniak, Z., Kuczynski, K. Limit strains in the process of stretch-forming sheet metal. *International Journal of Mechanical Sciences* 9: 609-620, 1967.

Marler, R. T., Arora, J. S. Review of Multi-Objective Optimization Concepts and Algorithms for Engineering. Optimal Design Laboratory, The University of Iowa, Report No. ODL-01.03, 2003, Iowa City

Matsuoka, T., Sudo, C. The effect of strain path on the fracture strain of steel sheets. *Sumitomo Search* 1: 71-80, 1969.

Mazumdar, M. "Approximate computation of power generating system reliability indexes." In *Quality Control and Reliability*, edited by Krishnaiah, P. R., Rao, C. R., 55-72. Amsterdam, Netherlands: Elsevier Science Publishers, 1988.

McCauley-Bell, P., Badiru, A. B. Fuzzy modeling and analytic hierarchy processing to quantify risk levels associated with occupational injuries - Part I: the development of fuzzy- linguistic risk levels & Part II: the development of fuzzy rule-based model for the prediction of injury. *IEEE Transactions on Fuzzy Systems* 4: 124-138, 1996.

Misra, K. B., Weber, G. G. Use of fuzzy set theory for level-I studies in probabilistic risk assessment. *Fuzzy Sets and Systems* 37: 139-160, 1990.

Morphy, G. Pressure-sequence and high-pressure hydroforming. *Tube and Pipe Journal* 9: 128-135, 1998.

Mortimer, J. BMW breaks new ground with hydroforming. *Assembly Automation* 21: 317-321, 2001.

Narasimhan, K., Zhou, D., Wagoner, R. H. Application of the Monte Carlo and finite element methods to predict the scatter band on forming limit strains. *Scripta metallurgica et materialia* 26: 41-46, 1992.

Nefussi, G., Combescure, A. Coupled Buckling and Plastic Instability for tube Hydroforming. *International Journal of Mechanical Sciences* 44: 899-914, 2002.

Numisheet 2005, Detroit, USA. 6th International Conference and Workshop on Numerical Simulation of 3D Sheet Forming Process. Benchmarks/Benchmark Simulation Study/Benchmark #2/File Downloads for Benchmark #2/BM2-AL5182.xls (Standard Material File for 5182-O aluminum), http://www.numisheet2005.org/FILES/Benchmarks/BM2/BM2-AL5182.xls

Onisawa, T. An application of fuzzy concepts to modeling of reliability analysis. *Fuzzy Sets and Systems* 37: 267-283, 1990.

Onisawa, T. An approach to human reliability in man- machine system using error possibility. *Fuzzy Sets and Systems* 27: 87-103, 1988.

Ozturk, F., Lee, D. Analysis of forming limits using ductile fracture criteria. *Journal of Materials Processing Technology* 147: 397-404, 2004.

Pagès, A., Gondran, M. *Fiabilité des Systèmes*. Paris, France: Eyrolles, 1980.

Park, K., Kim, Y. The effect of material and process variables on the stamping formability of sheet materials. *Journal Of Materials Processing Technology* 51: 64-78, 1995.

Peters, G. Fuzzy linear regression with fuzzy intervals. *Fuzzy Sets and Systems* 63: 45-55, 1994.

Rama, S. C., Ma, K., Smith, L. M., Zhang, J. M. A two-dimensional approach for simulation of hydroforming expansion of tubular cross-sections without axial feed. *Journal Of Materials Processing Technology* 141: 420-430, 2003.

Rao, S. S. *Reliability-Based Design*. New York: McGraw-Hill, 1992.

Rasmussen, S. N. Theoretical prediction of strain path dependence of limit strains in sheet materials. *Annals of the CIRP* 30, No. 1: 179-184, 1981.

Redden, D. T., Woodall, W. H. Further examination of fuzzy linear regression. *Fuzzy Sets and Systems* 79: 203-211, 1997.

Redden, D. T., Woodall, W. H. Properties of certain fuzzy linear regression models. *Fuzzy Sets and Systems* 64: 361-375, 1994.

Rees, D. W. A. Factors influencing the FLD of automotive sheet metal. *Journal of Materials Processing Technology* 118: 1-8, 2001.

Roberts, I. D., Samuel, A. E. The use of imprecise component reliability distributions in reliability calculations. *IEEE Transactions on Reliability* 45: 141-144, 1996.

Sang, H., Lloyd, D. J. The influence of biaxial prestrain on the tensile properties of three aluminum alloys. *Metallurgical Transactions A* 10: 1773-1776, 1979.

Sauvé, R. G. H3DMAP Version 6 - A General Three-Dimensional Linear and Nonlinear Analysis of Structures. Ontario Hydro Technologies, Report No. A-NSG-96-120, 1999, Toronto

Savic, D., Pedrycz, W. Evaluation of fuzzy regression models. *Fuzzy Sets and Systems* 39: 51-63, 1991.

Sawyer, J. P., Rao, S. S. Strength-based reliability and fracture assessment of fuzzy mechanical and structural systems. *AIAA Journal* 37: 84-92, 1999.

Shabeer, S., Wang, M. Y. Multi-objective optimization of sequential brakeforming processes. *Journal Of Materials Processing Technology* 102: 266-276, 2000.

Sing, W. M., Rao K. P. Predication of Sheet-metal Formability Using tensile-test Results. *Journal Of Materials Processing Technology* 37: 37-51, 1993.

Singh, H. Simulation of hydroforming. Automotive Tube Conference, Detroit, April 26-27, 1999.

Smith, L. M., Averill, R. C., Lucas, J. P., Stoughton, T. B., Matin, P. H. Influence of transverse normal stress on sheet metal formability. *International Journal of Plasticity* 19: 1567-1583, 2003.

Soliman, S. A., Helal, L, Al-Kandari, A. M. Fuzzy linear regression for measurement of harmonic components in a power system. *Electric power systems research* 50: 99-107, 1998.

Storen, S., Rice, J. R. Localized necking in thin sheets. *Journal of the Mechanics And Physics of Solids* 23: 421-441, 1975.

Stoughton, T. B. A General Forming Limit Criterion for Sheet Metal Forming. *International Journal of Mechanical Sciences* 42: 1-27, 2000.

Stoughton, T. B. The influence of material model on the stress-based forming limit criterion. *SAE paper 2002-01-0157*, 2002.

Stoughton, T. B. Stress-based forming limits in sheet metal forming. *ASME Journal of Engineering Materials and Technology* 123: 417-422, 2001.

Taguchi, G. *Systems of Experimental Design*, Vol. 1, Japanese Standards Association, 1976.

Taguchi, G. *Systems of Experimental Design*, Vol. 2, Japanese Standards Association, 1977.

Taguchi, G. *Introduction to Quality Engineering*. Tokyo: Asian Productivity Organization, 1999.

Takahashi, H. Automatic Speed Control Device Using Self-tuning Fuzzy Logic. *IEEE Decision and Control* 15: 65-71, 1988.

Takuda, H., Mori, K., Takakura, N., Yamaguchi, K. Finite element analysis of limit strains in biaxial stretching of sheet metals allowing for ductile fracture. *International Journal of Mechanical Sciences* 42: 785-798, 2000.

Hallquist, J. O. Preliminary User's Manuals for DYNA3D and DYNAP (Nonlinear Dynamic Analysis of Solids in Three Dimension, University of California, Lawrence Livermore National Laboratory, Report UCID-17268, 1976.

Tanaka, H. Fuzzy Data Analysis by Possibilistic Linear Models. *Fuzzy Sets and Systems* 24: 363-375, 1987.

Tanaka, H., Ishibuchi, H. Identification of possibilistic linear systems by quadratic membership functions of fuzzy parameters. *Fuzzy Sets and Systems* 41: 145-160, 1991.

Tanaka, H., Lee, H. Fuzzy linear regression combining central tendency and possibilistic properties. FUZZ-IEEE'97, Barcelona, Spain, July 1-5, 1997.

Tanaka, H., Uejima, S., Asai, K. Linear Analysis with Fuzzy Model. *IEEE Trans. Systems, Man and Cybernetics* 4: 903-907, 1982.

Tang, C. Y., Tai, W.H. Material damage and forming limits of textured sheet metals. *Journal of Materials Processing Technology* 99: 135-140, 2000.

Tang, J. Reliability assessment of mechanical components using fuzzy-set theory. *ASME Journal of Pressure Vessel Technology* 120: 270-275, 1998.

Tarng, Y. S., Yang, W. H., Juang, S. C. The Use of Fuzzy Logic in the Taguchi Method for the Optimisation of the Submerged Arc Welding Process. *International Journal of Aadvanced Manufacturing Technology* 16: 688-694, 2000.

Tjotta, S. "Formability and the growth of damage." In *Numerical Methods in Industrial Forming Processes*, edited by Wood, R. D., Zienkiewicz, O. C., 1992.

Van Minh, H., Sowerby, R., Duncan, J. L. Variability of forming limit curves. *International Journal of Mechanical Sciences* 16: 31-44, 1974.

We, L. W., Yu, Y. Computer simulation of forming automotive structural parts by hydroforming process. The Third International Conference Numisheet'96, Dearborn, USA, September 29 - October 3, 1996.

Wood, K. L., Antonsson, E. K. Computations with Imprecise Parameters in Engineering Design: Background and Theory. *Journal of Mechanisms, Transmission and Design* 111: 616-624, 1989.

Wu, P. D., Jain, M., Savoie, J., MacEwen, S. R., Tugcu, P., Neale, K. W. Evaluation of anisotropic yield functions for aluminum sheets. *International Journal of Plasticity* 19: 121-138, 2003.

Wu, P. D., MacEwen, S. R., Lloyd, D.J., Neale, K. W. A mesoscopic approach for predicting sheet metal formability. *Modelling and Simulation in Materials Science and Engineering* 12: 511-527, 2004.

Wu, P. D., Lloyd, D. J., Jain, M., Neale, K. W., Huang, Y. Effects of spatial grain orientation distribution and initial surface topography on sheet metal necking. *International Journal of Plasticity* 23: 1084-1104, 2007.

Xing, H. L., Makinouchi, A. Numerical Analysis and Design for Tubular Hydroforming. *International Journal of Mechanical Sciences* 43: 1009-1026, 2001.

Yager, R. R., et al., ed. *Fuzzy Sets and Applications: Selected Papers by L.A. Zadeh*. New York: John Wiley, 1987.

Yang, H. J., Hwang, P. J., Lee, S. H. A study on shrinkage compensation of the SLS process by using the Taguchi method. *International Journal of Machine Tools & Manufacture* 42: 1203-1212, 2002.

Yang, J., Jeon, B., Oh, S. Design sensitivity analysis and Optimization of the hydroforming process. *Journal Of Materials Processing Technology* 113: 666-672, 2001.

Yang, W. H., Tarng, Y. S. Design optimization of cutting parameters for turning operations based on the Taguchi method. *Journal Of Materials Processing Technology* 84: 122-129, 1998.

Yao, H., Cao, J. Prediction of forming limit curves using an anisotropic yield function with prestrain induced backstress. *International Journal of Plasticity* 18: 1013-1038, 2002.

Yoshitomi, Y. Estimation method for application of bulge forming to circular tubes. *Journal of the Japan Society for Technology of Plasticity* 28, No. 316: 432-437, 1987.

Zadeh, L. A. Fuzzy Sets. *Information and Control* 8: 338-352, 1965.

Zadeh, L. A. Probability Measures of Fuzzy Events. *Journal of Mathematical Analysis and Applications* 10: 421-427, 1968.

Zadeh, L. A. "Towards a theory of fuzzy systems." In *Aspects of Network and System Theory*, edited by Kalman, R. E., DeClaris, N., 469-490. New York: Holt. Rinehart & Winston, 1971.

Zhang, S. H. Developments in hydroforming. *Journal of Materials Processing Technology* 91, No. 1: 236-244, 1999.

Zhang, S. H., Wang, Z. R. Numerical simulation of the hydroforming process for 32-petal spherical vessels. *Journal Of Materials Processing Technology* 39: 109-118, 1993.

Zhao, L., Sowerby, R., Sklad, M. P. A theoretical and experimental investigation of limit strains in sheet metal forming. *International Journal of Mechanical Sciences* 38: 1307-1317, 1996.

Zhu, X., Weinmann, K., Chandra, A. A Unified Bifurcation Analysis of Sheet Metal Forming Limits. *ASME Journal of Engineering Materials and Technology* 123: 329-333, 2001.

Appendix A

Fuzzy Reliability Analysis of Metal Forming Process

An approach for the reliability analysis of the tube hydroforming process is proposed in this study, where the fuzzy linear regression method is used in cooperation with the finite element method. The finite element method is used as a numerical experiment tool to obtain a series of stress values, and then the fuzzy regression function of the stress is obtained by the fuzzy linear regression method. The regression coefficients of the obtained regression function for the stress are defined as triangular fuzzy numbers in this study, so the stress will be a triangular fuzzy number when its relative parameters are given in the nominal values. Similar with the stress-strength interference model in classical reliability theory, the fuzzy stress-random strength interference model is proposed in this study. A normal distribution is used to approximate the probability distribution of the material strength of the hydroformed tube, and its stress follows the triangular distribution, so the fuzzy reliability of the hydroformed tube can be evaluated. A tube hydroforming process for free bulging used in Chapter 3 is employed to illustrate the proposed approach.

A.1 Literature Review on Fuzzy Sets

A.1.1 Fuzzy Sets Theory

The traditional attitude toward uncertainty was seriously challenged by various developments in 20th century, such as the appearance of statistical mechanics and Heisenberg's uncertainty principle in quantum mechanics. While uncertainty became recognized as useful in statistical mechanics, it was for long time assumed that probability theory is the only way to deal with uncertainty and that uncertainty is fully captured by probability theory alone.

When probability theory can not satisfactorily deal with some special uncertainty such as subjective uncertainty, an important idea emerged in the second half of the 20th century, i.e., the idea of fuzzy sets, introduced by Zadeh (1965).

Fuzzy sets are defined on any given universal set of concern by functions analogous to characteristic functions of classical sets. These functions are called membership functions. A fuzzy set is characterized by a membership function mapping the elements of a domain, space or universe of discourse X to the unit interval [0, 1] (Zadeh, 1965). That is

$$A : X \rightarrow [0,1] \tag{A.1}$$

Many researchers have contributed to the development of foundations of fuzzy sets theory, but perhaps the most important role in its development, not only in its founding, was played by Zadeh. His selected papers on the period 1965-95 are well documented by two volumes edited by Yager et al. (1987) and Klir and Yuan (1995).

A.1.2 Fuzzy Numbers

In general, a fuzzy number is a fuzzy subset in R which is both "normal" and "convex". Normality implies that

$$\exists x \in R: \ \underset{x}{\forall} \mu_A(x) = 1 \tag{A.2}$$

Convex means that an α-cut which is parallel to the horizontal axis

$$A_\alpha = [a_{\min}^{(\alpha)} \quad a_{\max}^{(\alpha)}] \tag{A.3}$$

yields the property that

$$(\alpha' < \alpha) \Rightarrow (A_\alpha \subset A_{\alpha'}) \tag{A.4}$$

The most widely used fuzzy number is the triangular fuzzy number (Kaufmann & Gupta, 1988). The membership function of a triangular fuzzy number A (a, c) is defined by

$$\mu_A(z) = \begin{cases} 1 - \dfrac{|z-a|}{c} & a - c \le z \le a + c \\ 0 & others \end{cases} \tag{A.5}$$

where a is the center value of the fuzzy number A and c (c>0) is the width of the fuzzy number A (See Figure A.1).

The triangular fuzzy number A (a, c) has the following linear character

$$\begin{cases} ① & kA(a,c) = A(ka,kc),\ k > 0 \\ ② & A_1(a_1,c_1) + A_2(a_2,c_2) = A(a_1 + a_2, c_1 + c_2) \end{cases} \tag{A.6}$$

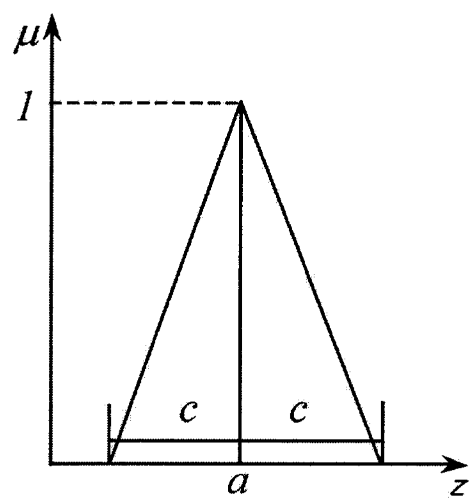

Figure A.1: Triangular Fuzzy Number

A.1.3 Fuzzy Regression

After Zadeh introduced fuzzy logic theory, many fuzzy methods analogous to statistical methods have been proposed for use in reliability, forecasting, linear regression and other areas.

Regression analysis is one of the most used statistical tools by engineers and scientists. In contrast to the ordinary regression that is based on probability theory, fuzzy regression is based on possibility theory (Dubois and Prade, 1988) and fuzzy sets theory (Zadeh, 1965). In fuzzy regression analysis, the deviations between observed values and estimated values are assumed to be due to the fuzziness of the model structure (Tanaka et al., 1982).

Generally, there are two main directions in fuzzy regression model development, fuzzy linear regression (FLR) and fuzzy least-squares regression (FLSR). The first direction includes the original FLR model proposed by Tanaka et al. (1982) and its variations such as the models in Tanaka (1987), Tanaka and Ishibuchi (1991), Peters (1994), Kim and Bishu (1998). The FLSR was firstly introduced by Celmins (1987) and Diamond (1988). Along the same line, there are several variations such as the ones in Savic and Pedrycz (1991), Chang and Lee (1996) and Tanaka and Lee (1997).

Between these two directions, FLR has been criticized significantly, especially in the original formulation of Tanaka et al. (1982). Savic and Pedrycz (1991) noted that not all data points are allowed to influence the estimated parameters in FLR. Furthermore, the model is sensitive to data outliers and prediction intervals become wider as more data are collected (Redden and Woodall, 1994, 1996). The original FLR with the objective function of minimizing the sum of parameter widths may yield some crisp parameter estimates (Celmins, 1987) and it is scale dependent (Jozsef, 1992). On the other hand, FLSR has had very few criticisms because of its similarity to traditional least-squares regression. However, the introduction of fuzzy parameters' modal values using conventional linear regression causes FLSR to be sensitive to outliers. Furthermore, FLSR should be used only when enough data are available. This results in losing one of the advantages of fuzzy regression in dealing with data insufficiency.

Fuzzy regression theory is still developing. The most applied fuzzy regression method in practice is the fuzzy linear regression method proposed by Tanaka (1987) (see Kim and Bishu, 1996; Soliman et al., 1998; Ip et al., 2003 etc).

In classical linear regression analysis, the deviations between real values of a function and estimated values are caused by the observation errors, or by the specification errors. According to Tanaka (1982), these deviations between the real values and the computed values depend on the fuzziness of the system structure, or in other words, the fuzziness of the system parameters. It is reflected in a fuzzy linear regression model that the regression coefficients of the regression function are fuzzy numbers.

When the relationship between the dependent variable Y and independent variables X is not linear but complicated, a method, so-called compound multiple linear regression analysis, can be used to solve the problem (Hu & Zhu, 1990). Let

$$\begin{aligned} U &= [u_1, u_2, \cdots, u_n, u_{n+1}, \cdots, u_{2n}] \\ &= [x_1, \cdots, x_n, x_1^2, \cdots, x_n^2] \end{aligned} \tag{A.7}$$

Similar to the classical linear regression method, a fuzzy linear regression is given by

$$y = A_0 + A_1 u_1 + A_2 u_2 + \cdots + A_{2n} u_{2n} \tag{A.8}$$

In fuzzy linear regression, the regression coefficient A_j is a fuzzy number. If A_j is defined as a triangular fuzzy number A_j (a_j, c_j), then the y in Eq. (A.8) is a triangular number and its membership function is as follows

$$\mu_y(y_i)=\begin{cases}1-\dfrac{\left|y_i-\sum_j a_j x_{ji}\right|}{\sum_j c_j x_{ji}} & \sum_j a_j x_{ji}-\sum_j c_j x_{ji}\le y\le \sum_j a_j x_{ji}+\sum_j c_j x_{ji} \\ 0 & others\end{cases} \tag{A.9}$$

The most suitable fuzzy linear function for the given data is the one in which the sum of the fuzzy width, denoted by $J=\sum c^T|x_i|$, is minimized. The degree of fitting, H, which ranges between 0 and 1, is an index that denotes the minimum value of the degree of fitting of the fuzzy linear regression model to the all samples. So the problem has turned to finding the fuzzy coefficients A_j *(j=0,…,2n)* which are the solution of the following linear programming problem

$$\begin{aligned} &Min && J=\sum c^T|x_i| \\ &Subject\ \ to && \sum_j a_j u_{ji}-(1-H)\sum_j c_j|u_{ji}|\le y_i \\ & && \sum_j a_j u_{ji}+(1-H)\sum_j c_j|u_{ji}|\ge y_i \\ & && c_j\ge 0,\quad i=1,\cdots,p\quad j=0,1,\cdots,2n \end{aligned} \tag{A.10}$$

This fuzzy linear regression method will be used in this research to obtain the regression function between the stress and its relative parameters.

A.1.4 Uncertainty and Fuzzy Sets in Reliability

When studying the reliability of a given system, the problem of partial information on the behavior of its components and uncertain character of the environment in which it operates are always encountered. Up to now, probability theory has been and is nowadays the main tool to analyze uncertainty associated with all type of problems, both systems modeling and failure theory. This is not surprising since the theory of probability has been a science since the 19th century, while other uncertainty theories, such as fuzzy sets or credibility theory (Bühlmann, 1967), have not appeared until the 1960's.

The main reasons to use fuzzy sets in reliability as a subset were explained by Zimmermann (1983). If problems are vague or diffuse by nature, the relations, the restrictions, the objects and the general system model must be fuzzy. Normally, the data we have for problem resolution are inaccurate, even more inaccurate if the observations are subjective. Although problems could be accurate, sometimes it is too costly or complex to obtain the exact solution, either analytically or numerically, and therefore, it is simpler to use the approximate and fuzzy solution.

To calculate the reliability of systems, many factors may be used, some of them are measurable quantitatively, and others are only qualitatively through experts' judgments. For this, fuzzy sets theory is a very useful tool to analyze those systems because it can treat two types of information, randomness and fuzziness, appropriately (Zadeh, 1971).

The utilization of fuzzy sets in failure analysis was first introduced by Kaufman (1975). Now that fuzzy sets theory has taken root in this area, there are many research topics such as fuzzy diagnostics (Mazumdar, 1988; Roberts & Samuel 1996); fuzzy mechanical reliability (Tang, 1998; Li, 2000; Harris, 2001), fuzzy software reliability (Bastani, 1985; Ebert, 1993; Cai, 1996); fuzzy human reliability (Onisawa, 1988, 1990);

fuzzy safety analysis (Karwowski & Mital, 1986; Misa & Weber, 1990; McCauley-Bell & Badiru, 1996) and fuzzy quality (Ebert, 1993; Cen, 1996).

A.2 Fuzzy Reliability Analysis

Similar to the stress-strength interference model, we present the fuzzy stress-random strength interference model here. The stress is modeled as a fuzzy variable with given membership function $\mu_{\tilde{S}}(x)$, and the strength is modeled as a random variable with given distribution function $f_\delta(x)$. An overlap will exist between the curves where failure may occur due to the probability of strength δ being less than stress $\tilde{S}$. Figure A.2 shows the region of "unreliability".

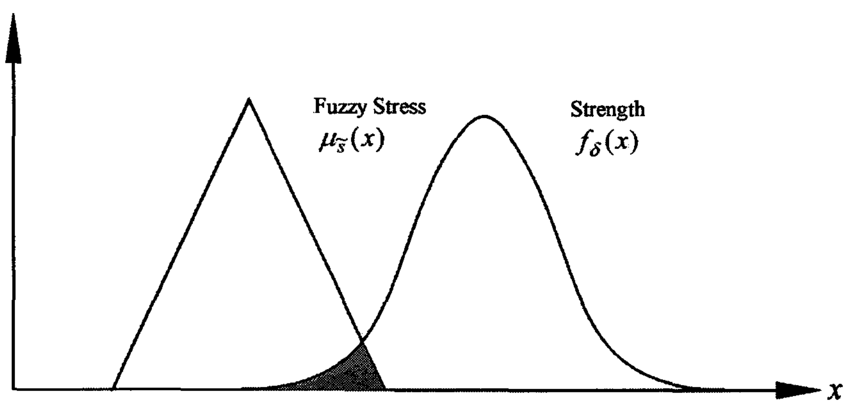

Figure A.2: Fuzzy stress-random strength interference model

The failure state of the structure, defined by $\delta < \tilde{S}$, is a fuzzy event, so according to the definition of the Zadeh's fuzzy probability (Zadeh, 1968), the failure probability of the structure is calculated by the following function

$$\tilde{F} = \int \mu_{\tilde{S}}(x) f_\delta(x) dx \tag{A.11}$$

The fuzzy reliability is then given as

$$\tilde{R} = 1 - \tilde{F} = 1 - \int \mu_{\tilde{S}}(x) f_\delta(x) dx \tag{A.12}$$

In this research, the stress is defined as a triangular fuzzy number, so the membership function of fuzzy stress $\tilde{S}$ will be

$$\mu_{\tilde{S}}(x) = \begin{cases} 1 - \dfrac{|x-m|}{n} & m-n \le x \le m+n \\ 0 & otherwise \end{cases} \tag{A.13}$$

where m is the center value of the fuzzy stress $\tilde{S}$ and n is the width of $\tilde{S}$.

When the distribution of the strength follows a normal distribution, its probability density function can be defined by

$$f_\delta(x) = \frac{1}{\sigma_\delta \sqrt{2\pi}} \exp[-\frac{1}{2}(\frac{x-\mu_\delta}{\sigma_\delta})^2] \tag{A.14}$$

where μ_δ is the mean value of the strength δ and the σ_δ is the standard deviation of δ.

Generally, as to the mean value and standard derivation of the strength, we have

$$\mu_\delta = k_1 \sigma_u \tag{A.15}$$

$$\sigma_\delta = k_2 \mu_\delta \tag{A.16}$$

where in this application σ_u is the ultimate tensile strength of the specimen of the tube material, k_1 is the manufacturing coefficient, k_2 is the differential coefficient (Kutz, 2002).

When Eqs. (A.13) and (A.14) are substituted into Eq. (A.11), the fuzzy failure probability of the structure can be described as

$$\widetilde{F}=\left(\frac{n+m-\mu_\delta}{n}\right)\times\Phi\left(\frac{m+n-\mu_\delta}{\sigma_\delta}\right)-\left(\frac{n-m+\mu_\delta}{n}\right)\times\Phi\left(\frac{m-n-\mu_\delta}{\sigma_\delta}\right)-2\times\left(\frac{m+\mu_\delta}{n}\right)\times\Phi\left(\frac{m-\mu_\delta}{\sigma_\delta}\right)+\frac{\sigma_\delta}{\sqrt{2\pi}n}\times\left\{\begin{array}{l}\exp\left[-\dfrac{(m+n-\mu_\delta)^2}{2\sigma_\delta^2}\right]+\\ \exp\left[-\dfrac{(m-n-\mu_\delta)^2}{2\sigma_\delta^2}\right]-\\ 2\exp\left[-\dfrac{(m-\mu_\delta)^2}{2\sigma_\delta^2}\right]\end{array}\right\} \tag{A.17}$$

where $\Phi(x)=\frac{1}{\sqrt{2\pi}}\int_x^{+\infty}\exp(-\frac{t^2}{2})dt$. According to Eq. (A.12), the fuzzy reliability $\widetilde{R}$ can be obtained as

$$\widetilde{R}=1-\widetilde{F} \tag{A.18}$$

A.3 Application

A.3.1 Finite Element Simulation

The same example as discussed in Chapter 3 is used here, which is a tube hydroforming process of free bulging of a straight tube with applying the internal pressure and axial force simultaneously. The FE simulation has been described in Section 3.3.1. The schematic view of the process is shown in Figure 3.3 and the material properties are listed in Table 3.1. The same method is applied to investigate the different forming parameters as listed in Table 3.4 for their effects on the hydroformability in terms of critical resulting stress by varying the value of each parameter over a range of ± 10% from the nominal value while keeping the remaining parameters constant. A series of stress values are obtained using FE simulation, the results are shown in Table A.1. All the denotation of the parameters shown in this table is same as described in Section 3.3.2. The critical stress in each run appeared at the same element, 3630.

Table A.1: The critical stress and its relative parameters

Run No.	L_0	t_0	r_e	W	n	P_f	m	μ	K	Von Mises stress of element 3630 (MPa)
1	200	1.5	10	100	0.227	40	0.4	0.06	537	473.26
2	180	1.5	10	100	0.227	40	0.4	0.06	537	490.31
3	190	1.5	10	100	0.227	40	0.4	0.06	537	486.68
4	210	1.5	10	100	0.227	40	0.4	0.06	537	474.44
5	220	1.5	10	100	0.227	40	0.4	0.06	537	454.39
6	200	1.35	10	100	0.227	40	0.4	0.06	537	476.41
7	200	1.425	10	100	0.227	40	0.4	0.06	537	474.37
8	200	1.575	10	100	0.227	40	0.4	0.06	537	468.60
9	200	1.65	10	100	0.227	40	0.4	0.06	537	462.05
10	200	1.5	9	100	0.227	40	0.4	0.06	537	465.20
11	200	1.5	9.5	100	0.227	40	0.4	0.06	537	467.16
12	200	1.5	10.5	100	0.227	40	0.4	0.06	537	470.00
13	200	1.5	11	100	0.227	40	0.4	0.06	537	471.72
14	200	1.5	10	90	0.227	40	0.4	0.06	537	456.84
15	200	1.5	10	95	0.227	40	0.4	0.06	537	460.15
16	200	1.5	10	105	0.227	40	0.4	0.06	537	479.93
17	200	1.5	10	110	0.227	40	0.4	0.06	537	489.36
18	200	1.5	10	100	0.2043	40	0.4	0.06	537	472.45
19	200	1.5	10	100	0.2157	40	0.4	0.06	537	472.60
20	200	1.5	10	100	0.2384	40	0.4	0.06	537	471.13
21	200	1.5	10	100	0.2497	40	0.4	0.06	537	469.57
22	200	1.5	10	100	0.227	36	0.4	0.06	537	441.59
23	200	1.5	10	100	0.227	38	0.4	0.06	537	454.21
24	200	1.5	10	100	0.227	42	0.4	0.06	537	480.44
25	200	1.5	10	100	0.227	44	0.4	0.06	537	494.69
26	200	1.5	10	100	0.227	40	0.36	0.06	537	472.36
27	200	1.5	10	100	0.227	40	0.38	0.06	537	472.68
28	200	1.5	10	100	0.227	40	0.42	0.06	537	472.26
29	200	1.5	10	100	0.227	40	0.44	0.06	537	472.37
30	200	1.5	10	100	0.227	40	0.4	0.054	537	471.34
31	200	1.5	10	100	0.227	40	0.4	0.057	537	472.36
32	200	1.5	10	100	0.227	40	0.4	0.063	537	472.93
33	200	1.5	10	100	0.227	40	0.4	0.066	537	472.76
34	200	1.5	10	100	0.227	40	0.4	0.06	483.3	437.65
35	200	1.5	10	100	0.227	40	0.4	0.06	510.15	456.28
36	200	1.5	10	100	0.227	40	0.4	0.06	563.85	486.09
37	200	1.5	10	100	0.227	40	0.4	0.06	590.7	499.36

A.3.2 Fuzzy Linear Regression Analysis for Fuzzy Stress

As discussed in the foregoing section, the stress is dependent on several relative parameters. In this study, the relative parameters set for the tube stress are selected as

$$X = [L_0, t_0, r_e, W, n, P_f, m, \mu, K] \tag{A.19}$$

where L_0 is length of tube; r_0 is outer radius of tube; t_0 is thickness of tube; r_e is die entry radius; W is bulge width; n is Hardening exponent; P_f is internal pressure; m is nominal stress ratio; μ is friction coefficient; and K is hardening coefficient.

The critical stress values and its relative parameters, as shown in Table A.1 are used as the data samples for the fuzzy linear regression analysis. According to Eq. (A.7), U is defined by

$$U = [L_0, t_0, r_e, W, n, P_f, m, \mu, K, L_0^2, t_0^2, r_e^2, W^2, n^2, P_f^2, m^2, \mu^2, K^2] \tag{A.20}$$

and according to the fuzzy linear regression method, the fuzzy stress of the hydroformed tube can be described as the following formula

$$\begin{aligned}\widetilde{S} = A_0 + A_1 L_0 + A_2 t_0 + A_3 r_e + A_4 W + A_5 n + A_6 P_f + A_7 m + A_8 \mu + A_9 K + \\ A_{10} L_0^2 + A_{11} t_0^2 + A_{12} r_e^2 + A_{13} W^2 + A_{14} n^2 + A_{15} P_f^2 + A_{16} m^2 + A_{17} \mu^2 + A_{18} K^2]\end{aligned} \tag{A.20}$$

when the nominal values of the L_0, t_0, r_e, W, n, P_f, m, μ and K are substituted into the above equation, the center value, width and membership function of the fuzzy stress can be obtained.

Applying the fuzzy linear regression method, following Tanaka (1987), the fuzzy threshold H was set equal to 0.5, the regression coefficients corresponding to the fuzzy stress regression function of the Element 3630 is shown in Table A.2. With reference to Table A.2, the fuzzy stress of the Element 3630 can be expressed as follows

$$\begin{aligned}\widetilde{S}_{3630} = {} & (-1621.1215,0)+(-2.8297,0.00004)L_0+(365.0624,0)t_0+(92.9981,0)r_e \\ & +(1.2574,0.00002)W+(1097.076,0)n+(32.0594,0.00001)P_f \\ & +(-51.7423,0)m+(633.0315,0)\mu+(1.9993,0.00009)K+(0.005,0)L_0^2 \\ & +(-137.0164,0)t_0^2+(-4.4911,0.00009)r_e^2+(0.0022,0)W^2 \\ & +(-2556.6814,0)n^2+(-0.318,0)P_f^2+(62.1779,0))m^2 \\ & +(-4328.0402,0)\mu^2+(-0.0013,0.00009)K^2]\end{aligned} \tag{A.21}$$

the estimated fuzzy stress value of $\widetilde{S}_{3630}$ can be obtained when the nominal values of each relative parameter are given, i.e., $\widetilde{S}_{3630}$ =(482.1221,27.2978) MPa, and then the membership function of $\widetilde{S}_{3630}$ is

$$\mu_{\widetilde{S}_{3630}}(x)=\begin{cases}1-\dfrac{|x-482.1221|}{27.2978} & 454.8243\le x\le 509.4199\\[2ex] 0 & otherwise\end{cases} \tag{A.22}$$

Table A.2: The regression coefficients of the fuzzy stress

A_j	a_j	c_j	A_j	a_j	c_j
0	-1621.1215	0.00000	10	0.0050	0.00000
1	-2.8297	0.00004	11	-137.0164	0.00000
3	365.0624	0.00000	12	-4.4911	0.00009
3	92.9981	0.00000	13	0.0022	0.00000
4	1.2574	0.00002	14	-2556.6814	0.00000
5	1097.0760	0.00000	15	-0.3180	0.00000
6	32.0594	0.00001	16	62.1779	0.00000
7	-51.7423	0.00000	17	-4328.0402	0.00000
8	633.0315	0.00000	18	-0.0013	0.00009
9	1.9993	0.00009			

A.3.3 Fuzzy Reliability of Tube Hydroforming Process

The material strength of the tube is assumed to follow a normal distribution. We let k_1=0.90 and k_2=0.05 in Eq. (A.15) and Eq. (A.16). As shown in Table 3.1, the tube material ultimate tensile strength is equal to 350 MPa, then the mean value and the standard deviation of the strength of the tube can be calculated, i.e., μ_δ=315 MPa and σ_δ =15.75 MPa. According to the Eq. (A.17) and Eq. (A.18), the fuzzy reliability of the Element 3630 of the hydroformed tube, which is the critical element in this example, is close to 0.0%. In this particular example, the prediction shows this tube hydroforming process will fail with the probability close to 100%.

A.4 Discussion and Conclusions

When the statistical information of the stress for reliability analysis of tube hydroforming process is not available or completed, fuzzy linear regression method provide an effective alternative to obtain the relationship between the stress and its relative forming parameters.

For the same tube hydroforming process, two different reliability analysis methods are presented in Chapter 3 and in this appendix based on strain and stress, respectively. From the calculated results, it can be found that this postulated hydroforming process has a high failure probability, 41.15% failure based on strain limit and almost 100% failure based on von Mises stress. The method presented in Chapter 3 gives more reasonable and practical prediction of the failure probability. The predicted failure probability in this appendix is based on the stress-strength interference model, this model generally does not expect that the resultant mean stress will be over the material mean ultimate strength. However, as we know, the ductile material true strain will keep increasing after reaching the ultimate stress point where the necking occurs until the fracture happens. The reliability analysis method presented in this appendix based on the fuzzy stress-random strength interference model is applicable for metal forming process only when the deformed part stress is less than the material ultimate strength. The reliability analysis method presented in Chapter 3 based on forming limit diagram is more suitable for the metal forming process which is mostly dealing with ductile material.

Usually, the non-zero width of the regression coefficient for certain parameter shows that the dependent variable is sensitive to the variation of this parameter. For the example given in this study, it can be found from Eq. (A.21) that the following parameters have the non-zero width of the regression coefficient: L_0 (length of tube); W (bulge width); P_f (internal pressure); K (hardening coefficient); r_e^2 (related to die entry radius) and K^2 (related to hardening coefficient). It means that these parameters (L_0, W, P_f, K and r_e) have more effects on the fuzzy stress than the other parameters. From Figure 3.7 in Chapter 3 for the forming parameters effects on the bulge ratio, it can be found that the similar set of parameters (L_0, W, P_f and K) have significant effects on the bulge ratio. The fuzzy linear regression method presented in this study to obtain the fuzzy stress not only can give out the relationship between the stress and its related parameters, but also can provide the sensitivity information through the value of the width of each regression coefficient.